

ADA058041

LEVEL II

(2)

RADC-TR-78-156
Phase Report
June 1978



ELECTROMAGNETIC PROPERTIES AND EFFECTS OF ADVANCED
COMPOSITE MATERIALS: MEASUREMENT AND MODELING

Georgia Institute of Technology
Syracuse University
State University of New York
USAF Academy

AD NO. _____
DDC FILE COPY

Approved for public release; distribution unlimited.

ROME AIR DEVELOPMENT CENTER
Air Force Systems Command
Wright-Patterson Air Force Base, New York 13441

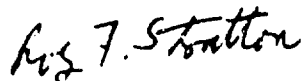
DDC
RECEIVED
AUG 23 1978

Best Available Copy

This report has been reviewed by the RADC Information Office (OI) and is releasable to the National Technical Information Service (NTIS). At NTIS it will be releasable to the general public, including foreign nations.


RADC-TR-78-156 has been reviewed and is approved for publication.

APPROVED:



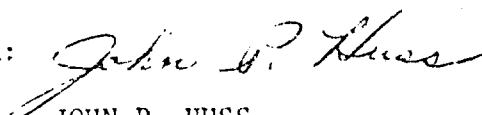
ROY F. STRATTON
Project Engineer

APPROVED:



JOSEPH J. NARESKY
Chief, Reliability & Compatibility Division

FOR THE COMMANDER:



JOHN P. HUSS
Acting Chief, Plans Office

If your address has changed or if you wish to be removed from the RADC mailing list, or if the addressee is no longer employed by your organization, please notify RADC (RBCT) Griffiss AFB NY 13441. This will assist us in maintaining a current mailing list.

Return this copy. Retain or destroy.

Best Available Copy

A058041

ERRATA

September 1978

RADC-TR-78-156 dated June 1978

Title: Electromagnetic Properties and Effects of Advanced Composite
Materials: Measurement and Modeling

Please add the following author's name and address to cover and
block 7 of DD Form 1473:

Dr. Roy F. Stratton
Rome Air Development Center

Rome Air Development Center
Air Force Systems Command
Griffiss Air Force Base, New York 13441

78 10 06 121

UNCLASSIFIED

SECURITY CLASSIFICATION OF THIS PAGE (When Data Entered)

REPORT DOCUMENTATION PAGE		READ INSTRUCTIONS BEFORE COMPLETING FORM
1. REPORT NUMBER RADC-TR-78-156	2. GOVT ACCESSION NO.	3. RECIPIENT'S CATALOG NUMBER
6. ELECTROMAGNETIC PROPERTIES AND EFFECTS OF ADVANCED COMPOSITE MATERIALS: MEASUREMENT AND MODELING		7. TYPE OF REPORT & PERIOD COVERED Phase Report 1 Oct 76 - 30 Sept 77
7. AUTHOR(s) See Reverse		8. CONTRACT OR GRANT NUMBER(s) See Reverse
9. PERFORMING ORGANIZATION NAME AND ADDRESS See Reverse		10. PROGRAM ELEMENT, PROJECT, TASK AREA & WORK UNIT NUMBERS 62702F 23380306 170314
11. CONTROLLING OFFICE NAME AND ADDRESS Rome Air Development Center (RBCT) Griffiss AFB NY 13441		12. REPORT DATE June 1978
14. MONITORING AGENCY NAME & ADDRESS (if different from Controlling Office) Same (12) 176 P.		13. NUMBER OF PAGES 160
15. DISTRIBUTION STATEMENT (of this Report) Approved for public release; distribution unlimited. (15) F30602-75-C-0121		16. SECURITY CLASS. (of this report) UNCLASSIFIED
17. DISTRIBUTION STATEMENT (of the abstract entered in Block 20, if different from Report) Same (10) A. T. / Adams, W. J. / Gajdos, R. E. / Heintz W. F. / Walker		18. DECLASSIFICATION/DOWNGRADING SCHEDULE N/A
19. SUPPLEMENTARY NOTES RADC Project Engineer: Roy F. Stratton (RBCT)		
20. KEY WORDS (Continue on reverse side if necessary and identify by block number) Electromagnetic shielding Shielding Effectiveness Advanced Composite Materials Conductivity Permittivity Permeability Method of Moments Antennas		
21. ABSTRACT (Continue on reverse side if necessary and identify by block number) This report covers several areas: 1. Electromagnetic properties of composite materials are given for the range DC to 30MHz. 2. Techniques of measurement are discussed in the range DC to 1 GHz. 3. Electromagnetic shielding theory is discussed. Surface transfer impedance and the two loop method are related to the conductivity. A matrix method		

DD FORM 1 JAN 73 1473

UNCLASSIFIED

SECURITY CLASSIFICATION OF THIS PAGE (When Data Entered)

339 78 08 22 00

UNCLASSIFIED

SECURITY CLASSIFICATION OF THIS PAGE (When Data Entered)

for the calculation of shielding effectiveness for laminated anisotropic materials (perpendicular incidence) is presented.

4. The modification required by the method of moments to allow calculation involving non-perfect conductors are discussed.
5. A comparison of antenna patterns over a graphite/epoxy ground plane and an aluminum ground plane for dipole and monopole antennas at 370 MHz and 837 MHz is given.

Blocks 7, 8, 9:

<u>Author</u>	<u>Affiliation and Performing Organ.</u>	<u>Contract no. and Prime Contractor, if Different</u>
J. L. Allen	University of South Florida	F30602-75-C-0118 Georgia Inst of Tech
A. T. Adams	Syracuse University on sabbatical leave	F30602-75-C-0122 State Univ of NY
W. J. Gajda	Univ of Notre Dame	F30602-75-C-0121 Syracuse Univ
R. E. Heintz W. F. Walker	Rochester Inst of Tech	F30602-75-C-0121 Syracuse Univ
Lt. Col. O. Graham Capt. J. E. Erickson	US Air Force Academy	JON # 95670212

UNCLASSIFIED

SECURITY CLASSIFICATION OF THIS PAGE (When Data Entered)

The following educational institutions support this investigation:

<u>Author</u>	<u>Affiliation and Performing Organ.</u>	<u>Contact no. and Prime Contractor, if Different</u>
J. L. Allen	Univ of South Florida	F30602-75-C-0118 Georgia Inst of Tech
A. T. Adams	Syracuse University on sabbatical leave	F30602-75-C-0122 State Univ of NY
W. J. Gajda	Univ of Notre Dame	F30602-75-C-0121 Syracuse Univ
R. E. Heintz W. F. Walker	Rochester Inst of Tech	F30602-75-C-0121 Syracuse Univ
Lt. Col. O. Graham Capt. J. E. Erickson	US Air Force Academy	JON # 95670212

ACCESSION	
NTIS	<input checked="" type="checkbox"/>
DTIC	<input type="checkbox"/>
AD	<input type="checkbox"/>
<div style="border: 1px solid black; padding: 5px; display: inline-block;">A</div>	

PREFACE

This effort was conducted by Notre Dame University and Rochester Institute of Technology subcontracting through Syracuse University, by the University of South Florida subcontracting through Georgia Institute of Technology, by the Air Force Academy and by a Syracuse University professor (on sabbatical) subcontracting through the State University of New York under the sponsorship of the Rome Air Development Center Post-Doctoral Program for Rome Air Development Center. Dr. Roy F. Stratton, RADC/RBCT, was project engineer and provided overall technical direction and guidance.

The RADC Post-Doctoral Program is a cooperative venture between RADC and some sixty-five universities eligible to participate in the program. Syracuse University (Department of Electrical Engineering), Purdue University (School of Electrical Engineering), Georgia Institute of Technology (School of Electrical Engineering), and State University of New York at Buffalo (Department of Electrical Engineering) act as prime contractor schools with other schools participating via sub-contracts with prime schools. The U.S. Air Force Academy (Department of Electrical Engineering), Air Force Institute of Technology (Department of Electrical Engineering), and the Naval Post Graduate School (Department of Electrical Engineering) also participate in the program.

The Post-Doctoral Program provides an opportunity for faculty at participating universities to spend up to one year full time on exploratory development and problem-solving efforts with the post-doctorals splitting their time between the customer location and their educational institutions. The program is totally customer-funded with current projects being undertaken for Rome Air Development Center (RADC), Space and Missile Systems Organization (SAMSO), Aeronautical System Division (ASD), Electronics Systems Division (ESD), Air Force Avionics Laboratory (AFAL), Foreign Technology Division (FTD), Air Force Weapons Laboratory (AFWL), Armament Development and Test Center (ADTC), Air Force Communications Service (AFCS), Aerospace Defense Command (ADC), Hq USAF, Defense Communications Agency (DCA), Navy, Army, Aerospace Medical Division (AMD), and Federal Aviation Administration (FAA).

Further information about the RADC Post-Doctoral Program can be obtained from Mr. Jacob Scherer, RADC/RBC, Griffiss AFB, NY, 13441, telephone Autovon 587-2543, Commercial (315) 330-2543.

ACKNOWLEDGEMENTS

Even though this phase of our work has been primarily research oriented, a relatively large number of people have given assistance in one form or another. We want to acknowledge the helpful assistance of the following: Aerospace Corporation - W. McDonald and E. Kendall; Avco - T. Schoenberg; Boeing - J. Browne and R. Force; Hercules - S. Cross; Narmco - D. Black and N. Sunshine; National Aeronautics & Space Agency (NASA-Langley) - R. Pride and S. Lorenz; (NASA-Lewis) - R. Glayas and T. Serafini; Naval Air Systems Command (NASC) - J. Birken; Rand - A. Hiebert; United Technologies - R. Pike; and Wright-Patterson AFB - R. Achard, J. Corbin, R. Ditmer, V. Mangola, R. Neff, and D. Shirrel.

<u>TABLE OF CONTENTS</u>		Page
ACKNOWLEDGEMENTS.....		i
1.0	<u>INTRODUCTION</u>	1
1.1	SUMMARY.....	1
1.1.1	Introduction.....	1
1.1.2	Section 2.....	1
1.1.3	Section 3.....	1
1.1.4	Section 4.....	1
1.1.5	Section 5.....	2
1.1.6	Section 6.....	2
1.2	BACKGROUND.....	2
1.3	VALUABLE REFERENCE.....	3
REFERENCES.....		4
2.0	<u>MEASUREMENT OF THE ELECTRICAL PROPERTIES OF ADVANCED COMPOSITES IN THE FREQUENCY RANGE OF DC TO 30 MHz</u>	5
2.1	SUMMARY OF PROGRESS TO DATE.....	5
2.1.1	Permeability of Advanced Composite Materials.....	5
2.1.2	Permittivity of Advanced Composite Materials.....	5
2.1.3	Conductivity of Advanced Composite Materials.....	5
2.2	GOALS AND OBJECTIVES.....	6
2.3	SAMPLE TYPES AND SAMPLE PREPARATION.....	7
2.3.1	Materials.....	7
2.3.2	Lay-Up Procedures.....	7
2.3.3	Curing.....	7
2.3.4	Electrical Contact Formation.....	7
2.4	MEASUREMENT TECHNIQUES.....	12
2.4.1	Permeability.....	12
2.4.2	Permittivity.....	14
2.4.3	Conductivity.....	14
2.5	PROPERTIES OF CONSTITUENTS.....	16
2.5.1	Electrical Properties of Fibers.....	16
2.5.2	Electrical Properties of Epoxies.....	17

	Page
2.6	MEASURED ELECTRICAL PROPERTIES OF ADVANCED COMPOSITES..... 18
2.6.1	Permeability..... 18
2.6.2	Permittivity..... 18
2.6.3	DC Conductivity..... 20
2.6.4	High Field Effects..... 22
2.6.5	Summary..... 25
2.7	CONDUCTIVITY - FREQUENCY BEHAVIOR OF GRAPHITE/EPOXY..... 27
2.7.1	Measurement Techniques and Results..... 27
2.7.2	Skin Effect..... 34
2.8	CONDUCTIVITY MODELS..... 36
2.8.1	Current in Longitudinal Directions..... 36
2.8.2	Current in Transverse Directions..... 36
2.8.3	Conductance of Multiple-Ply Samples..... 38
2.9	MOISTURE EFFECTS..... 40
2.10	TEMPERATURE EFFECTS..... 40
2.11	CONCLUSIONS AND SUMMARY..... 41
	APPENDIX 2-A CALCULATION OF SKIN EFFECT..... 42
	APPENDIX 2-B RANDOM FIBER MODEL..... 44
	REFERENCES..... 46
3.0	<u>MEASUREMENT OF THE ELECTRICAL PROPERTIES OF ADVANCED</u> <u>COMPOSITES IN THE FREQUENCY RANGE OF 30 MHz TO 1.0 GHz.....</u> 47
3.1	SUMMARY OF PROGRESS TO DATE..... 47
3.1.1	Parallel Plate Sample Tester..... 47
3.1.2	Slotted Line Stripline Tester..... 47
3.1.3	Early Results in Parameter Measurement..... 48
3.1.3.1	Results from Parallel-Plate Tester..... 48
3.1.3.2	Results from 10 cm Slotted Stripline..... 48
3.2	DEVELOPMENT OF A PARAMETER MEASUREMENT METHOD..... 48
3.2.1	The Parallel Plate Tester..... 48
3.2.2	The Slotted Stripline..... 51
3.2.2.1	Physical Description..... 51
3.2.2.2	Measurement Method..... 51
3.2.2.3	Advantages of the Stripline Method..... 54
3.2.2.4	Limitations of the Slotted Stripline Method..... 54

	Page
3.2.3 Measurement Results.....	55
APPENDIX 3-A THE ANALYTICAL BASIS FOR THE SLOTTED STRIPLINE.....	57
APPENDIX 3-B COMPUTER ANALYSIS OF MEASURED DATA.....	64
REFERENCES.....	73
4.0 <u>ELECTROMAGNETIC SHIELDING EFFECTIVENESS OF ADVANCED</u>	
<u>COMPOSITE MATERIALS</u>	74
4.1 INTRODUCTION.....	74
4.2 BACKGROUND.....	74
4.3 MEASUREMENT TECHNIQUES AND THEORY.....	75
4.3.1 Plane Wave Normally Incident on Infinite Flat Plate.....	75
4.3.2 Two-loop/Infinite Flat Plate Configuration.....	78
4.3.3 Quasistatic Shielding Formulas for Electrically Thin-Shell Ellipsoids.....	81
4.3.4 Surface Transfer Impedance and Effective Conductivity.....	81
4.3.5 Transverse Flat Plate Samples in Waveguide and Transmission Line Structures.....	86
4.3.5.1 General Case.....	86
4.3.5.2 Rectangular Waveguide.....	89
4.4 AN ANISOTROPIC MODEL FOR PLANE WAVE PROPAGATION THROUGH SINGLE AND MULTILAYER ADVANCED COMPOSITES.....	92
4.4.1 Unidirectional Samples.....	94
4.4.2 Unidirectional Sample with Normally Incident, Arbitrarily Polarized Plane Wave.....	94
4.4.3 Multilayer Samples with Normally Incident, Arbitrarily Polarized Plane Waves.....	98
4.4.4 Scattering Matrix for a Multilayer Composite Structure with Normally Incident, Arbitrarily Polarized Plane Waves.....	98
4.4.5 Extension to Oblique Angles of Incidence.....	100
APPENDIX 4-A DERIVATION OF EQUATION (4-9).....	103
SYMBOLS USED IN SECTION 4.....	105
REFERENCES.....	107
5.0 <u>NUMERICAL TECHNIQUES FOR THE ANALYSIS OF COMPOSITE</u>	
<u>MATERIALS</u>	108
5.1 BASIC PROBLEMS AND TECHNIQUES.....	108
5.1.1 The Electromagnetic Problem.....	108

	Page
5.1.2 Characteristics of Advanced Composites.....	112
5.1.3 Available Numerical Techniques.....	112
5.1.4 Basic Methods for Analysis of Composite Materials.....	113
5.1.4.1 The Polarization Current Method.....	113
5.1.4.2 The Equivalent Surface Current Method.....	115
5.1.4.3 Wire-Grid Loading Techniques.....	118
5.1.4.4 Surface Loading Techniques.....	122
5.1.4.5 Body of Revolution Methods.....	122
5.1.4.6 Aperture Coupling Methods.....	122
5.1.5 Special Problems in Composites.....	123
5.2 LOAD TECHNIQUES FOR THIN WIRES AND SURFACES.....	124
5.2.1 Loading Techniques for Thin Wires.....	124
5.2.2 Loading Techniques for Surfaces.....	134
5.2.3 Application of the Load Techniques.....	136
APPENDIX 5-A THE POLARIZATION METHOD AND SURFACE LOADING.....	137
SYMBOLS USED IN SECTION 5.....	139a
REFERENCES.....	141
6.0 <u>ANTENNA CHARACTERISTICS</u>	143
6.1 THE GROUND PLANE.....	143
6.2 INPUT IMPEDANCE.....	143
6.3 ANTENNA PATTERNS.....	143
6.3.1 Monopole Antennas.....	143
6.3.2 Dipole Antennas.....	151
6.3.3 Blade Antenna.....	151
REFERENCES.....	160

LIST OF ILLUSTRATIONS		Page
Figure 2-1	Abrading of Epoxy Rich Layers.....	9
Figure 2-2	Broken Fibers in Narmco 5213.....	10
Figure 2-3	Vacuum System.....	11
Figure 2-4	Sketch of Contact Formation.....	11
Figure 2-5	Permeability Measurement.....	13
Figure 2-6	Vibrating Sample Magnetometer.....	13
Figure 2-7	Two-Point Conductivity Measurement.....	15
Figure 2-8	Cross Plane Measurements on Boron/Epoxy.....	19
Figure 2-9	DC Resistance Measurements.....	20
Figure 2-10	Volume Fraction of Boron Fibers.....	22
Figure 2-11	Longitudinal Current Density vs Applied Field.....	24
Figure 2-12	Transverse Current Density vs Applied Field.....	24
Figure 2-13	Current vs Temperature in Transverse Sample.....	26
Figure 2-14	(a) Sample in Shielded Metal Box Attached to the Front of the Oscilloscope.....	28
	(b) Composite Sample is the Horizontal Post Current Sampling Resistor is at Right Angles to the Composite Post.....	28
Figure 2-15	Conductivity vs Frequency for Sample #15.....	29
Figure 2-16	Conductivity vs Frequency for Sample #16.....	29
Figure 2-17	Conductivity vs Frequency for Sample #16.....	29
Figure 2-18	Conductivity vs Frequency for Sample #20.....	30
Figure 2-19	Conductivity vs Frequency for Sample #27.....	30
Figure 2-20	Conductivity vs Frequency for Sample #21.....	30
Figure 2-21	Conductivity vs Frequency for Sample #21.....	31
Figure 2-22	Conductivity vs Frequency for Sample #23.....	31
Figure 2-23	Conductivity vs Frequency for Sample #25.....	31
Figure 2-24	Conductivity vs Frequency for Sample #30.....	32
Figure 2-25	Conductivity vs Frequency for Sample #30.....	32
Figure 2-26	Conductivity vs Frequency for Sample #31.....	32
Figure 2-27	Conductivity vs Frequency for Sample #31.....	33
Figure 2-28	Conductivity vs Frequency for Sample #29.....	33
Figure 2-29	Conductivity vs Frequency for Sample #14.....	33

	Page
Figure 2-30 Skin Effect Geometry.....	35
Figure 2-31 Skin Effect Results.....	35
Figure 2-32 Model for Determination σ_L	37
Figure 2-33 Model for Determination σ_T	37
Figure 3-1 Parallel Plate Tester.....	49
Figure 3-2 Schematic Diagram of Parallel Plate Tester.....	49
Figure 3-3 Slotted Stripline - Cross Section.....	52
Figure 3-4 Slotted Stripline - Side View.....	52
Figure 3-5 Standing Wave Data.....	56
Figure 3-6 Slotted Stripline.....	58
Figure 3-7 Fields & Currents in the Stripline.....	58
Figure 3-8 Lossy Parallel Plate Guided Wave Structures.....	60
Figure 3-9 Transmission Line Cross Section.....	60
Figure 3-10 Lossy Line Standing Waves.....	65
Figure 4-1 (a) Elementary Plane Wave Shielding.....	76
(b) Transmission Line Analogy.....	76
(c) ABCD Parameter Representation.....	76
Figure 4-2 Two-loop/Infinite Flat Plate Configuration.....	79
Figure 4-3 Quasistatic Ellipsoidal Shields.....	82
Figure 4-4 Two-port Impedance Representation.....	83
Figure 4-5 Two Types of Measurement Structures Included in the Generalized Analysis.....	87
Figure 4-6 Generalized Transmission Line Model for Measurement Structure.....	87
Figure 4-7 Insertion Loss and Phase Delay for a Lossy Transverse Slab in L-band Rectangular Waveguide.....	91
Figure 4-8 Propagation and Material Coordinates for Treating Aniso- tropic Material with "OpticAxis" in z Direction.....	93
Figure 4-9 Shielding Effectiveness of a Single Layer Anisotropic Shield for Various Fiber Orientations.....	101
Figure 4-10 Shielding Effectiveness of 4-Layer and 7-Layer Anisotropic Shields.....	102
Figure 5-1 Basic EM Scattering Problems for Composites.....	110
Figure 5-2 Basic EM Radiation Problems for Composites.....	111
Figure 5-3 The Equivalent Surface Current Method.....	116

	Page
Figure 5-4 Wire-Grid Method for Composite Problems.....	120
Figure 5-5 Composite Problems.....	125
Figure 5-6 Thin Wire Antennas.....	126
Figure 5-7 The Typical Expansion Function.....	127
Figure 5-8 A Typical Driven, Loaded Group of Subsections.....	129
Figure 5-9 Thin-Wire Loading.....	133
Figure 5-10 A Rectangular Section of a Composite Structure.....	135
Figure 6-1 Impedance of a Monopole Antenna (360-430 MHz).....	144
Figure 6-2 Impedance of a Monopole Antenna (780-900 MHz).....	145
Figure 6-3 The Coordinate Systems Used for the Antenna Patterns.....	146
Figure 6-4 Monopole Antenna at 370 MHz.....	147
Figure 6-5 Monopole Antenna at 370 MHz.....	148
Figure 6-6 Monopole Antenna at 837 MHz.....	149
Figure 6-7 Monopole Antenna at 837 MHz.....	150
Figure 6-8 Dipole Antenna at 370 MHz.....	152
Figure 6-9 Dipole Antenna at 370 MHz.....	153
Figure 6-10 Dipole Antenna at 370 MHz.....	154
Figure 6-11 Dipole Antenna at 837 MHz.....	155
Figure 6-12 Dipole Antenna at 837 MHz.....	156
Figure 6-13 Dipole Antenna at 837 MHz.....	157
Figure 6-14 The Coordinates Used on the Blade Antenna.....	158
Figure 6-15 Blade Antenna at 370 MHz.....	159

LIST OF TABLES

	Page
Table 2-1 Samples Cured at Flight Dynamics Laboratory.....	8
Table 2-2 High Field Nonlinear Thresholds.....	23
Table 2-3 Summary of Electrical Properties of Measured Composites....	25

1.0 INTRODUCTION

1.1 SUMMARY

1.1.1 Introduction

This report is intended to represent a first step toward providing the engineer with the tools required to deal with composite materials in a systematic manner and integrating these tools into the Air Force Intrasytem Analysis Program (IAP). Another report with the same title by the Naval Air Systems Command (1-1) provides additional information.

This report consists of five stand-alone sections, each containing its own set of references. Sections 2 through 5 are interim reports on work still in progress. Therefore, the results presented must be considered as interim results. Section 6 is a very much shortened version of a report (1-2) to be published by the USAF Academy; their work on antennas is completed.

Throughout this report σ , ϵ , and μ are used for conductivity (in mhos/meter), permittivity (in farads/meter) and permeability (in henries/meter). ϵ_0 and μ_0 are the permittivity and permeability of free space. In general ϵ is a complex number which includes the conductivity, but the real part and the conductivity are usually quoted separately. See for example Table 2-3 which quotes the relative permeability (μ/μ_0), relative permittivity (ϵ/ϵ_0), and the conductivity for several materials.

1.1.2 Section 2

This section by W. Gajda of the University of Notre Dame deals with methods for measuring the electrical properties of composite materials in the range DC to 30 (or 50) MHz. Table 2-3, section 2.5.5, gives the results of measurements for the materials used; and these results are in reasonable agreement with other published results. Nevertheless, the number of samples was too small to allow one to assume that all materials of the types studied will fall near the values obtained.

1.1.3 Section 3

Section 3 by R.E. Heintz and W.F. Walker of Rochester Institute of Technology deals with methods for measuring the electrical properties of composite materials in the range 30 MHz to 1 GHz. They have devised a method for measuring the conductivity which is independent of contacts. This method is still being tested.

1.1.4 Section 4

Section 4 by J.L. Allen of the University of South Florida deals with the theory of shielding effectiveness. Equations are presented relating various shielding effectiveness results and methods. In particular, the surface transfer impedance is related to the conductivity of a material.

An interesting model is developed for anisotropic multi-layer materials in section 4.4.

A fold-out table of symbols is located at the end of this section.

1.1.5 Section 5

Section 5 by A.T. Adams of Syracuse University is concerned with the application of the method of moments to nonperfectly conducting materials - particularly to composite materials.

Those already familiar with the method of moments and electromagnetic compatibility may want to skip over section 5.1.

A fold-out table of symbols is provided at the end of this section.

1.1.6 Section 6

Section 6 by Captain John E. Erickson and Lt Colonel Oscar D. Graham of the USAF Academy presents most of the data from a report (1-2) to be published by the same authors. The discussion presented here is minimal. The reader is referred to the complete report for more information.

1.2 BACKGROUND

Composite materials in the form of fiber-reinforced matrix materials (e.g., graphite/epoxy) have found steadily increasing use in structural and surface components in modern aircraft. This growth has proceeded over the past decade from limited use in control surfaces to the formation of major fuselage and wing sections. The impetus behind this transition has been the markedly improved strength-to-weight ratio of these composite materials. This trend is expected to continue.

Along with the increased usage of composite materials came the realization that the electrical properties were relatively unknown and would present a new challenge to the electromagnetic compatibility (EMC) engineer.

The IAP was developed as an EMC analysis tool for use by the USAF Products Divisions, Logistic Command and their prime contractors. In its present form it cannot deal with composite materials.

Several earlier studies (1-3, 1-4, 1-5) were felt to be insufficient to completely satisfy the needs of the IAP. Therefore in 1975 a study was initiated by RADC through the Post-Doctoral program. The results of this study (1-6) led to the work described in this report. Further work is planned to integrate the capability to deal with composite materials or other anisotropic poorly conducting materials into the IAP.

3.0 VALUABLE REFERENCE

Additional results which both complement and supplement the results presented in this report are given in a report [1-7] just released.

REFERENCES

- 1-1 J. Birken, Electromagnetic Properties and Effects of Advanced Composite Materials: Measurement and Modeling, Vol. II, NAVAIR Report 520-1, late 1978.
- 1-2 Capt John E. Erickson, Lt. Col. Oscar D. Graham, Maj Jerry D. McCannon, Capt Michael J. O'Brien, Performance of Graphite/Epoxy as an Antenne Ground Plane, To be published by the U.S. Air Force Academy, CO.
- 1-3 D. Strawe, L. Piszkes, Interaction of Advanced Composites with Electromagnetic Pulse (EMP) Environment, AFML-TR-75-141, September 1975, (AD-D011927).
- 1-4 D.G. Kim, G.A. DuBro, and R.C. Beavin, Measurement of Advanced Composite Materials Shielding Effectiveness, AFFDL-TR-74-30, June 1974.
- 1-5 C.D. Skouby, Electromagnetic Effects of Advanced Composite Materials, Final Report on Contract N 00014-74-C-0200, January 1975.
- 1-6 W.F. Walker, et. al., A Technology Plan for Electromagnetic Characteristics of Advanced Composites, RADC TR-76-206, July 1976.
- 1-7 R. Force, P. Geren, D. Strawe, and A. Schmidt, Investigation of Effects of Electromagnetic Energy on Advanced Composite Aircraft Structures and Their Associated Avionic/Electrical Equipment, Boeing Report D-180-20186-4 Volume 1, Final Report on Navy Contract N 00019-76-C-0497, draft date September 1977.

2.0 MEASUREMENT OF THE ELECTRICAL PROPERTIES OF ADVANCED COMPOSITES IN THE FREQUENCY RANGE OF DC TO 30 MHZ.

2.1 SUMMARY OF PROGRESS TO DATE

This section of the report concerns procedures and results involving the measurement of the intrinsic electrical parameters (conductivity σ , permittivity ϵ and permeability μ) of advanced composite materials over the frequency range of DC to 50 MHz. The work was carried out from October 1, 1976 to September 30, 1977, in the Department of Electrical Engineering of the University of Notre Dame.

2.1.1 Permeability of Advanced Composite Materials

Permeabilities of representative samples of graphite/epoxy, boron/epoxy and Kevlar/epoxy were determined at DC and 60 Hz by measuring sample weight changes as a function of magnetic field. Permeabilities were also measured at 100 Hz using a vibrating sample magnetometer.

All three materials were weakly diamagnetic with magnetic susceptibilities on the order of -10^{-7} . The low frequency permeabilities of these materials are essentially equal to that of free space.

2.1.2 Permittivity of Advanced Composite Materials

Permittivities of representative samples of boron/epoxy and Kevlar/epoxy were determined by measuring the capacitance of rectangular slabs using bridges over the frequency range of 10 kHz to 50 MHz. The relative permittivities were 5.6 for boron/epoxy and 3.6 for Kevlar/epoxy.

A similar approach with graphite/epoxy failed to produce useful results because of the high conductance associated with the samples. The impedance of the samples was essentially resistive even at 30 MHz. It was concluded that the permittivity of graphite/epoxy is indeterminate over the frequency band investigated.

2.1.3 Conductivity of Advanced Composite Materials

Representative conductivities were measured using two-point techniques. A known current was injected across one face of a rectangular sample and extracted from the opposite face.

For graphite/epoxy, conductivities ranged from 10^2 to $2(10^4)$ mhos/m, while boron/epoxy displayed conductivities from $2(10^{-8})$ to 30 mhos/m. The larger values are associated with current parallel to fibers in unidirectional samples while the lower values are found when current is orthogonal to the fiber axis. The conductivities of non-unidirectional samples fall between these bounds.

The conductivity of Kevlar/epoxy was 10^{-9} mhos/m. and showed no geometric anisotropy.

2.2 GOALS AND OBJECTIVES

Although Section 2.1 summarizes the major results of the low frequency (DC to 30 MHz) measurements, this section examines the goals and objectives of the research program in detail. The general objective is the development of techniques and experimental fixtures for the measurement of the intrinsic electrical properties (conductivity, permittivity and permeability) of representative samples of advanced composite material panels of the types to be used as aircraft surfaces. In addition, techniques and experimental fixtures are to be developed to allow measurements of the intrinsic parameters of the individual fibers and slabs of the binding matrix. The frequency range examined is DC to 30 MHz.

The techniques and fixtures are to be designed to accommodate the following ranges of variables. The excitation levels extend from low level, where the sample shows a linear current-voltage characteristic, to that high level which causes irreversible electrical breakdown of the sample. The measurements are to be performed over a broad range of independently varying temperature and relative humidity. The samples include single-ply boron/epoxy and graphite/epoxy; multiple-ply configurations of these materials and Kevlar/epoxy in a variety of commonly used lay-up patterns; and individual fibers and individual slabs of the binding materials.

It is to be determined what experimental techniques for inhomogeneous and/or anisotropic materials are necessary. Appropriate experimental techniques are to be developed to accommodate the range of variables outlined above.

In conjunction with the development of the experimental approaches, analytical derivations are to be used to justify the measurement techniques and the data obtained from their use. In addition, analytical expressions are to be developed to predict intrinsic parameters as a function of frequency, temperature and relative humidity from a limited set of experimental measurements and to predict the intrinsic parameters of advanced composite samples in arbitrary lay-up configurations, given the intrinsic parameters of the individual fibers and individual slabs of binding matrix as functions of frequency, temperature and relative humidity.

This task includes the development of suitable sample preparation methods to allow effective and reliable coupling of excitation and response sensors to the advanced composite material samples. The full development of the measurement techniques necessarily involves the specification of the sample preparation methods.

Of the goals presented above, work has been initiated in all areas except the effects of relative humidity. A simple set of experiments in which samples are immersed in water for extended periods and effects upon electrical conductivity are noted was completed and is discussed in Section 2.9.

2.3 SAMPLE TYPES AND SAMPLE PREPARATION

2.3.1 Materials

Many advanced composites exist but the work in this program has been restricted to materials which are widely used in defense systems. In particular, three types of graphite/epoxy were examined: Hercules 3501, Narmco 5208 and Narmco 5213. The Hercules fibers were type AS while both Narmco materials were reinforced with Thornel T300 fibers. The boron/epoxy was provided by Avco (type 5505). Detailed manufacturer specifications of the Kevlar/epoxy samples are not known.

2.3.2 Lay-Up Procedures

The multiple-ply, unidirectional samples of Narmco 5213 were laid-up and cured by Narmco personnel. Other multiple-ply samples were laid-up from pre-preg tapes by the principal investigator, either at the Composites Facility of the Air Force Flight Dynamics Laboratory at Wright-Patterson Air Force Base or at the University of Notre Dame. Normal composite handling procedures were followed. Rubber gloves were worn during the handling and curing of the tapes and care was taken to insure a clean working environment. The samples were then individually wrapped in storage bags and placed in a freezer in the Composite Materials Facility to await an autoclave run.

2.3.3 Curing

All samples (other than those of Narmco 5213) were cured in autoclaves in the Flight Dynamics Laboratory. The specifications for pressure, temperature and time given by the various manufacturers were followed in all cases. This information is available from the manufacturers and is not included here. The thicknesses of the cured plies closely approached the nominal values suggested by the manufacturers. For example, the Hercules 3501 panels had a median ply thickness of 0.013 cm. (0.005 in.) A total of 38 samples were fabricated as detailed in Table 2-1. The Narmco 5213 samples are not included but are identified separately in the following sections.

2.3.4 Electrical Contact Formation

The basic difficulty in making electrical measurements, especially of conductivity, using composite materials involves the ill-defined nature of the samples. In particular, the lack of a standardized sample caused concern. A typical composite part is produced by stacking a series of pre-preg tapes, followed by a curing process which involves elevated temperatures and pressures. Each manufacturer makes detailed recommendations regarding the proper procedures to be used in curing the tapes. These processes often result in the formation of epoxy-rich layers at the sample surfaces. These layers are quite evident in some samples, although they are different for different materials and curing procedures. The type of bleeder cloths used to remove excess resin during the curing also affects the nature of these layers.

Identification	Plies- Material	Lay-up Orientation	Identification	Plies- Material	Lay-up Orientation
A	10-B	u	16	5-H	[0 45 90] _S
B	3-N	[0 90 0] _T	17	5-N	[0 45 90] _S
C	4-N	u	18	6-N	[0 0 90 0 0] _T
D	4-H	u	19	7-N	[0 45 -45 90] _S
E	4-B	u	20	7-H	[0 45 -45 90] _S
1	1-N	u	21	9-H	[0 45 -45 0 90] _S
2	20-B	u	22	9-N	[0 45 -45 0 90] _S
3	3-B	[0 90 0] _T	23	11-H	[0 45 -45 0 90 90] _S
4	9-B	[0 0 90 90 0] _S	24	11-N	[0 45 -45 0 90 90] _S
5	2-B	u	25	15-H	[0 90 0 45 -45 45 -45 90] _S
6	4-B	[0 90 90 0] _T	26	16-N	u
7	5-B	[0 90 0] _S	27	1-H	u
8	5-B	u	28	1-H	u
9	17-B	u	29	2-H	u
10	destroyed	u	30	10-H	u
11	3-N	[0 90 0] _S	31	6-H	u
12	5-N	[0 90 0 0] _S	32	4-N	u
13	7-N	u	33	6-N	u
14	10-N	[0 90] _S			
15	3-H				

NOTATION

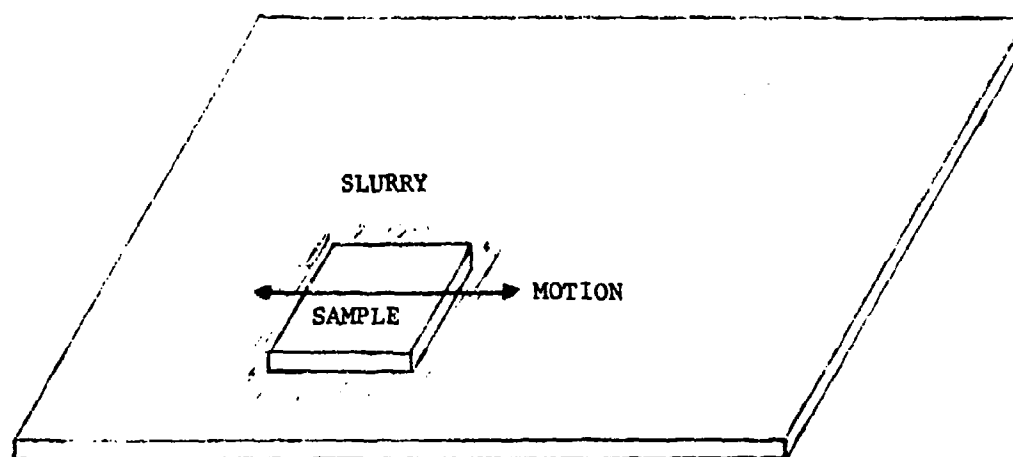
B: Avco Boron/Epoxy
H: Hercules 3501 Graphite/Epoxy
N: Narmco 5208 Graphite/Epoxy
u: Unidirectional
T: total ply lay-up sequence is given
S: right ply is regarded as a mirror, e.g., [0 90 0]_S = [0 90 0 90 0]_T

SAMPLES CURED AT FLIGHT DYNAMICS LABORATORY

TABLE 2-1

From a conceptual viewpoint, a graphite/epoxy composite consists of graphite fibers embedded in an epoxy matrix and the most satisfying model of such a solid involves a repetition of this basic structure from surface-to-surface through the thickness of the sample. This means that the presence of an epoxy-rich surface layer is at variance with the intrinsic bulk properties of a graphite/epoxy sample. The proper measurement of the intrinsic bulk electrical properties, in particular, the accurate measurement of the conductivity of graphite/epoxy, depends upon a careful removal of this surface layer.

The epoxy-rich surface layers were removed by abrading the top and bottom surfaces of the samples. A glass plate was coated with diamond paste (0.04 μm particle size) and the sample rubbed across the surface in a "sanding" motion (Figure 2-1). The samples were periodically removed and rinsed in distilled water to allow inspection of the abraded surface. The removal of the



ABRADING OF EPOXY RICH LAYERS

FIGURE 2-1

resin-rich layer is accompanied by a notable dulling of the surface as the optical reflectivity is decreased. With both surfaces properly abraded, a radio frequency bridge cannot be balanced with the composite connected across its measurement terminals. This is a consequence of the high conductivity displayed by the graphite/epoxy. For samples with cross-sectional areas of a few square centimeters and thicknesses up to 0.4 cm., this method has been successful in detecting the removal of the epoxy. The measurements are made simply by sandwiching the composite between two aluminum plates which are then connected to the bridge.

The resin-rich layer problem only arises in making measurements which involve current flow across surfaces which were part of the original surface of the cured sample. In cases in which a small section is cut from the interior of the lay-up, current flowing in the plane of the sample will not cross

a resin-rich surface and no difficulties occur.

It is important to recognize that resin-rich layers are of no concern in composites composed of insulating fibers or of fibers which do not touch. Of the materials investigated in this work, Kevlar/epoxy is in the former category while boron/epoxy is in the latter.

The surface of a composite material presents a problem in making good electrical contact for current-voltage measurements. The presence of epoxy rules out any high temperature method of forming metal contacts. In addition, localized point contacts will not yield valid conductivities because of the presence of broken fibers (especially in graphite/epoxy). Figure 2-2 shows such fibers in a sample of Narmco 5213.



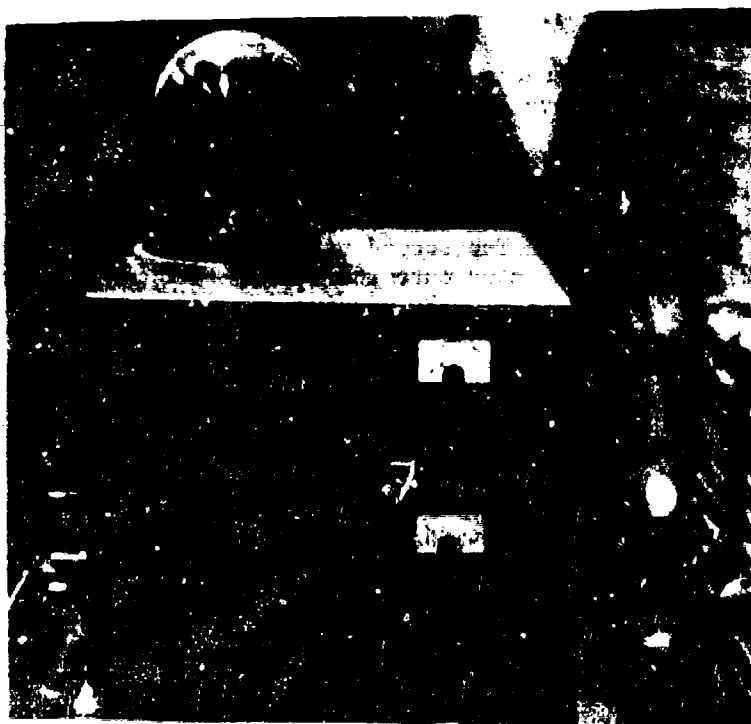
40X

BROKEN FIBERS IN NARMCO 5213

FIGURE 2-2

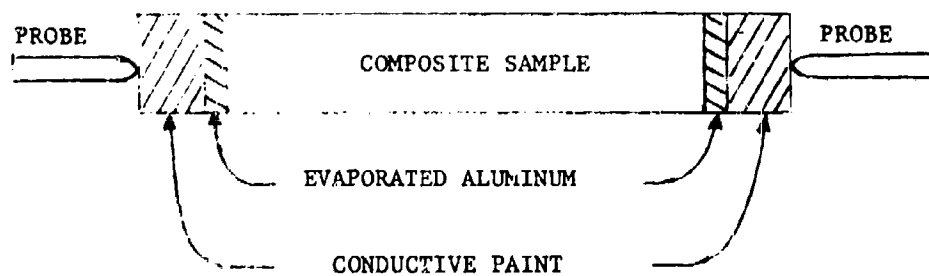
With these factors in mind, a number of methods of contacting composite samples was investigated. The most successful was the vacuum evaporation of aluminum films onto the composite surfaces. The evaporation apparatus is shown in Figure 2-3. Aluminum wire (99.99% pure) was etched in dilute NaOH, rinsed in distilled water and methanol. The aluminum wire was loaded into a tungsten boat for subsequent evaporation. The composite samples were placed on quartz chimneys above the boat and the system evacuated to a pressure of $2(10^{-4})$ torr. The aluminum was then deposited by passing current through the tungsten.

The aluminum adhered well, but the evaporated films were necessarily thin



VACUUM SYSTEM

FIGURE 2-3



SKETCH OF CONTACT FORMATION

FIGURE 2-4

and were coated with conductive paint to provide a thick "pad" onto which probes could be placed to allow connection of the measurement apparatus (Figure 2-4).

The resultant contacts displayed ohmic behavior. The current-voltage characteristics were linear and the slope was independent of polarity.

Because the procedure of contact formation is time-consuming, two alternatives were investigated. The first involved the rubbing of indium onto the sample surfaces and the application of conductive silver paint over the rubbed indium. The second utilized a conductive epoxy (Able-bond 36-2) which was painted onto the sample surfaces and then cured at a temperature of 150°C for 60-90 minutes.

Of these methods, only the rubbed indium approach proved ineffective. These contacts displayed an aging phenomenon in which they degrade with time and yield non-reproducible data. The conductive epoxy method has been used in the bulk of this work.

In nearly all cases, the samples were chemically cleaned prior to contact formation. The process consisted of ultrasonic agitation in trichlorethylene, followed by rinses in acetone and methanol and drying in a purified nitrogen stream. All chemicals were reagent grade. Once the samples were cleaned, the contacts were applied using the procedures detailed above. Although careful cleaning was observed through most of this work, a few samples were prepared by simply rinsing the samples in water and methanol after the removal of the epoxy-rich layers. The conductivities were independent of the cleaning procedure.

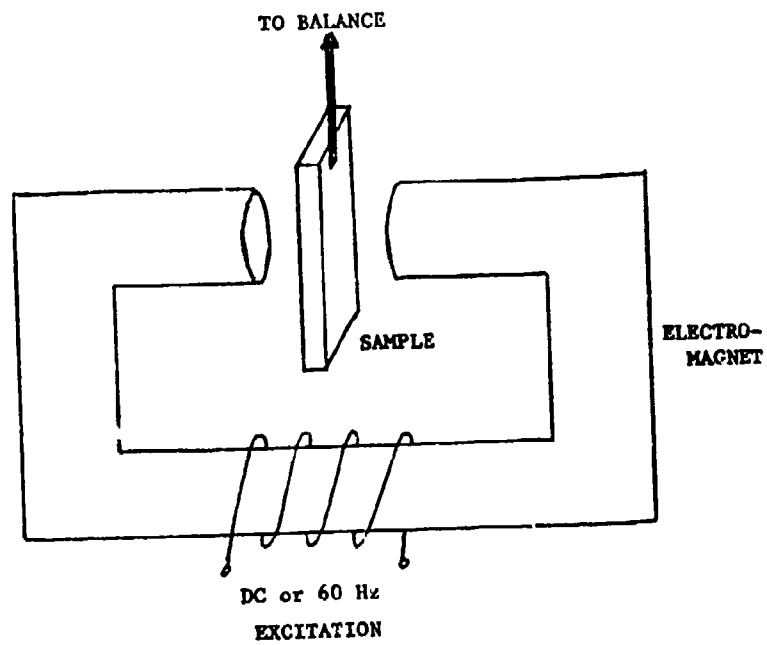
The autoclave-cured specimens were too large for convenient laboratory handling and smaller samples were cut using either an abrasive slurry string saw or a diamond wheel circular saw. The samples used for measurements below 5 MHz were in the form of rectangular slabs (cross-sectional areas approximately 2. x 4. cm. (0.8 by 1.6 in.) and varying thickness). Above 5 MHz, samples were posts with lengths on the order of 10 cm. (4 in.) and cross-sectional areas on the order of 4mm² (.006 in.²).

2.4 MEASUREMENT TECHNIQUES

2.4.1 Permeability

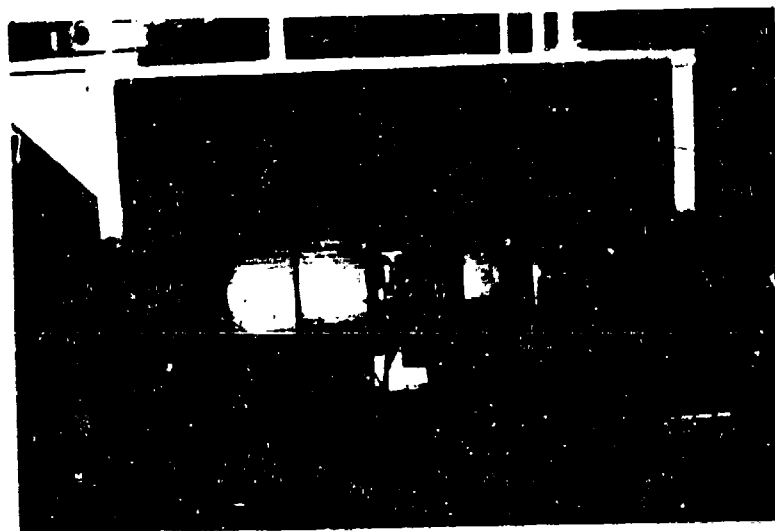
An ASTM standard method²⁻¹ was used to determine the DC permeability of graphite/epoxy, boron/epoxy and Kevlar/epoxy. Slabs of each material were prepared with lengths of 10 cm. (3.9 in.), widths of 0.8 cm. (0.3 in.) and thicknesses of 0.15 cm. (0.06 in.). The end of the slab was cemented (Eastman 910) to a metal weight holder which was attached to a balance with a sensitivity of 0.1 mg.

The sample was placed between a pair of magnetic poles with a 2 by 4 cm. (0.8 by 1.6 in.) area and a spacing of 2 cm. (0.8 in.). The apparatus is sketched in Figure 2-5. The maximum flux density was 0.8 Wb/m².



PERMEABILITY MEASUREMENT

FIGURE 2-5



VIBRATING SAMPLE MAGNETOMETER

FIGURE 2-6

The sample is weighed; a magnetic field H (in oersteds) is applied and the sample reweighed. The difference in weight is the magnetic force F (in mg). The material permeability is

$$\mu = \mu_0 \left[1 + \frac{24.6F}{AH^2} \right] \text{ henries/meter}$$

where A (in cm²) is the area of the pole pieces and μ_0 is the permeability of free space. The measurements were made on both Narmco and Hercules graphite/epoxy, Avco boron/epoxy and Kevlar/epoxy. Both DC and 60 Hz magnetic fields were used in determining μ .

With the balance sensitivity cited above, an upper bound (2.1) of 0.0001 can be placed on the term $24.6F/AH^2$ if no magnetic force F is observed. In such a case, the conclusion is that the sample permeability μ is equal to the permeability of free space to within one part in 10,000.

A vibrating sample magnetometer (Figure 2-6) was used to determine permeability at 100 Hz. To reduce the geometric anisotropy, cube-shaped samples of the materials of interest were prepared. Results are presented in Section 2.6.1.

Since there is no reason to expect that the permeability of these materials will be significantly different from that of free space, techniques for measuring permeabilities at high frequency were not developed.

2.4.2 Permittivity

The standard method used to measure this property involves fabricating a composite material capacitor by placing a sample between two metal electrodes and measuring the resistance and capacitance exhibited by the resulting structure. An effective conductivity and permittivity may be calculated from the measured values R and C via the formulas

$$R = \frac{L}{\sigma A} \qquad C = \frac{\epsilon A}{L}$$

$$\text{or} \qquad \sigma = \frac{L}{RA} \qquad \epsilon = \frac{CL}{A}$$

where L is the sample length and A the cross-sectional area.

This method worked well with boron/epoxy and Kevlar/epoxy but failed, for fundamental reasons, with graphite/epoxy. As will be discussed in Section 2.6.2, it is unlikely that any experiment will allow a determination of the permittivity of graphite/epoxy over the frequency range of DC to 30 MHz.

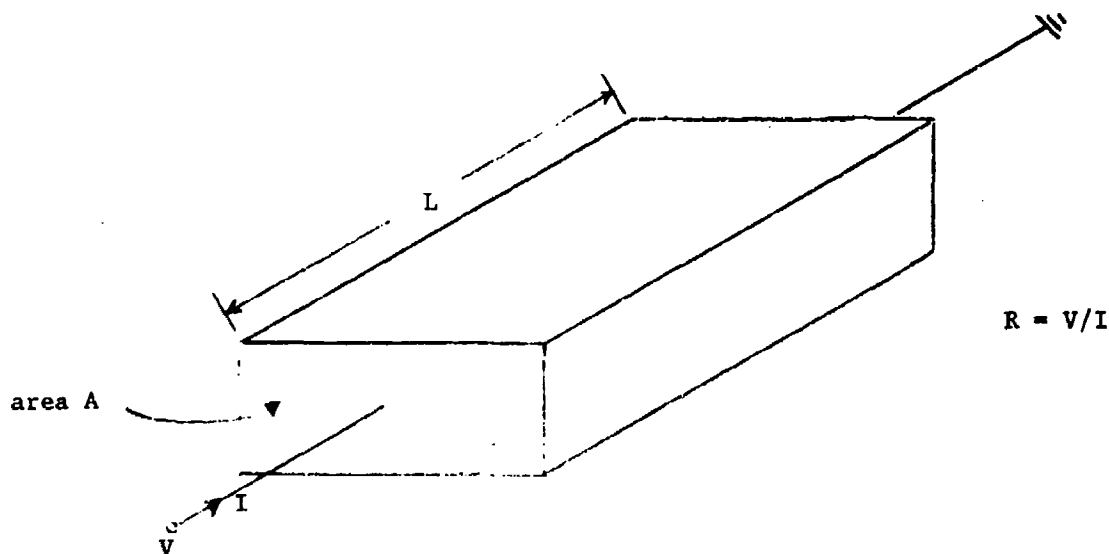
2.4.3 Conductivity

Two methods of measuring the low frequency, low excitation level conductivities of materials have received widespread support and use. These

are specified by the American Society for Testing and Materials and are known as the two-point and four-point probe techniques.²⁻² The two-point probe method is the most precise for determining electrical conductivities. In this method, ohmic contacts are attached to the ends of a rectangular cross-section sample of the material of interest. A known, fixed current is passed through the sample via the contacts and the associated voltage drop across the sample is measured. The ratio of voltage to current defines a sample resistance R and an effective sample conductivity is determined by

$$\sigma = \frac{L}{RA}$$

where L is the sample length between the contacts and A the cross-sectional area as shown in Figure 2-7. This result requires a uniform distribution of current across the area A and a homogeneous material if the measured conductivity is to equal the local conductivity. The contact resistance must also be negligibly small when compared with the sample resistance. In the case of a multiple-ply composite the assumption of



TWO-POINT CONDUCTIVITY MEASUREMENT

FIGURE 2-7

homogeneity is not valid, but the measured value of conductivity is a useful measure of the current-carrying capability of the sample. The technique is quite simple in concept and interpretation and has been successfully used in this work from DC to 50 MHz.

The four-point probe method was not used because it involves contacts to the sample surface and has been developed for isotropic materials.

There are, in addition, significant theoretical difficulties in interpreting the results of four-point probe measurements on anisotropic, inhomogeneous materials.

The measurement of non-linear, high-level excitation effects can also be easily made by means of a two-point probe configuration. This is done by simply increasing the excitation levels until deviations from a linear current-voltage characteristic are observed. The results of these investigations are reported in Sections 2.6.3 and 2.6.4.

2.5 PROPERTIES OF CONSTITUENTS

2.5.1 Electrical Properties of Fibers

The electrical conductivities of graphite and boron fibers were studied in detail and the results of this work have been reported elsewhere.²⁻³ These results are summarized here.

The graphite fibers may be accurately characterized as good conductors. For this reason their relative permittivity cannot be measured in the range of frequencies of interest. The conduction current is always much larger than the displacement current in any measurement situation. In addition, it is known that graphite is a non-magnetic material. The relative permeability of these fibers is unity. For these reasons, the investigations have focused on the fiber conductivity. Fiber tows were cleaned by immersion in solvents, and individual fibers were mounted on pre-cleaned microscope slides for subsequent investigation. This mounting was accomplished by applying conductive inks to the fiber ends to provide mechanical adhesion and ohmic electrical contact. The current-voltage characteristics were found to be linear over the range of electric fields from zero to 4000 volts/m and the measured conductivities averaged 20,600 mhos/m for a total of 60 different fibers. The results are for Thorne T300 fibers, and all reported values were made at DC. It was verified that the low frequency conductivities are independent of frequency by exciting fibers using a step generator and finding no differences in measured conductivities associated with the higher frequency components of the excitation.

Boron fibers are much larger and easier to handle than graphite fibers. In particular, individual graphite fibers have diameters on the order of $7(10^{-4})$ cm., while boron fibers have diameters of $2(10^{-2})$ cm. While larger, the boron fibers are significantly more difficult to contact electrically. The use of conductive silver paint was investigated as well as indium. In both situations it was found that the electrical characteristics displayed by the boron fibers were non-linear.

It is important to recognize that boron fibers consist of two well-defined separate components; the first being a core with a diameter of $1.8(10^{-3})$ cm. which is composed of WB_4 and W_2B_5 , the other being the boron sheath itself. No elemental tungsten remains in the core after boron growth.²⁻⁴ The difficulty in making electrical contact occurs in attempting to contact only the boron without touching the central core of tungsten

borides. This problem was finally solved by plating nickel onto the boron sheaths.²⁻³ This procedure results in excellent, reproducible, linear current-voltage characteristics.

By making measurements in which the nickel plating contacts the core, as well as measurements in which it does not, the following values for conductivity were determined.

$$\sigma_{\text{core}} = 3(10^5) \text{ mhos/m.}$$

$$\sigma_{\text{Boron}} = 0.19 \text{ mhos/m.}$$

The electrical conductivity of boron fibers is thus seen to be highly anisotropic. For current along the fiber axis, the local conductivity is more than six orders of magnitude greater than that associated with current perpendicular to the fiber axis.

The fiber conductivity σ_f is defined by the equation

$$\begin{aligned} G_{\text{fiber}} &= G_{\text{core}} + G_{\text{Boron}} \\ &= \frac{\sigma_c A_c}{l} + \frac{\sigma_B A_B}{l} = \frac{\sigma_f A_f}{l} \end{aligned}$$

where σ_c , σ_B , σ_f are the core, boron, fiber conductivities,

A_c , A_B , A_f , the core, boron and fiber areas and

l is the fiber length.

Solving for σ_f yields

$$\sigma_f = \sigma_c \left(\frac{A_c}{A_f} \right) + \sigma_B \left(\frac{A_B}{A_f} \right).$$

Substituting the values given above results in

$$\sigma_f = 2.4(10^3) \text{ mhos/meter.}$$

2.5.2 Electrical Properties of Epoxies

Samples of uncured epoxy resins were obtained from the manufacturers of graphite/epoxy (Narmco and Hercules) and boron/epoxy (Avco). In order to characterize the epoxies electrically, they were heated until they flowed and were cast into rectangular slabs. These slabs were then cured following temperature-time cycles identical to those used for the autoclave processing of the associated tapes. No pressure was applied however. The cured slabs of epoxy were placed between aluminum electrodes and their equivalent resistance and capacitance were measured at a frequency of 1 MHz. Measurements of the sample impedance at other frequencies over the range of interest indicate that the conductivity and permittivity

of these materials is independent of frequency. Although there is some variation between the various types of epoxy, the following numbers are representative of the electrical properties.

$$\epsilon_R = 3.4$$

$$\sigma \leq 6(10^{-8}) \text{ mhos/m}$$

It is important to recognize the large difference between the fiber conductivities and those of the epoxy matrix. While the epoxy matrix may be classed as an excellent insulator, the graphite and boron fibers are both imperfect conductors.

2.6 MEASURED ELECTRICAL PROPERTIES OF ADVANCED COMPOSITES

2.6.1 Permeability

The results of the permeability investigations were in accordance with expectations. The sample weighing experiments indicated that the relative permeabilities of samples of graphite/epoxy, boron/epoxy and Kevlar/epoxy were all unity to within 1 part per thousand at DC and 60 Hz.

The vibrating sample magnetometer (Department of Metallurgical Engineering and Materials Science) has significantly better resolution than the sample weighing technique. These measurements indicated that all three materials are weakly diamagnetic at 100 Hz and have relative susceptibilities on the order of -10^{-7} . The permeabilities of the materials may be written as

$$\mu = \mu_0(1 + \chi_m)$$

where $\chi_m \approx -10^{-7}$

In view of these results, it can be assumed that these three advanced composite materials essentially have the permeability of free space with no significant loss in model accuracy. No further investigations of magnetic properties of these materials are envisioned.

2.6.2 Permittivity

To begin a discussion of the permittivity of graphite/epoxy, it is helpful to start with the sinusoidal steady state form of Maxwell's Equations.

$$\nabla \times \vec{H} = (\sigma + j\omega\epsilon)\vec{E}$$

In this equation, the conductivity and permittivity are shown to be linked together. In any physical situation the conduction and displacement currents will flow through the medium and their relative magnitudes will depend upon the relative values of conductivity σ and $\omega\epsilon$. Anticipating the results of later sections, the conductivity of graphite/epoxy was seen to be between 10^2 and 10^4 mhos/m. At the maximum frequency (50 MHz)

investigated in this work, the radian frequency has a value of $3.14 (10^8) \text{ sec}^{-1}$. In order for the product $\omega\epsilon$ to be comparable to the conductivity,

$$10^2 \approx 3(10^8)\epsilon$$

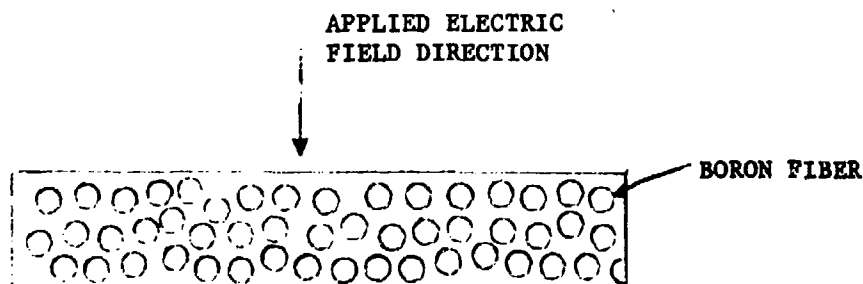
or $\epsilon \approx 3(10^{-7}) \text{ f/m}$

or $\epsilon_R = \epsilon/\epsilon_0 \approx 38000.$

Since the epoxy matrix has a relative dielectric constant on the order of three and it is difficult to conceive any artificial dielectric effects of sufficient strength to increase the relative dielectric constant by four orders of magnitude, it is found that the permittivity of graphite/epoxy is essentially unmeasurable by any low frequency technique. In the sense that the low frequency permittivities of metals are indeterminate, the same conclusion is valid for the relative permittivity of graphite/epoxy. In order to consistently measure a permittivity, it is necessary that the capacitive reactance be comparable to the resistance. Such will not be the case for graphite/epoxy until the excitation frequencies are on the order of 10^{12} Hz .

Kevlar/epoxy is a good insulator and the measurement of its relative permittivity poses no difficulty at the frequencies of interest. The relative permittivity is a constant value of 3.6 over a frequency range from 10 kHz to 50 MHz.

The case of boron/epoxy is intermediate between that of graphite/epoxy and Kevlar. The only measurements made of permittivity for this material involved a geometry in which the excitation fields were normal to the axes of the fibers. In short, cross-plane geometries were investigated, in which the fibers lie in the plane as sketched in Figure 2-8. In these cases, the relative permittivity is also independent of frequency from 10 kHz to 50 MHz and has a value of 5.6. It is expected that similar values of permittivity will be measured in cross-plane situations



CROSS PLANE MEASUREMENTS ON BORON/EPOXY

FIGURE 2-8

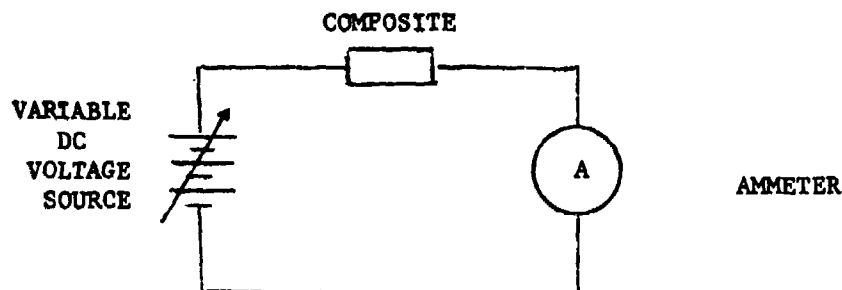
in which the electrodes are parallel to the fiber axis. Of course, in the orthogonal situation in which the electrodes contact opposite ends of continuous fibers, the large resultant effective conductivity will make a measurement of permittivity impossible.

2.6.3 DC Conductivity

In this subsection, the values of DC conductivity measured for the three classes of composite materials of interest are reported. The use of a separate section for these data is intended to point out the relatively large concentration on the frequency response of graphite/epoxy (Section 2.7). It can be seen that relatively few experimental measurements of the frequency responses of Kevlar and boron/epoxy were made. Some Kevlar/epoxy and boron/epoxy samples have been examined from DC to 50 MHz. The preliminary conclusion is that the conductivities and relative permittivities are independent of frequency over this range. Additional measurements and modeling must be done to adequately buttress this conclusion.

DC conductivities were measured by a simple series combination of a DC power supply, electrometer and composite sample (Figure 2-9). The applied voltage and resultant current were measured. Their ratio provides the effective resistance. The effective conductivity is defined using the familiar formula

$$\sigma = \frac{L}{RA}.$$



DC RESISTANCE MEASUREMENTS

FIGURE 2-9

For Kevlar/epoxy, the conductivity is $6(10^{-9})$ mhos/m. This value was independent of direction.

For a seven-ply boron/epoxy sample with the stacking sequence

$$[0 \ 0 \ 0 \ 90]_S,$$

two values of conductivity were measured; σ_0 associated with current in

the direction of the fibers in the six 0 plies and σ_{90} for current orthogonal to the six plies. The resultant conductivities were

$$\sigma_0 = 25 \text{ mhos/m}$$

$$\sigma_{90} = 3.8 \text{ mhos/m.}$$

These values are the effective conductivities for the entire sample and will be further discussed in Section 2.8. It is anticipated that these results would be independent of the exact stacking sequence although no direct confirming experiments have been done.

For unidirectional samples of boron/epoxy, the longitudinal conductivity (associated with current flow in the sample plane and parallel to the fiber axis) and a transverse conductivity (associated with current flow also in the plane of the sample and perpendicular to the fiber axis) were measured. The measured values were

$$\sigma_L = 30 \text{ mhos/m}$$

$$\sigma_T = 2(10^{-8}) \text{ mhos/m.}$$

For current flow through the plane of the sample, conductivities equal to σ_T were measured.

The difference between σ_{90} for the seven-ply [0 0 0 90]₇ sample and σ_T for the unidirectional sample is explained by the presence of the one 90 layer in the former.

The large anisotropy ratio

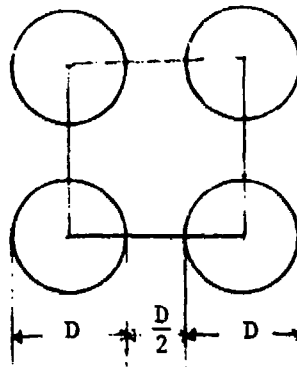
$$\frac{\sigma_L}{\sigma_T} = 1.5(10^9)$$

for boron/epoxy is of interest because it indicates that current flow orthogonal to the fiber axis is controlled by the resistivity of the epoxy matrix. In short, there is not a significant degree of fiber contact present in these samples. Optical micrographs of polished boron/epoxy surfaces also indicate that this is so. The fiber-to-fiber spacing is approximately 1.5D where D is the fiber diameter. This structure is sketched in Figure 2-10. The volume fraction f of fibers is

$$f = \frac{\pi D^2/4}{(1.5)^2 D^2} = .35$$

This expression is derived in Figure 2-10.

In the case of unidirectional graphite/epoxy samples, the anisotropy ratio is found to be significantly lower. Typical longitudinal and transverse conductivity values for graphite/epoxy samples are



$$\text{Area of Square} = (1.5D)^2$$

$$f = \frac{\pi D^2/4}{(1.5D)^2} = 0.35$$

VOLUME FRACTION OF BORON FIBERS

FIGURE 2-10

$$\sigma_L = 2(10^4) \text{ mhos/m}$$

$$\sigma_T = 100 \text{ mhos/m.}$$

As detailed in Section 2.7, precise values differ for samples from different manufacturers but the above are good "ballpark" values.

The anisotropy ratio

$$\frac{\sigma_L}{\sigma_T} = 200$$

indicates that the large epoxy resistance is being shunted by a high degree of fiber-to-fiber contact. Optical micrographs confirm that this is the case.

Preliminary examination of a unidirectional sample of graphite/polyimide obtained from NASA Lewis Research Center indicates that the anisotropy ratio in this material is approximately the same as that of graphite/epoxy. The small diameter nature of the graphite fibers which necessitates their being wound into tows prior to the manufacturing of the pre-preg tape necessarily results in a high degree of fiber contact in cured composite specimens.

2.6.4 High Field Effects

Although the data reported above for graphite/epoxy are for Hercules 3501, the non-linear work was done with some of the first samples of graphite/epoxy received. These were single-ply, unidirectional samples of Narmco 5213 which were cured by the manufacturer. As a consequence, the values of conductivity and the anisotropy ratio differ from those values given in the preceding section. This difference is explained by

the differences in material and curing procedure. Investigations of the non-linear thresholds of Narmco 5208, Hercules 3501, boron/epoxy or Kevlar/epoxy have not yet been made.

The non-linear thresholds for these unidirectional samples were measured using a DC power supply in series with an ammeter and the sample. Again, the current-voltage characteristics were measured in both longitudinal and transverse directions with current flow being confined, in all cases, to the plane of the sample. Results are shown in Figures 2-11 and 2-12 and are summarized in Table 2-2. For current in the longitudinal direction, the characteristic is linear up to a well-defined threshold at which the current begins to increase more rapidly than an extrapolation of the linear response would indicate. The result is precisely the opposite for current in the transverse direction; the current is linear to a threshold and then increases at a rate less than the extrapolation of the linear response. An adequate explanation for the longitudinal response has not been determined. The curve is similar to that of the thermal runaway in a semiconductor but simple thermal models are inadequate and more detailed investigation of this non-linear response is required.

Current Direction	E_{NL} (volts/m)	J_{NL} (amps/m ²)
Longitudinal	250	$4(10^5)$
Transverse	4000	$1(10^4)$

HIGH FIELD NON-LINEAR THRESHOLDS

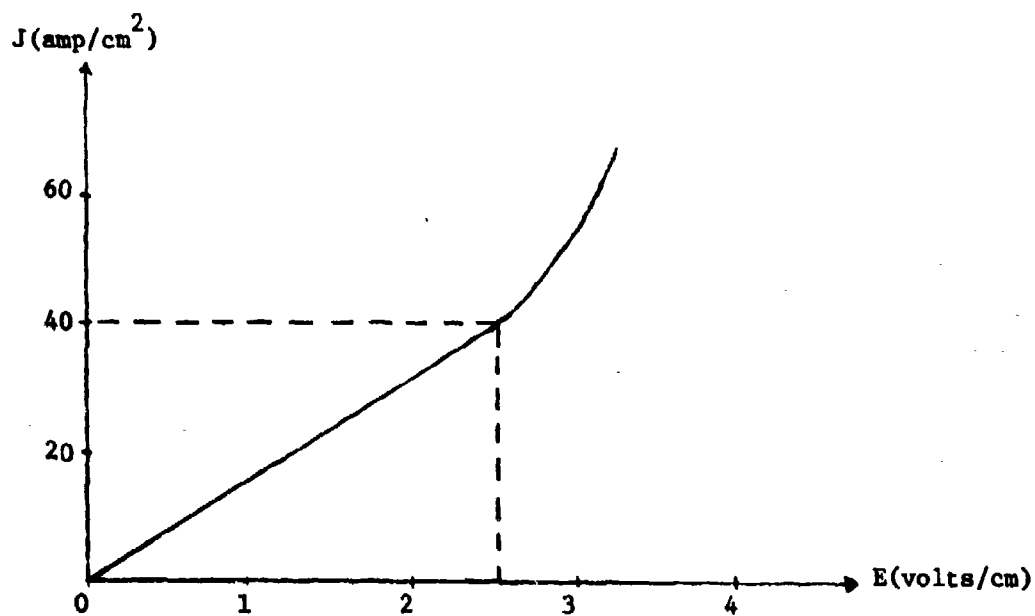
Narmco 5213 Graphite/Epoxy

TABLE 2-2

A plausible explanation of the transverse response can, however, be made. The relatively large value of transverse conductivity can only be explained by a high degree of fiber-to-fiber contact present in graphite/epoxy. As the current density in the transverse direction is increased, local heating occurs which is accompanied by some softening of the epoxy matrix. This results in a sag in the sample with some regions being placed in tension. The fiber-to-fiber contact is reduced and the incremental sample conductance is negative. As a consequence, the current does not increase as rapidly as the linear region response would indicate.

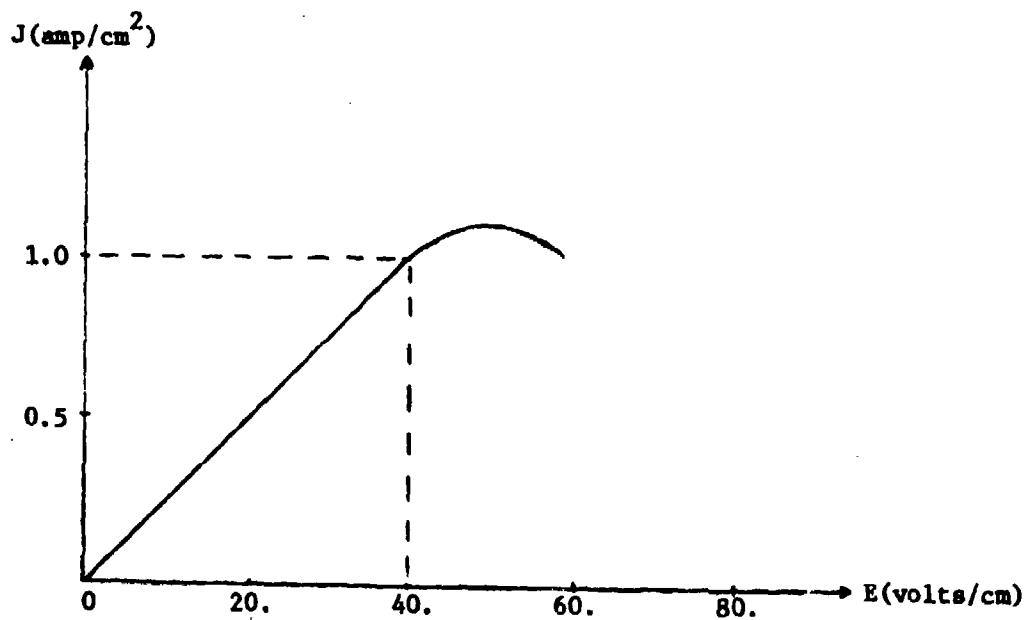
The values of the high field thresholds for electric field and current density are given in Table 2-2.

In order to confirm this contact reduction mechanism as an explanation



LONGITUDINAL CURRENT DENSITY vs. APPLIED FIELD

FIGURE 2-11



TRANSVERSE CURRENT DENSITY vs. APPLIED FIELD

FIGURE 2-12

for the non-linear response with transverse currents, a thermocouple was placed on the surface of a graphite/epoxy sample which was then transversely excited at a current density corresponding to the threshold value. The current remained constant as the surface temperature increased and then displayed a sharp drop when the surface temperature reached 110°C, as is shown in Figure 2-13. This sudden reduction at a surface temperature near that of the epoxy softening temperature indicates that the sample indeed underwent a mechanical change with a resultant local decrease in average fiber contact. The softening effect was observed in less than a minute.

The non-linear responses of other graphite/epoxy types, boron/epoxy and Kevlar/epoxy will be examined in future work.

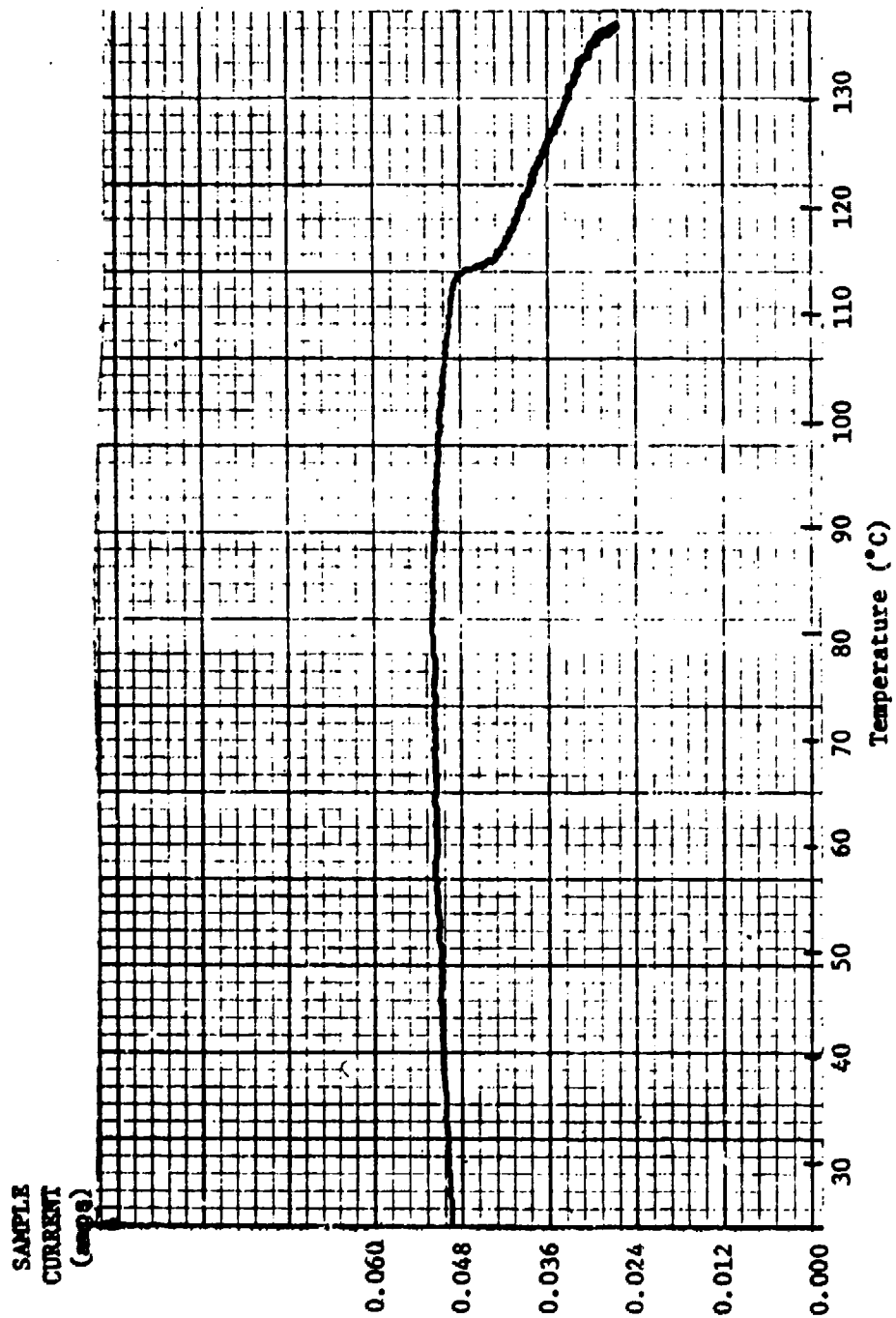
2.6.5 Summary

The results of the permeability, permittivity, DC conductivity and high field thresholds are summarized in Table 2-3. The graphite/epoxy data, although listed in a single column, were taken from different samples. In particular, the DC conductivity is that associated with Hercules 3501. The high field thresholds are those of Narmco 5213.

	<u>Graphite/Epoxy</u>	<u>Boron/Epoxy</u>	<u>Kevlar</u>
Permeability μ_R	1	1	1
Permittivity ϵ_R	Indeterminant	5.6	3.6
DC Conductivity (mhos/m)			
longitudinal σ_L	$2(10^4)$	30	$6(10^{-9})$
transverse σ_T	100	$2(10^{-8})$	$6(10^{-9})$
Anisotropy Ratios (σ_L/σ_T)	200	$1.5(10^9)$	1
High Field Thresholds			
longitudinal			
E_{NL} (volts/m)	250	not	not
J_{NL} (amps/m ²)	$4(10^5)$	measured	measured
tranverse			
E_{NL} (volts/m)	4000	not	not
J_{NL} (amps/m ²)	$1(10^4)$	measured	measured

SUMMARY OF ELECTRICAL PROPERTIES OF MEASURED COMPOSITES

TABLE 2-3



CURRENT vs. TEMPERATURE IN A TRANSVERSE SAMPLE

FIGURE 2-13

Advanced composite materials are seen to be non-magnetic and to range from a good conductor (graphite/epoxy) with an infinite permittivity to a good insulator (Kevlar) with a relative permittivity of 3.6. Boron/epoxy is an intermediate material which is characterized by an extreme anisotropy ratio such that the conductivity in the direction of the fibers is more than nine orders of magnitude greater than the conductivity in a direction across the fibers.

2.7 CONDUCTIVITY - FREQUENCY BEHAVIOR OF GRAPHITE/EPOXY

2.7.1 Measurement Techniques and Results

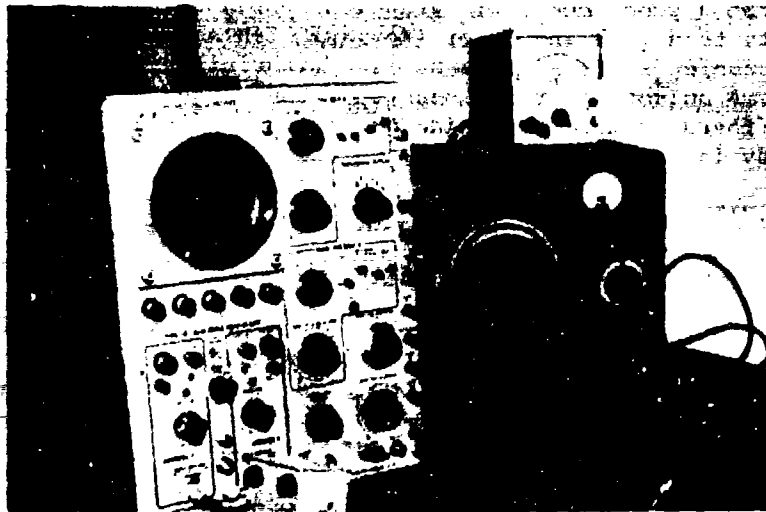
An upper measurement frequency of 50 MHz was chosen in order to allow overlap with the work described in Section 3 of this report. To avoid parasitic coupling, the composite samples and the sampling resistor were placed in a shielded enclosure. Coaxial leads from this enclosure to the measuring instrumentation were allowed to be no longer than 10 cm. The basic equipment consisted of a General Radio 1001-A signal generator with a maximum operating frequency of 50 MHz connected to a series combination of a sampling resistor of fixed value and a narrow post of the composite of interest. The cross-sectional areas of the samples along with their lengths are given in the Figures 2-15 to 2-29 which present the conductivity-frequency results. The fixed, current sampling resistor was, in all cases, selected with resistance comparable to that of the composite sample at low frequencies. The voltages developed across the sampling resistor and the composite sample were fed to a Tektronix 547 oscilloscope with a type 1A1 dual trace plug-in. Figure 2-14 shows the apparatus and sample holder. The amplitudes of the two voltage waveforms were recorded and the sample resistance and conductivity were calculated directly.

$$I = V_1 / R_K \quad R_C = V_2 / I \quad \sigma_C = \frac{L}{R_C A}$$

where V_1 is the voltage across the sampling resistor,
 R_K the value of the sampling resistor,
 V_2 the voltage across the composite post,
 L the composite length,
 A its cross-sectional area and
 σ_C the sample conductivity.

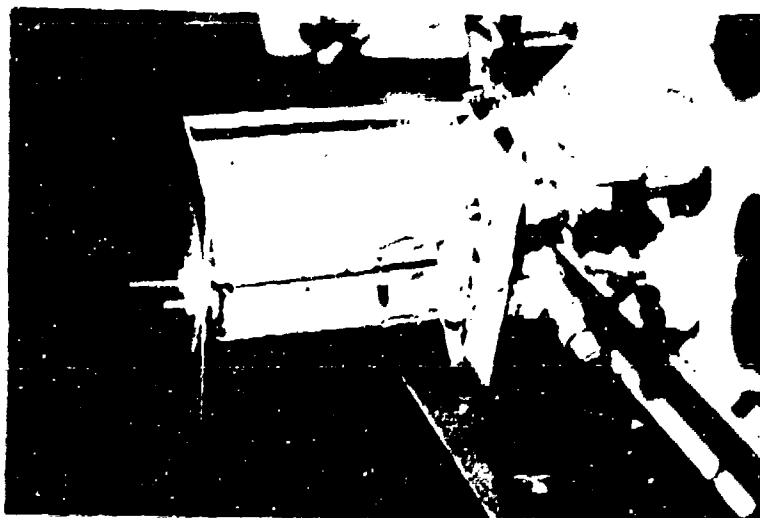
The results of the measurement procedure are shown in Figures 2-15 through 2-29 for a total of ten samples, some of which were excited in two different in-plane directions. This was done by cutting posts out of the same composite lay-up in orthogonal directions. The effective conductivity of graphite/epoxy is independent of frequency over the range DC to 5 MHz.

Above this frequency, there are variations in the effective conductivities. For unidirectional samples excited in the transverse direction



SAMPLE IN SHIELDED METAL BOX
ATTACHED TO THE FRONT OF THE OSCILLOSCOPE

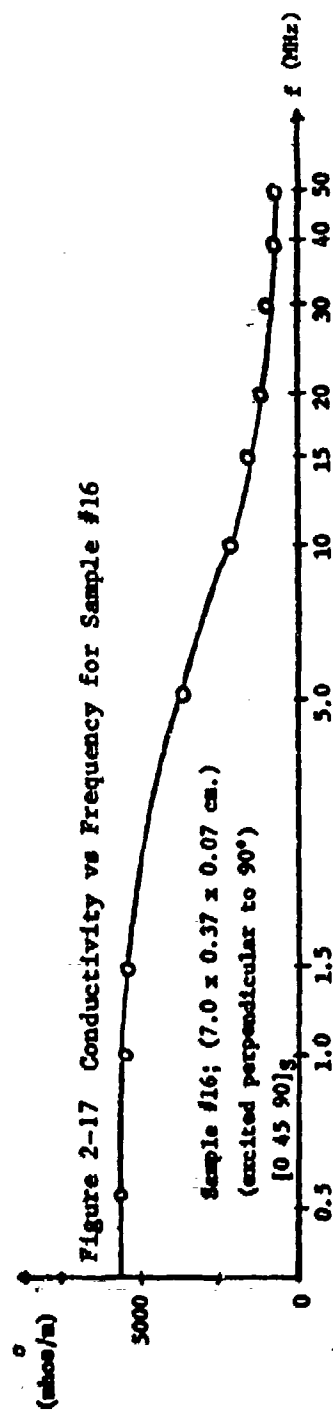
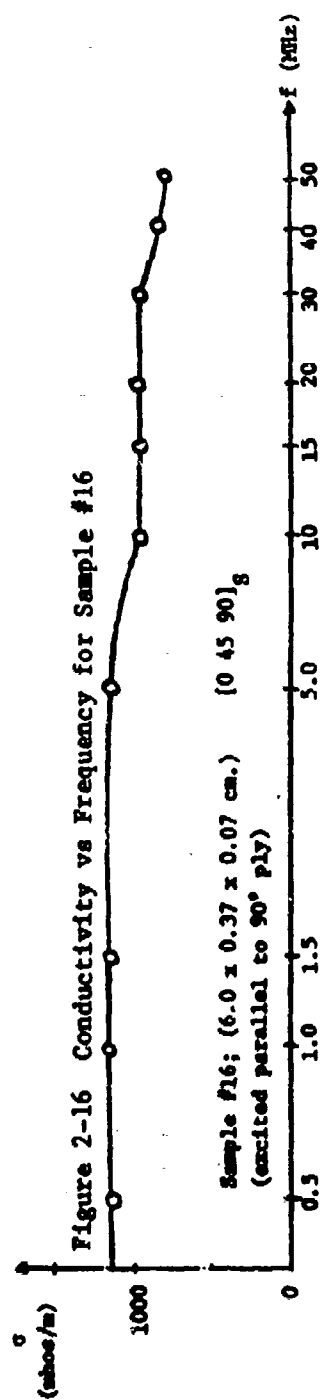
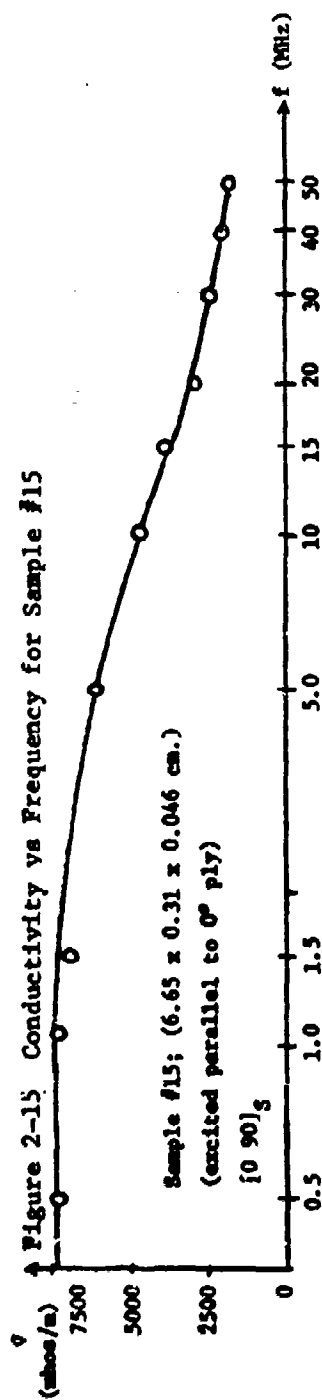
(a)

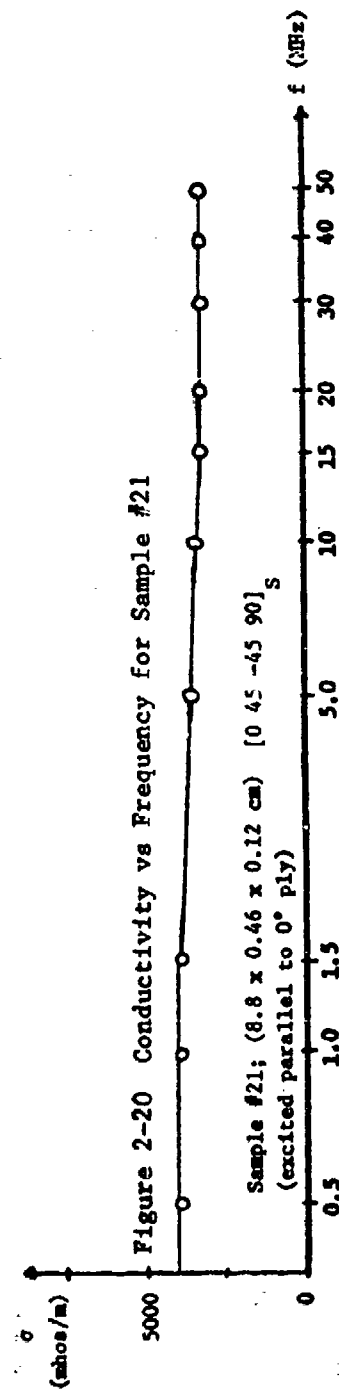
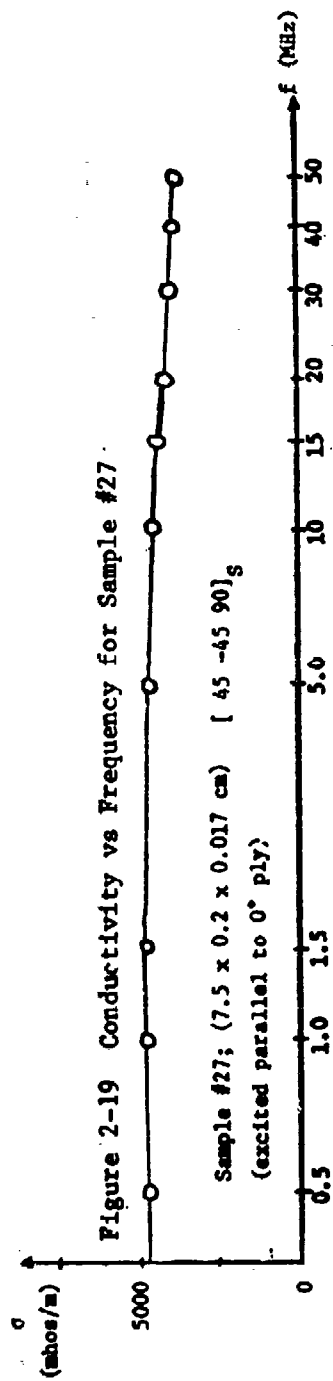
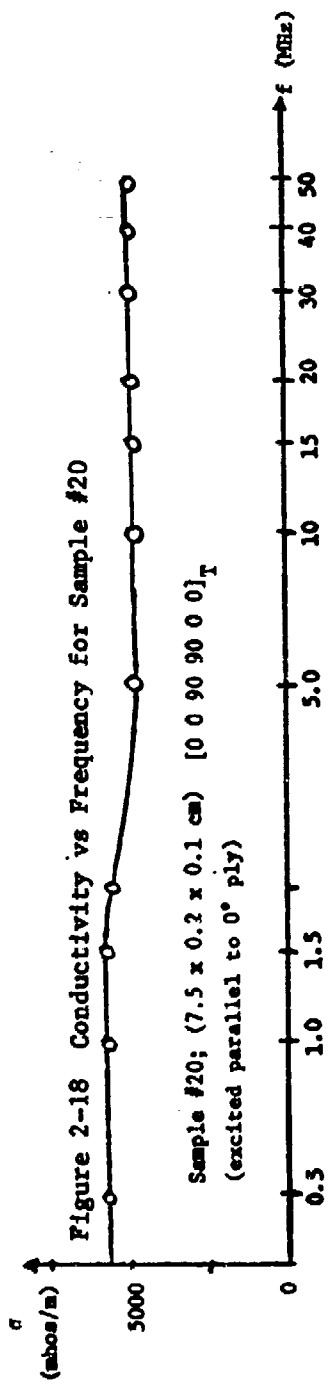


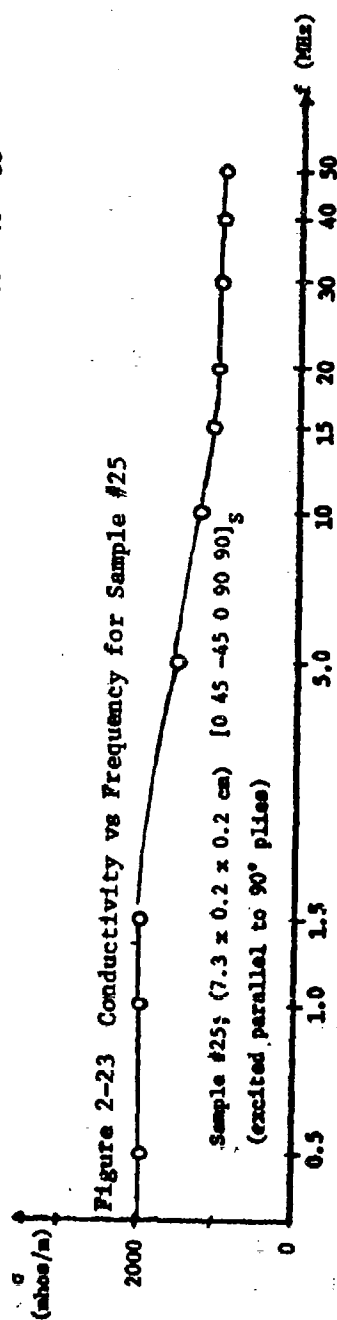
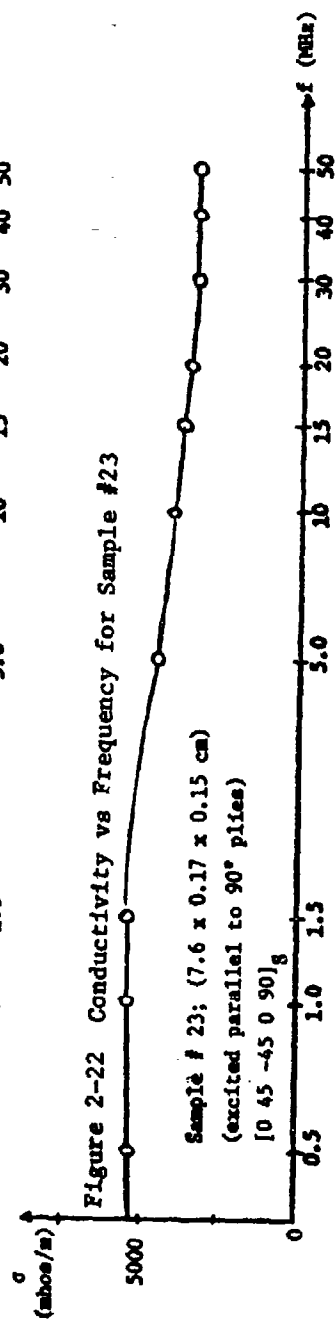
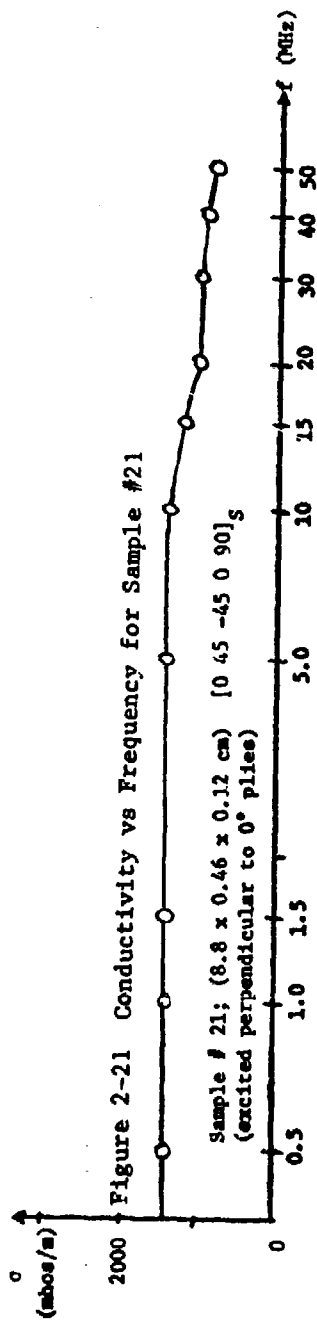
COMPOSITE SAMPLE IS THE HORIZONTAL POST
CURRENT SAMPLING RESISTOR IS AT RIGHT ANGLES TO COMPOSITE POST

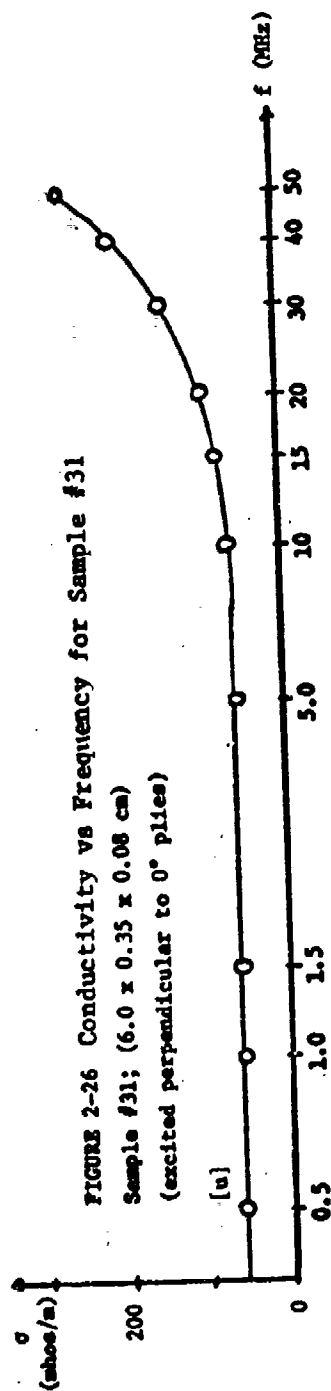
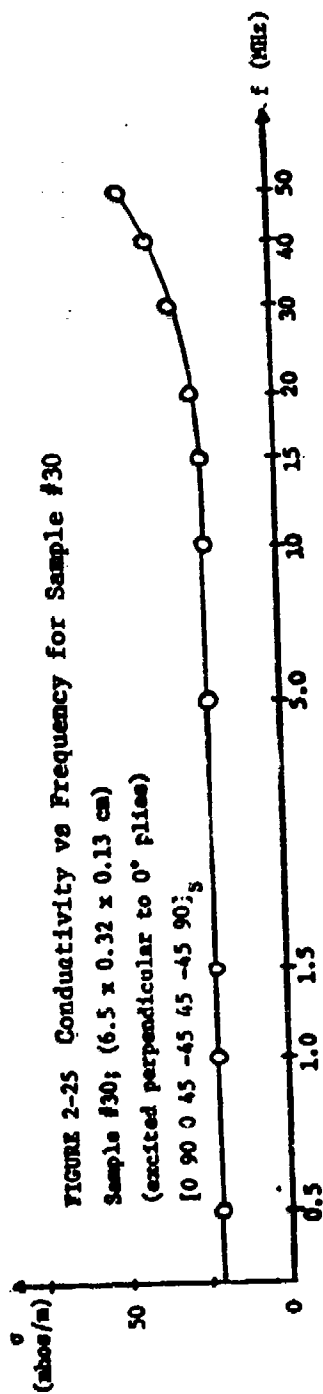
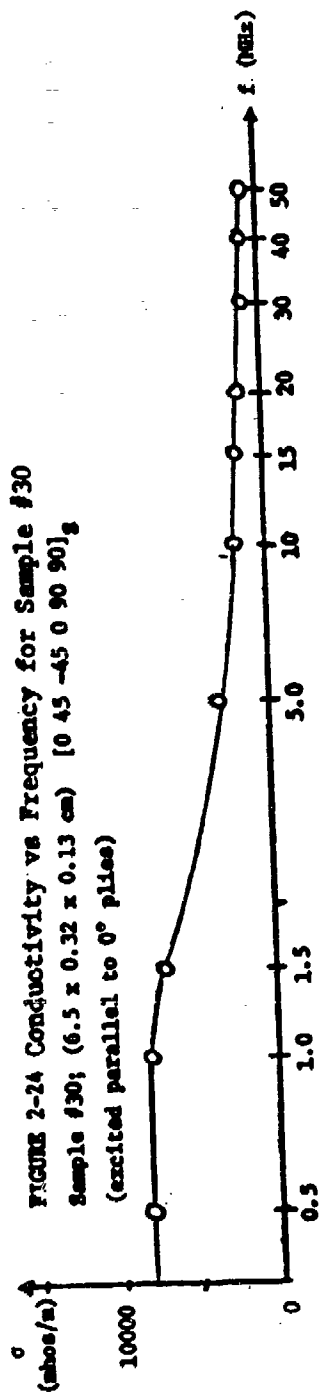
(b)

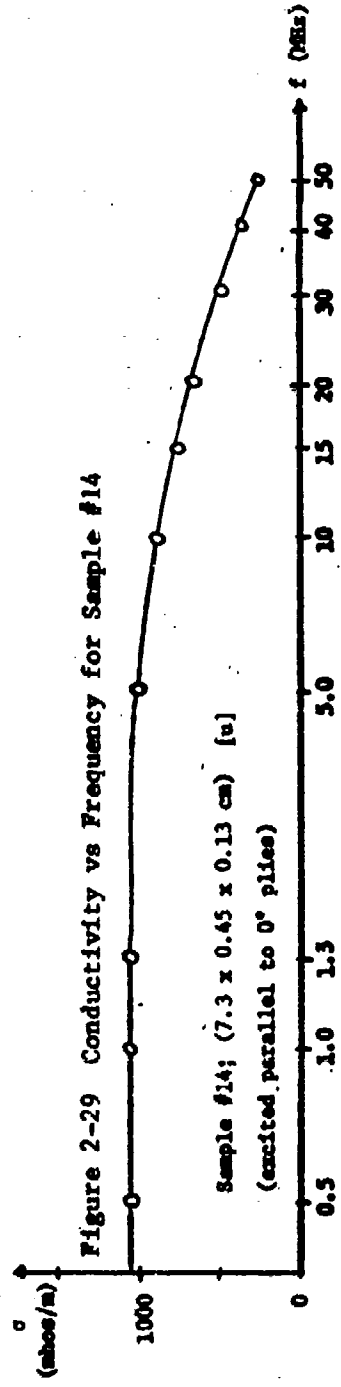
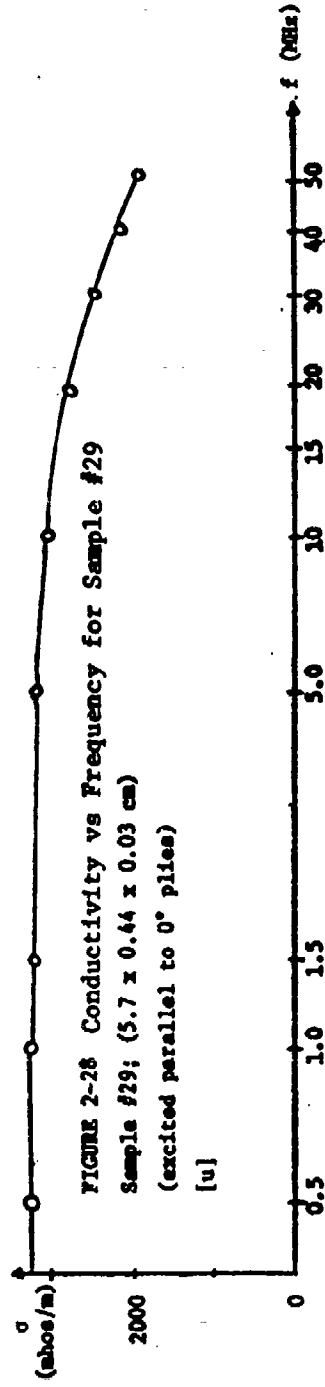
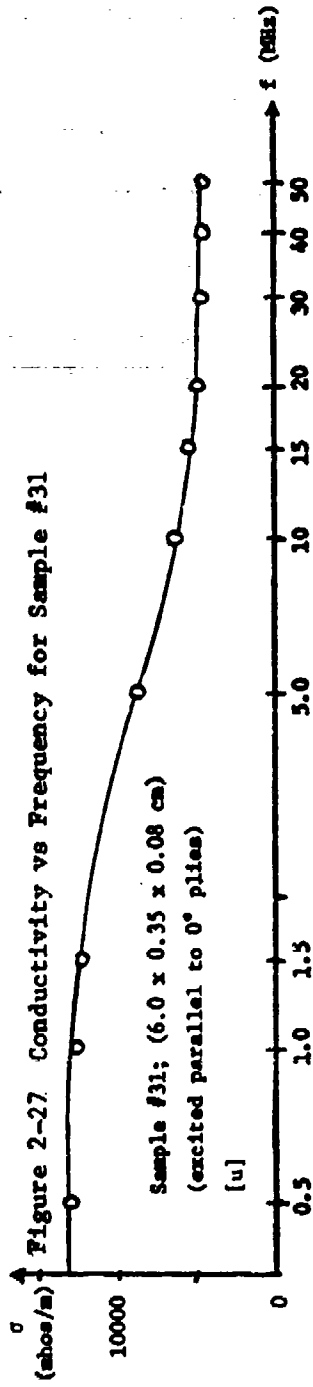
FIGURE 2-14











(current normal to the fiber axis), the effective conductivity increases with frequency. From a circuit point-of-view, this looks, like a capacitive effect but this phenomenon is not fully understood at this time.

For unidirectional samples excited in the longitudinal direction or multiple-ply samples, the effective conductivity decreases with frequency above 5 MHz. This effect is explainable by a combination of skin effect and the distributed inductance of the samples. Inductance effects have not yet been modeled, but skin effect is discussed in the next section.

2.7.2 Skin Effect

Although the samples measured were inhomogeneous and had rectangular cross-sections, an easily analyzed model results by assuming homogeneity and a circular cross-section. Following Ramo, et al.²⁻⁵, the current density distribution for the geometry of Figure 2-30 is

$$J(r) = J_0 \left(\frac{\text{Ber } u + j \text{Bei } u}{\text{Ber } u_0 + j \text{Bei } u_0} \right)$$

where $u = \sqrt{2} r / \delta$, $u_0 = \sqrt{2} r_0 / \delta$,
 $\delta = 1/(\pi f \mu \sigma)^{1/2}$, (the skin depth), meters,
 f = the frequency of excitation, Hz,
 σ, μ have their usual meanings,
 r, r_0 are defined in Figure 2-30, meters,
 Ber, Bei are the real and imaginary parts of the zero order Bessel function, and
 J_0 is the current density at the surface $r = r_0$.

A FORTRAN program (Appendix 2-A) was written to integrate this equation and yield the current i .

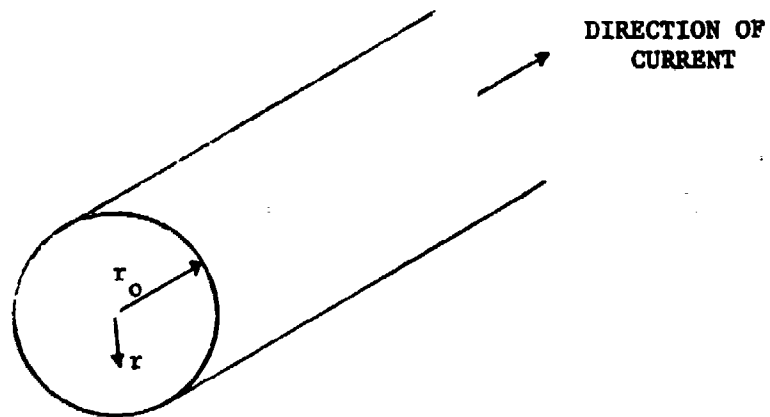
$$i = \int_0^{r_0} 2\pi r J(r) dr$$

The surface current density J_0 is calculated as

$$J_0 = \sigma E_0 = \sigma \frac{V}{L}$$

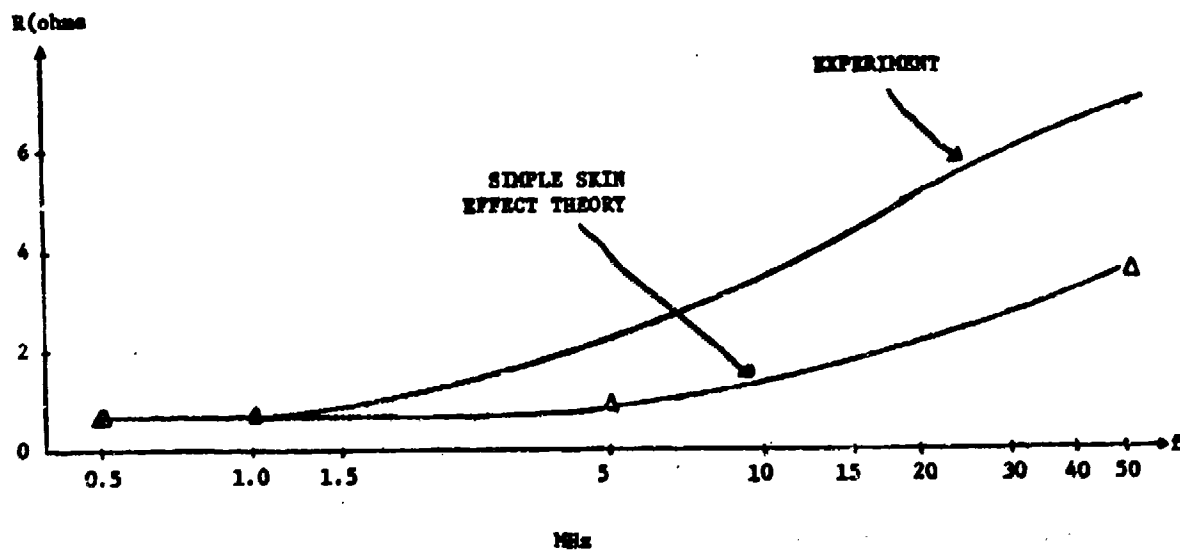
where V is the applied voltage and L the sample length. The resultant sample resistance is plotted in Figure 2-31 as a function of frequency from 0.5 MHz to 50. MHz for sample 23, 11 plies of Hercules 3501 with a stacking sequence [0 45 -45 0 90 90]_S.

The agreement with experiment is qualitative and shows the correct trend. Extensions to rectangular, inhomogeneous solids are in progress.



SKIN EFFECT GEOMETRY

FIGURE 2-30



SKIN EFFECT RESULTS

FIGURE 2-31

2.8 CONDUCTIVITY MODELS

2.8.1 Current in Longitudinal Directions

The effective conductance of a single ply of a graphite/epoxy or boron/epoxy material for current in the longitudinal direction is simply the sum of the conductances of the individual fibers. This is so because the conductivity of the resin matrix is orders of magnitude less than the conductivity of the fibers. Figure 2-32 shows the geometry of interest. The conductance, G_f , of an individual fiber may be written

$$G_f = \frac{\sigma_f A_f}{L}$$

where

σ_f is the fiber conductivity,

A_f the fiber area and

L the sample length.

The total sample conductance, G , is simply a summation of the individual fiber conductances. Assuming N identical fibers, we write

$$G = NG_f = \frac{\sigma_f A_f N}{L}$$

We define a composite conductivity in the longitudinal direction via the equation

$$G = \frac{\sigma_L A}{L}$$

where A is the sample area. Combining these last two equations allows us to write

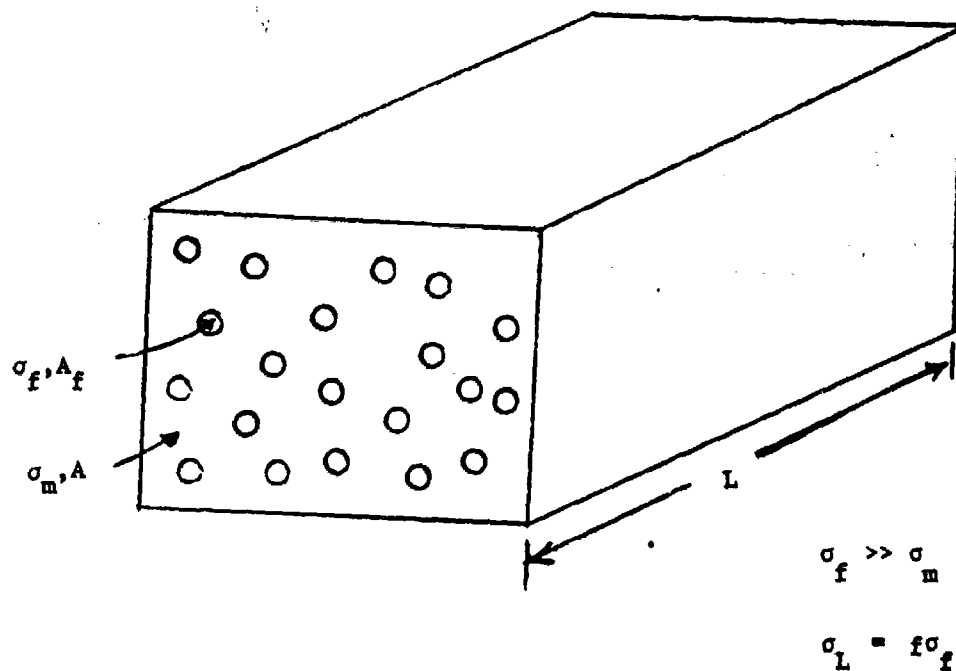
$$\sigma_L = \frac{A_f N}{A} \sigma_f = f \sigma_f$$

where f is the volume fraction of fiber in the composite.

The measured conductivity of graphite fibers is $2(10)^4$ mhos/m. Typical volume fractions are on the order of 0.6 and this results in a longitudinal conductivity of $1.2(10^4)$ mhos/m. This is in excellent agreement with the values reported in the last section for Hercules 3501.

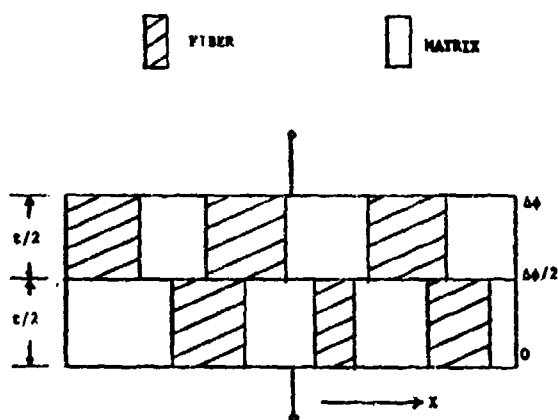
2.8.2 Current in Transverse Directions

The basic model for transverse currents in a unidirectional sample is shown in Figure 2-33 and is based on dividing the sample into a family of parallel planes, with fibers being distributed at random across each plane in accordance with the overall volume fraction f . Simplifying assumptions (Appendix 2-B) are applied to this random fiber model to



MODEL FOR DETERMINATION OF σ_L

FIGURE 2-32



MODEL FOR DETERMINATION OF σ_T

FIGURE 2-33

allow direct calculation of the transverse conductivity. For two planes, the effective conductivity (assuming the plane boundaries are equipotentials--a drastic assumption) is of the form

$$\sigma_T = f^2 \sigma_f + 8f(1-f)\sigma_m + (1-f)^2 \sigma_m$$

where σ_m is the matrix conductivity. The detailed derivation is given in Appendix 2-B.

For graphite/epoxy, the fiber conductivity is much greater than the matrix conductivity, and the above equation simplifies to

$$\sigma_T = f^2 \sigma_f$$

for all cases in which the volume fraction f is not near zero.

Assuming a volume fraction f of 0.6, the transverse conductivity of graphite/epoxy is calculated to be

$$\sigma_T = (.6)^2 (2)(10^4) = 7.2(10^3) \text{ mhos/m.}$$

This theoretical prediction is a factor of 70 greater than the experimentally measured quantities. The simple two-plane random fiber model is then seen to be inadequate. Analysis using more precise models is being carried on.

2.8.3 Conductance of Multiple-Ply Samples

In calculating the effective conductance or conductivity of a multiple-ply sample, the basic assumption is that the individual plies may be treated as conductances in parallel. This approach works well for situations in which the samples are uniformly excited by electrodes over opposing faces of a rectangular sample. The measured values and those theoretically predicted in this section are not applicable to problems similar to that of lightning attachment because, in such cases, the current is injected at a point, or a series of points, along a surface. The key assumption of uniform excitation is not present.

Defining G_i as the conductance of the i^{th} layer in the direction of interests, we may write the sample conductance G as a simple summation

$$G = \sum_{i=1}^N G_i.$$

We assume the sample has a length L , a uniform width W and that each ply has a thickness Δ . The quantity G_i may then be written

$$G_i = \frac{\sigma_i W \Delta}{L}$$

where σ_i is the conductivity associated with the i^{th} layer. The total sample conductance may be expressed in terms of effective conductivity by the equation

$$G = \frac{\sigma_e A}{L} = \sum_{i=1}^N \frac{\sigma_i W \Delta}{L} \quad (A = WN\Delta).$$

Upon cancelling common terms, we obtain

$$\sigma_e = \frac{1}{N} \sum_{i=1}^N \sigma_i.$$

It is essential to recognize that this derivation assumes that all plies have identical thicknesses. With this final result, the effective conductivity of any multiple-ply sample can be calculated as long as the values of conductivity to be associated with the angular orientations of individual plies are known.

The longitudinal and transverse conductivities are already known from the measurements on unidirectional samples. To predict the conductivity of any arbitrary lay-up of 0, 45 and 90 plies, it is necessary to assign a value to the conductivity of a ply which is oriented at 45° with respect to the exciting electrodes. For the Hercules 3501, a value of 0.5(10⁴) mhos/m. provides a good fit to experimental data as will be shown. For this material, we have

$$\begin{aligned} \sigma_L &= 1.0(10^4) \text{ mhos/m.} \\ \sigma_T &= 100 \text{ mhos/m.} \\ \sigma_{45} &= 0.5(10^4) \text{ mhos/m.} \quad (45^\circ \text{ layer}) \end{aligned}$$

For the 11-ply graphite/epoxy sample (23), with a ply stacking sequence of

$$[0 \ 45 \ -45 \ 0 \ 90 \ 90]_S,$$

the conductivity is calculated as

$$\frac{(4)(10^4) + (4)(.5)(10^4) + (3)(100)}{11} = 8.2(10^3) \text{ mhos/m.}$$

This compares with an experimentally measured value of conductivity of 5.61(10³) mhos/m. The agreement between this model and measured values is shown for three other samples below.

Sample ID	20	21	25
σ_{theory} (mhos/m)	7.14(10 ³)	6.67(10 ³)	5.33(10 ³)
σ_{exp} (mhos/m)	4.96(10 ³)	4.14(10 ³)	4.97(10 ³)

The model provides consistently good agreement with the experiment and requires only careful numerical determination of the three values of conductivity: longitudinal, transverse and 45°.

2.9 MOISTURE EFFECTS

To obtain information concerning the effects of absorbed moisture on the electrical properties of composite materials, a simple set of experiments were planned in which the DC electrical conductivity of samples was measured before and after immersion, for several days, in water.

The experiments were performed using rubbed indium contacts and revealed that the transverse conductivities decreased with increasing water content while no significant changes were observed in longitudinal conductivities. These results fit in quite well with the model of transverse conduction depending upon fiber-to-fiber contact. One can hypothesize that the water is absorbed into the epoxy, the epoxy swells, and fiber contact is reduced. After seeing these effects over a period of months, the behavior of electrodes on samples which had not been immersed in water were studied. It was found that the resistance of these samples was also increasing. This effect appears to occur only on the rubbed indium-silver paint electrodes and casts suspicion on all of the earlier work in the effects of water immersion because all samples involved in these experiments had such indium contacts.

This recognition appeared quite late in the reporting period and only a brief effort has been expended to investigate the effects of moisture on samples with evaporated aluminum contacts. However, over a period of two to four weeks immersion in water, the transverse conductivity of graphite/epoxy samples with such contacts decreases by a factor of four. An attempt to reverse this effect by drying the samples has been made, but the water absorption process displays hysteresis and is not completely reversible. This is, of course, a direct consequence of the random-walk diffusion mechanism whereby the water molecules enter the composite material.

In summary, the first set of experiments produced meaningless results because of unrecognized difficulties with contact aging. The second set of experiments, on a preliminary basis only, indicates that there are effects on the transverse conductivities in unidirectional samples. In a typical multiple-ply sample of a normal stacking sequence, these effects would not be observable because of the dominating presence of fibers running longitudinally between the measurement electrodes.

2.10 TEMPERATURE EFFECTS

Only a very small effort has been devoted to measuring changes in the conductivity of graphite/epoxy as a function of temperature. The apparatus for this work has been constructed but several other problems that arose during this period of the effort were more important.

Over the entire temperature range from liquid nitrogen (77°K) to room temperature (300°K), a relatively small change in electrical conductivity was recorded for multiple-ply, non-directional samples. The total conductivity change over this temperature shift was on the order of 15%. These were the only experiments regarding temperature effects.

2.11 CONCLUSIONS AND SUMMARY

Simple measurement techniques may be used to obtain data to characterize composite materials over the frequency range DC to 50 MHz as long as care is taken to avoid parasitics in the upper range of frequencies. The circuits used to measure conductivity and permittivity for Kevlar/epoxy and boron/epoxy (for excitation orthogonal to the fiber axis) are simple bridges with signal generators covering the frequency range of interest. For graphite/epoxy, a simple series circuit consisting of a voltage source of the frequency of interest, sampling resistor and the composite itself is sufficient.

The magnetic properties of these materials were measured by the sample weighing technique and a vibrating sample magnetometer. All three materials were found to be weakly diamagnetic. For any numerical calculations involving shielding effectiveness, the relative permeability of any of these advanced composites may be taken to be unity with no significant loss in computational accuracy.

Permittivities are measurable for boron/epoxy (excited orthogonal to the fiber axis) and Kevlar/epoxy. The permittivity of Kevlar/epoxy is essentially that of the resin matrix, while the permittivity of boron/epoxy is larger because of the artificial dielectric phenomenon. The permittivity of graphite/epoxy is indeterminate at the frequencies with which this section is concerned.

Kevlar/epoxy is electrically isotropic and may, for shielding effectiveness calculations, be considered a good dielectric. Boron/epoxy has an anisotropy ratio on the order of 10^9 and displays behavior ranging between that of an imperfect conductor and a good dielectric depending upon the direction in which it is excited. Graphite/epoxy may be considered to be a good conductor with an anisotropy ratio on the order of 200. These results were obtained for small amounts of material, each type from a single part of a production run. For example, all samples of Hercules 3501 were fabricated from a single roll of pre-preg tape; no data representing statistical averaging over several different production times has been recorded. The values given in this report should not be taken as necessarily representative of all composites.

The bulk of the investigation of frequency dependence focused on graphite/epoxy. The conductivities of these materials are independent of frequency from DC to 5 MHz and, above this frequency, vary in ways which are not totally understood. Skin effect and distributed inductance account, in qualitative terms, for the behavior of samples with at least some layers perpendicular to the exciting electrodes. The behavior of transverse conductivity above 5 MHz is not understood at this time.

APPENDIX 2-A CALCULATION OF SKIN EFFECT

Skin effect was discussed in Section 2.7.2. In numerically determining sample resistance and conductivity, series expansions were used for ber(u) and bei(u).²⁻⁶

$$\text{ber}(u) = 1 - \frac{u^4}{(2 \cdot 4)^2} + \frac{u^8}{(2 \cdot 4 \cdot 6 \cdot 8)^2} - \dots$$

$$\text{bei}(u) = \frac{u^2}{2} - \frac{u^6}{(2 \cdot 4 \cdot 6)^2} + \frac{u^{10}}{(2 \cdot 4 \cdot 6 \cdot 8 \cdot 10)^2} - \dots$$

The following are the definitions of variables and the FORTRAN program used to calculate the impedance changes resulting from skin effect.

TPI: 2π ,
 N: index to fix length of Bessel function expansions, number of terms equals $N/4$,
 A: radius of cylinder (m),
 SIG: DC conductivity of sample (mhos/m.),
 ZMU: magnetic permeability of sample (henries/m.),
 VDC: voltage used to normalize calculations to experiment to DC (volts),
 RDC: DC sample resistance (ohms),
 ZL: sample length (meters),
 RP: area/length ratio for sample (meters),
 FREQ(J): array of frequencies, DC to 50 MHz in 1 MHz increments,
 W: radian frequency
 SKD(J): array of skin depths, DC to 50 MHz (meters),
 U: $\sqrt{2}/\delta$,
 ZII: imaginary part of current,
 ZIR: real part of current,
 RI(J): array of resistance values, DC to 50 MHz (ohms) and
 C(J): array of conductivities, DC to 50 MHz (mhos/m.).

PROGRAM LISTING

```

DIMENSION SKD(51),QI(51),R(51),P(51),K(17),ZK(17),FREQ(51),C(51)
TPI=6.283
N=4
A=.00081
SIG=13800.
ZMU=12.566E-7
ZU=SQRT(2.)
  
```

```

VDC=1.
RDC=2.62
AO=VDC/RDC
ZL=.0745
RP=(2.06E-6)/ZL
FREQ=1.0E6
DO 10 L=2,N,2
ZK(1)=1.
DO 5 J=1,L/2
ZJ=FLOAT(J)
5 ZK(L)=ZK(L)*2.*ZJ
10 CONTINUE

DO 50 J=1,51
ZJ=FLOAT(J)
FREQ(J)=(ZJ-1.)*FREQ
Q=TPI*FREQ(J)
IF (W.GT. 0.) GO TO 30
ZIR=(TPI*A**2.)/2.
ZII=0.
GO TO 40
30 SKD(J)=SQRT(2./(SIG*ZMU*W))
U=ZU/SKD(J)
ZIR=0.
ZII=0.
BEI=0.
BER=0.
DO 20 I=1,1
M=4*I
ZM=FLOAT(M)
ZI=FLOAT(I)
BER=BER+((-1.)*I)*((U*A)**ZM)/(ZK(M)**2)
BEI=BEI+((-1.)*I+1)*((U*A)**ZM-2)/(ZM(M-2)**2)
ZIR=ZIR+((-1.)*I)*TPI*A**ZM*(U**ZM)/((ZK(M)**2.)*ZM+2.)
20 ZII=ZII+((-1.)*I+1)*TPI*A**ZM*(U**ZM-2.)/((ZK(M-2)**2.)*ZM)
ZIR=ZIR+(TPI*A**2.)/2.
BER=1.-BER
ZII=(ZII*BER-ZIR*BEI)/(BER**2+BEI**2)
ZIR=(ZIR*BER-ZII*BEI)/(BER**2+BEI**2)
40 QI(J)=SQRT(ZIR**2+ZII**2)
IF (J.NE. 1) GO TO 45
RI=QI(1)
45 QI(J)=AO*QI(J)/RI
R(J)=VOC/QI(J)
P(J)=RP*R(J)
50 C(J)=1./P(J)
DO 60 I=1,51
60 WRITE (6,*) FREQ(I),R(I),P(I),C(I)
CALL PLOT (2,FREQ,R,51,1,1)
STOP
END

```

APPENDIX 2-B RANDOM FIBER MODEL

To calculate the transverse conductivity of two layers of fiber, it is assumed that the boundaries of the two layers are equipotentials. Further, f represents the volume fraction of fibers, σ_f the fiber conductivity, σ_m the matrix conductivity.

At any lateral point x , there are four possibilities concerning the material in the z direction:

- i) both layers are fiber; probability f^2
- ii) the first layer is fiber, the second matrix; probability $f(1-f)$
- iii) the first layer is matrix, the second fiber; probability $(1-f)f$
- iv) both layers are matrix; probability $(1-f)^2$,

The total current flow is the sum of the currents associated with each of the four cases. For case i,

$$J_i = \sigma_f E = \sigma_f (\Delta\phi/2t)$$

because the electric field is uniform through the two layers, $\Delta\phi/t$, where $\Delta\phi$ is the potential drop and t the thickness of the two layers.

In type ii situations, the electric fields in the fiber, E_f , and matrix, E_m , are determined from the conservation of current density

$$J_f = \sigma_f E_f = J_m = \sigma_m E_m$$

and from the fact that the potential drop is $\Delta\phi$,

$$E_f(t/2) + E_m(t/2) = \Delta\phi$$

Solving simultaneously yields

$$E_f = 2\left(\frac{\sigma_m}{\sigma_f + \sigma_m}\right)(\Delta\phi/t)$$

The current density is

$$J_{ii} = \sigma_f E_f = 2\left(\frac{\sigma_f \sigma_m}{\sigma_f + \sigma_m}\right)(\Delta\phi/t)$$

Similarly, for the other two cases,

$$J_{iif} = 2\left(\frac{\sigma_f \sigma_m}{\sigma_f + \sigma_m}\right)(\Delta\phi/t)$$

$$J_{iv} = \sigma_m(\Delta\phi/2t)$$

The total current density is found by weighting each of four individual cases by their respective probabilities and summing.

$$J = f^2 J_i + f(1-f) J_{if} + (1-f)f J_{iif} + (1-f)^2 J_{iv}$$

Recognizing that $J = \sigma_T E$ and that $E = \Delta\phi/2t$ yields

$$\sigma_T = \sigma_f f^2 + 8\left(\frac{\sigma_f \sigma_m}{\sigma_f + \sigma_m}\right)f(1-f) + \sigma_m(1-f)^2$$

For $\sigma_f \gg \sigma_m$ (the case in graphite/epoxy), this reduces to the expression given in Section 2.8.2.

$$\sigma_T = \sigma_f f^2 + 8\sigma_m f(1-f) + \sigma_m(1-f)^2$$

REFERENCES

- 2-1. 1974 Book of ASTM Standards, Part 44, p. 36, (1974).
- 2-2. 1974 Book of ASTM Standards, Part 43, p. 206, (1974).
- 2-3. W. J. Gajda, Jr., "A Fundamental Study of the Electromagnetic Properties of Advanced Composite Materials," Final Report, Rome Air Development Center (1978).
- 2-4. T. Schoenberg (Private Communication), AVCO Corporation, Lowell, MA (1977).
- 2-5. Ramo, Whinnery and Van Duzer, "Fields and Waves in Communication Electronics," J. Wiley and Sons, New York (1965).
- 2-6. W. C. Johnson, "Transmission Lines and Networks," McGraw-Hill, New York (1950).

3.0 MEASUREMENT OF THE ELECTRICAL PROPERTIES OF ADVANCED COMPOSITES IN THE FREQUENCY RANGE OF 30 MHZ TO 1.0 GHZ

3.1 SUMMARY OF PROGRESS-TO-DATE

This section of the report treats the work done in connection with the measurement of the electrical parameters of composite materials over the frequency range of 30 MHz to 1 GHz during the period from October 1, 1976 to September 30, 1977. This work has concentrated on two basic methods: a) a Parallel-Plate sample tester and b) a Slotted Stripline tester.

3.1.1 Parallel Plate Sample Tester

This method will be described quite briefly since it was pursued only far enough to identify its various difficulties and shortcomings. The essence of the method was the measurement of the impedance of a small composite post placed across a parallel-plate transmission line. It was hoped that the simplicity of the field geometry relative to the post would then enable the determination of the admittivity $\hat{y}_c = (\sigma_c + j\omega\epsilon_c)$ of the post material from the measured post impedance. The principal difficulties with the method were:

- a) necessarily small post dimensions causing inconvenient and unrealistic sample sizes
- b) uncertain contact resistance which contaminated impedance measurements
- c) coaxial-to-parallel-plate transmission line discontinuities which made impedance measurements inaccurate.

The method is described below in section 3.2.1 in somewhat more detail.

3.1.2 Slotted Line Stripline Tester

The shortcomings of the parallel plate method listed above stimulated the development of a technique which avoided most of these difficulties. The slotted-line tester consists of a transmission line whose outer conductors are parallel aluminum plates and whose center conductor is a flat strip of composite material. The result is a lossy transmission line whose complex propagation constant, $\gamma = \alpha + j\beta$, is determined by the line geometry and the admittivity, $\hat{y}_c = (\sigma_c + j\omega\epsilon_c)$ of the composite center conductor. The measurement technique consists of determining γ from standing wave patterns on the line and then calculating \hat{y}_c from γ .

The analysis and development of a line of this type has received the full attention of the investigators over the period January 1, 1977 through September, 1977. A three-foot line based on this method is nearly complete and preliminary measurements on a crude version have demonstrated the feasibility of the technique. The slotted stripline method and equipment is described in detail in Section 3.2.2 and in the

Appendices, 3A and 3B.

3.1.3 Early Results in Parameter Measurement

3.1.3.1 Results From Parallel-Plate Tester

Contact resistance and measurement uncertainties in this method prevented the determination of anything other than a loose "lower bound" on the conductivity of graphite posts of about $\sigma_c > 3 \times 10^2$ mhos/meter between 140 MHz and 1.0 GHz.

3.1.3.2 Results From 10 cm Slotted Stripline

A simplified experimental model of the slotted stripline was assembled to determine the feasibility of the method. This line had a useable length of approximately 10 cm. A preliminary set of measurements on the short slotted stripline indicate values of σ_c for uni-directional graphite/epoxy of greater than 3×10^4 mhos/m in the direction of the fibers. Some sample preparation involving the removal of surface regions having low fiber density will tend to improve the accuracy of these results. Accuracy will also be improved, of course, by the greater precision of the one meter line.

3.2 DEVELOPMENT OF A PARAMETER MEASUREMENT METHOD

The central aim of the program at the Rochester Institute of Technology for the period October 1, 1976 to September 30, 1977 was the development of a suitable technique for the measurement of the intrinsic electrical parameters (σ, μ, ϵ) of advanced composite materials over the frequency range from 30 MHz to 1.0 GHz. Since measurements (at Notre Dame University) at D.C. revealed no detectable magnetic properties (i.e. $\mu = \mu_0 = 4\pi \times 10^{-7}$ henries/meter) and because of the non-magnetic nature of the constituent materials, this effort concentrated on the admittivity ($Y = \sigma + j\omega\epsilon$) of the materials. As mentioned above, two distinct methods were pursued.

3.2.1 The Parallel Plate Tester

This method sought to determine admittivity by relating the two-terminal impedance of a composite material post to its conductivity. The basic scheme is depicted in Figure 3-1.

The parallel plate line enables the excitation of the sample post with an E-Field of simple and classical geometry relative to that of the post. Figure 3-2 presents a circuit schematic of the test system.

Scattering parameter measurements of the two-port (port A to port B) and a knowledge of the geometry of the line were used to determine the impedance, z_p , of the sample post as a lumped two-terminal impedance. The impedance z_p was then related to geometry and material of the post by

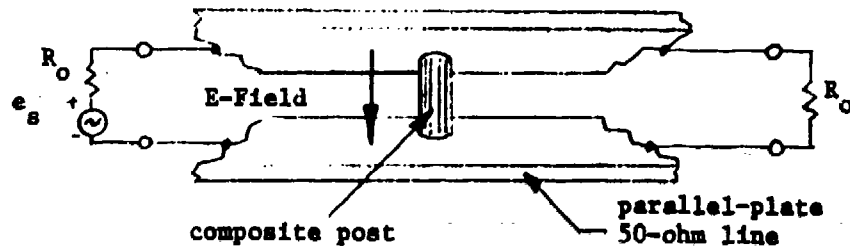


Figure 3-1 - Parallel Plate Tester

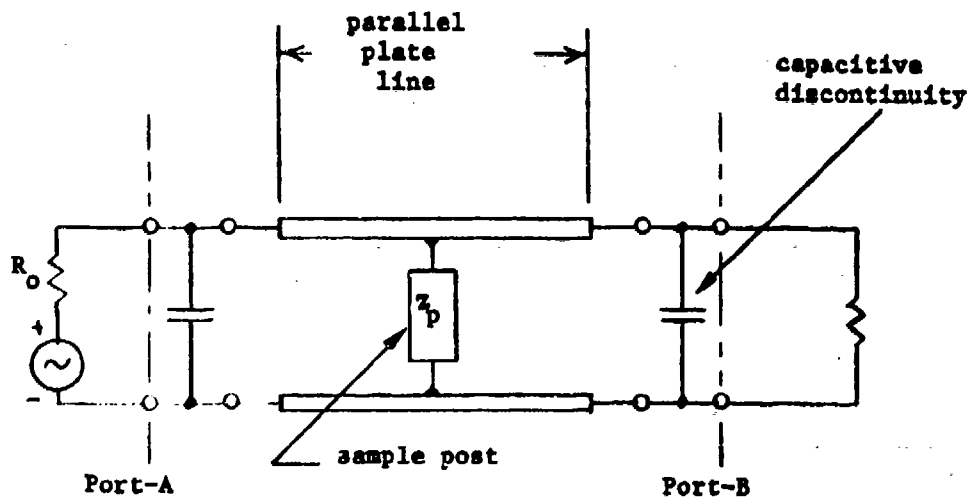


Figure 3-2 Schematic Diagram of Parallel Plate Tester

$$z_p = \frac{V}{I} = j\omega L_p + R_p = j\omega L_p + \frac{l}{\sigma_c \delta C}$$

where, V = Transmission line voltage at the post

I = Total current through the post in amperes

R_p = Post resistance in ohms

L_p = Inductance of the sample in henries

l = Post length in meters

C = Post circumference in meters

$\delta = \sqrt{\frac{2}{\omega \mu_0 \sigma_c}} = \text{skin depth (meters)}$

σ_c = Conductivity of the post in mhos/meter.

As may be appreciated, this method has several features which make the accurate determination of σ_c difficult and ultimately led to disenchantment with the technique. The difficulties are:

- a) Measurement of z_p must be made indirectly through measurement of P the total A-B two-port.
- b) Contact resistance at the top and bottom of the post is difficult to control and may not be negligible in the case of highly-conductive samples.
- c) In order to produce post impedances which are accurately determinable in a 50 Ω system (e.g. Hewlett-Packard Network Analyzer), the post dimensions are quite small (within an order of magnitude of fiber diameters).
- d) The post inductance is a function of the geometry of the complete tester and must be determined separately.
- e) The inductive term, $j\omega L_p$, tends to exceed the resistive term at higher frequencies sufficiently to make accurate determination of R_p difficult.

A line of this type was built and tested with unidirectional graphite/epoxy posts. The difficulties listed were such as to prevent accurate measurement of σ_c . The best that could be done was to place a "lower

bound" on σ of between 10^2 and 10^3 mhos/meter. Low frequency measurements and subsequent measurements by the slotted stripline method have indicated higher conductivity, σ_c , of the order of 3×10^4 mhos/meter.

3.2.2 The Slotted Stripline

3.2.2.1 Physical Description

The slotted stripline tester is a "coaxial" type slotted line similar in construction to Hewlett Packard's 805 C coaxial slotted line. A cross section of the slotted line tester is shown in Fig. 3-3. The center conductor is a flat strip of composite material. The outer conductors are two aluminum channels joined together at each end by aluminum end-plates.

The dielectric is a thin strip of Teflon .020" or .040" thick. One dielectric, containing one or more Teflon layers, is used on each side of the center conductor. In general, dimension "a", the width of the dielectric, is an integral multiple of .020". In use, the aluminum outer conductors are clamped together to form a Teflon-composite-Teflon sandwich.

The standing waves are measured by a magnetic probe, a loop of small diameter semi-rigid coaxial cable. The probe is attached to a probe carriage which moves along the slotted line. The distance between the probe and the center conductor is variable.

A side view (a vertical section through the center of the line) of the line is shown in Fig. 3-4. The slotted line is fed at one end via a type N coaxial connector. At the other end the composite material is cut off short of the end of the slotted line providing an open circuit termination for the slotted line.

3.2.2.2 Measurement Method

The slotted stripline tester forms a lossy transmission line whose propagation characteristics are determined by the line geometry and the electrical properties of the composite material center conductor. In operation the line is left "open-circuited" at the far end and driven from the other with a resulting standing wave pattern (voltage or current) characteristic of a lossy line. With a perfectly conducting center conductor the line would be a purely TEM guided-wave system. With a lossy center conductor the electric field has a small component in the propagating direction which is a maximum adjacent to the center conductor and vanishes at the outer conductor inner surfaces (see Figure 3-7). It is this longitudinal component of the E-Field which interacts with the admittivity of the center conductor to produce the lossy VSWR pattern. The use of unidirectional composite specimens for the center conductor permits the measurement of admittivity both parallel to and perpendicular to the fiber direction depending upon how the length of the center strip is oriented relative to the fibers.

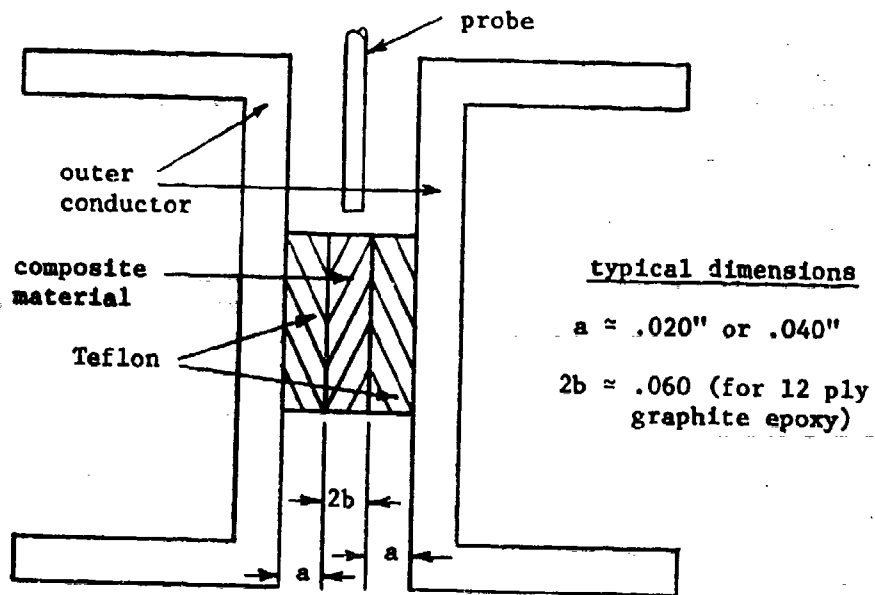


Figure 3-3 Slotted Stripline - Cross Section

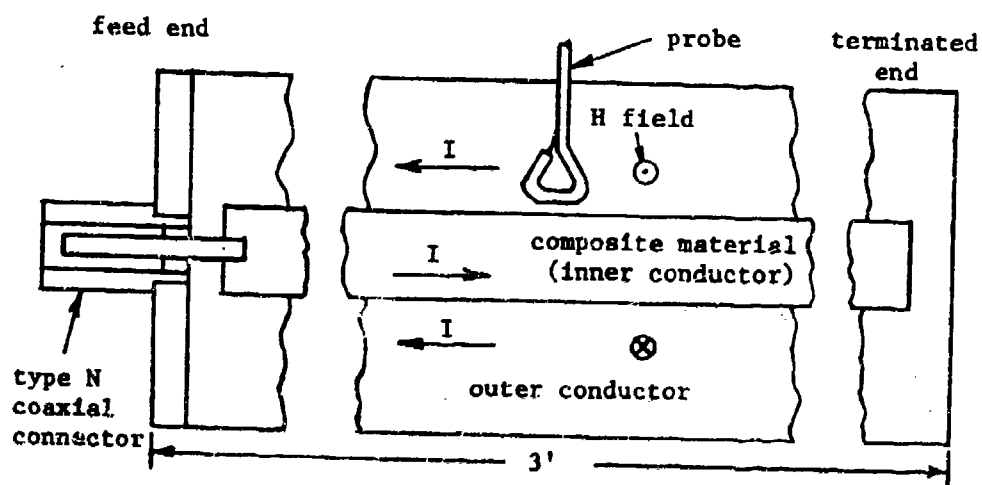


Figure 3-4 Slotted Stripline - Side View
(vertical section through center of line)

The voltage along the line as measured by a standing wave detector, is given by:

$$|e(x)| = |C| \cosh \{(u + \alpha x) + j(\phi + \beta x)\}$$

where C = amplitude term proportional to the driving signal voltage

α = real part of the transmission line propagation factor, γ , in nepers/meter

β = imaginary part of γ in radians/meter

u, ϕ = "offset" terms associated with the termination (u, ϕ are zero for a pure "open circuit" termination)

x = distance in meters from the termination to the point where $|e(x)|$ is measured.

The measurement method used with the line consists of taking data of $|e(x)|$ vs. x over the length of the line. These data are then analyzed (by the computer program described in section 3-B) to provide estimates of α and β . When the effective conductivity of the composite strip is such that its "skin depth" is small compared to its thickness, the admittivity ($\hat{y}_c = \sigma_c + j\omega\epsilon_c$) of the composite material in the direction of line propagation may be determined from α , β and the line geometry by (see Appendix 3-A, equations (11) and (12)):

$$|\hat{y}_c| = |\sigma_c + j\omega\epsilon_c| = \frac{|-j\omega\mu_0| \omega^2 \epsilon_d^2}{a^2 |[(\alpha^2 + \omega^2 \mu_0 \epsilon_d - \beta^2) + j\alpha\beta]^2|}$$

where, ω = operating radian frequency

μ_0 = free space permeability

ϵ_d = permittivity of dielectric separating inner and outer conductors (F/m)

a = separation between inner and outer conductors (m).

With perfect data, the absolute value signs above could be removed and the parameters σ and ϵ could, in principle, be determined separately. As a practical matter, however, for graphite composite as measured so far the typical values of α, β , and $\omega^2 \mu_0 \epsilon_d$ are such that small percentage variations in these values produce a substantial change in the angle associated with $(\sigma_c + j\omega\epsilon_c)$, although the magnitude is relatively unchanged. For example, if $\sigma_c = 10^4$ mhos/m, the value $|\hat{y}_c|$ is

relatively unaffected by values of ϵ_c up to and including $\epsilon_c = 8.85 \times 10^7$ farads/meter: - that is, relative dielectric constant, k_c^1 , up to 10^5 !

3.2.2.3 Advantages of the Stripline Method

There are a number of features of the stripline method which make it extremely attractive as compared to other techniques (e.g. the parallel plate method or schemes where the composite acts as a transmission barrier).

- a) The method is essentially independent of any conductive joints between the composite sample and the rest of the test apparatus. The quantities measured reflect a direct and simple interaction of adjacent fields and the test specimen.
- b) The instrumentation (signal generator and standing wave indicators) are such as would be available in the most modest of RF laboratories.
- c) The dimensions and geometry of the test samples (thin flat strips of the order of 2-4 cm in width by 1 meter or more in length) are such that ease of sample preparation and desired fiber orientation are readily achieved. The sample sizes are such that the results also provide something of a bulk average.
- d) Measurement data consists of a large number of data points (a meter or more of standing wave data) at a single frequency so that appreciable data averaging (and error reduction) is accomplished at each measurement frequency.
- e) The method is essentially "broad-band" in that no physical adjustment or "tuning" is necessary as the frequency is changed over a range of nearly 1-1/2 decades.

3.2.2.4 Limitations of the Slotted Stripline Method

As indicated above, the slotted stripline method has a number of attractive features in terms of its ability to measure parameters in the region 100 MHz to 1 GHz and above. There are, however, limitations to the scheme:

- a) The technique and the calculations of the admittivity, $\hat{y} = \sigma + j\omega\epsilon_c$, are based on a model of the composite material center conductor which is homogeneous. This, of course, is not strictly true of the fibrous nature of graphite/epoxy, boron/epoxy and Kevlar/epoxy composite materials. In addition the model assumes that the admittivity is isotropic in any direction perpendicular to the fibers, but may vary with respect to its value parallel to the fibers. The result is that the

calculated admittivity provides, effectively, a "bulk" value based on this model.

- b) The calculated admittivity varies inversely as the square of the spacing "a" between the composite strip and the outer conductor. As a result this value must be known accurately and care must be taken in sample preparation to remove outer layers of low fiber density before measurement. In this respect the method is somewhat less desirable than one which measures the transfer impedance of a composite panel directly and calculates a bulk admittivity from that measurement. Such transfer impedance methods, however, are generally subject to leakage effects occurring at the boundary of the test panel and the fixture which holds it.
- c) For materials such as graphite which tend to display values of $|\hat{y}|$ in the direction of the fibers of $10^4 - 10^5$ mhos/meter, the method would be hard-pressed to differentiate between unidirectional samples and (for instance) $0^\circ - 90^\circ - 0^\circ$ - laminated samples where the outer ply was parallel to the propagation direction. This would be because of the very small power penetration beyond the first layer.
- d) As indicated earlier, the method has difficulty in determining σ and ϵ_c separately for any combination of $\omega\epsilon_c \leq \sigma/5$. For graphite/epoxy specimens at 1.0 GHz, this implies that relative dielectric constants of 10^4 or lower would not be detected.

In summary then, the method is most appropriate to the measurement of unidirectional samples of uniform fiber density.

3.2.3 Measurement Results

A simplified form of the slotted stripline test was assembled having the following physical characteristics:

- 1) Composite Sample: unidirectional graphite/epoxy
16 mm wide by 2 mm thick by 23 cm long
- 2) Dielectric Spacer: Mylar 0.254 mm thick, dielectric constant 2.2 (relative).

Voltage standing wave data were taken at 900 MHz on this line (shown as $|e^2|$, relative in Figure 3-5). The data were then processed to compute the complex propagation factor, $\gamma = \alpha + j\beta$, from which the admittivity, $\hat{y}_c = |\sigma_c + j\omega\epsilon_c|$ was calculated.

The result for this specimen was $|\sigma_c + j\omega\epsilon_c| = 1.9 \times 10^5$ mhos/meter. This value is felt to be high by a factor of 3 or 4 compared to what

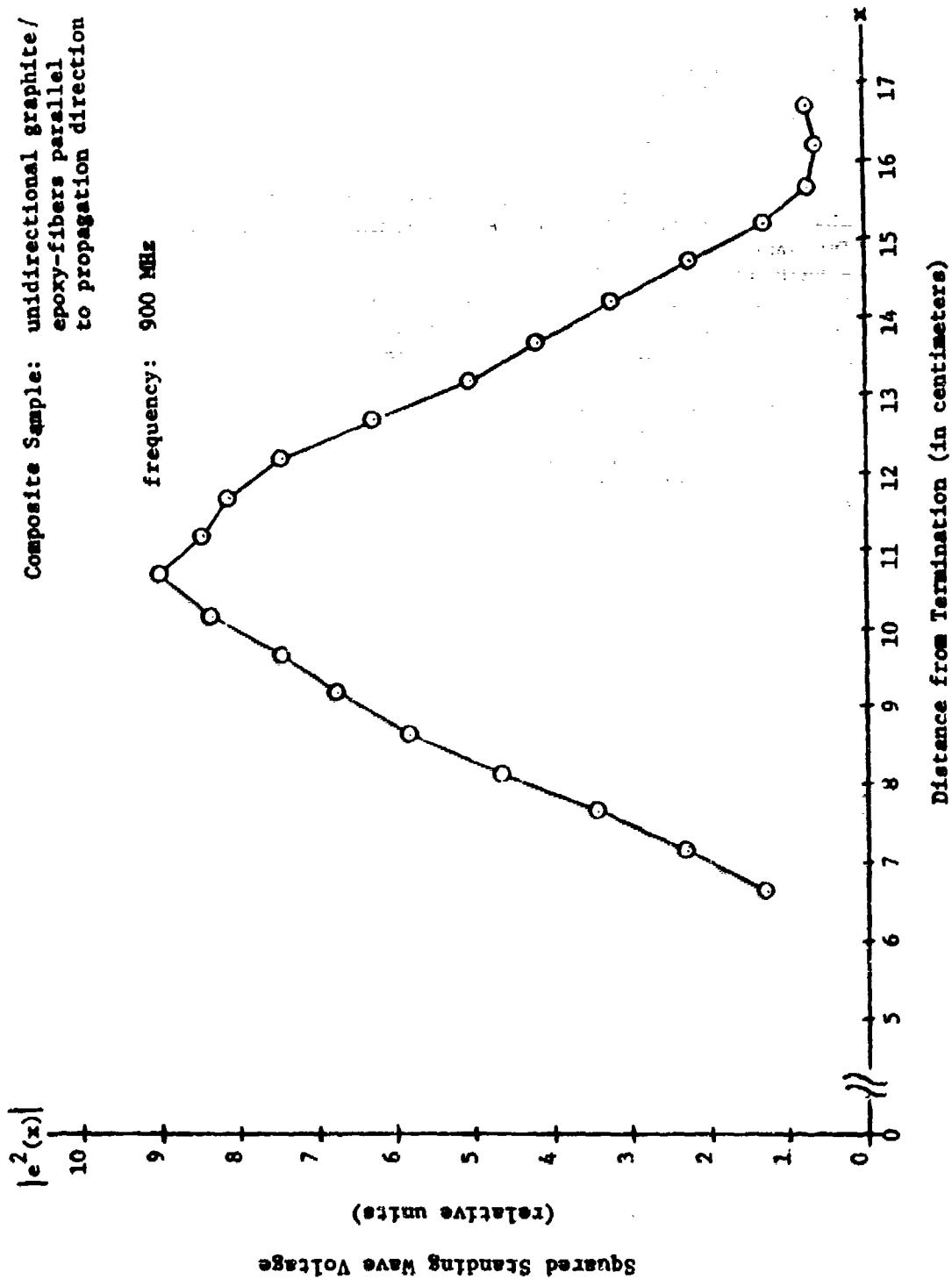


Figure 3-5 Standing Wave Data

was expected for unidirectional graphite/epoxy in the direction of the fibers. One feature of the specimen which would contribute to a higher apparent value of $|\hat{y}|$ is a surface layer of epoxy containing either a very low carbon fiber density or no fibers at all. This is a common characteristic of finished molded composite panels. This layer makes the effective dielectric spacing greater between the inner and outer conductors and, as shown in Appendix 3-A, the calculated admittivity is inversely proportional to the square of this spacing.

In the final use of the slotted stripline, this outer layer of epoxy should be removed, or the dielectric spacing should be increased so that the effect of the epoxy layer is negligible.

APPENDICES A AND B

3-A The Analytical Basis for the Slotted Stripline

Earlier methods aimed at the measurement of the intrinsic parameters (σ, ϵ, μ) of composite materials (e.g. coaxial transmission systems (1), or the parallel-plate technique described previously) have suffered from the uncertainties associated with the boundary between the composite test sample and the rest of the test apparatus. The result has either been signal leakage or contact resistance which interfered with the accurate measurement of the sample. The slotted stripline method described in this report was developed in order to avoid or minimize these "boundary" effects. Two objectives were emphasized in its design:

- a) To produce a measurable interaction between the composite material and adjacent EM fields--wherein this interaction could be measured without interference from conductive joints, leakage, or extraneous circuit elements.
- b) To be able to accommodate the effects of fiber orientation relative to the excitation fields.

The basic notion behind the slotted stripline is to produce a lossy transmission line. Standing wave pattern measurements on this line may then be used to determine electrical characteristics of the composite sample (conductivity, σ , in the case of graphite/epoxy, and perhaps complex permittivity, in the case of boron/epoxy and kevlar). Figure 3-6 illustrates the scheme.

Each half of the line approximates a parallel plate guided wave structure consisting of a lossy material (conductivity, σ) for one plate and a perfect conductor for the other plate with a spacing of "a" meters between them, as shown in Figure 3-8 (a). This structure is capable of propagating a "Quasi-TEM" wave in any direction parallel to the plate faces. The field structure between the faces for such waves is essentially identical to that in the lower half of the related parallel plate guide system shown in Figure 3-7, for waves propagating in the same direction. Guided wave systems such as that in Figure 3-8 (b) have been treated in the literature (3-2). These treatments provide

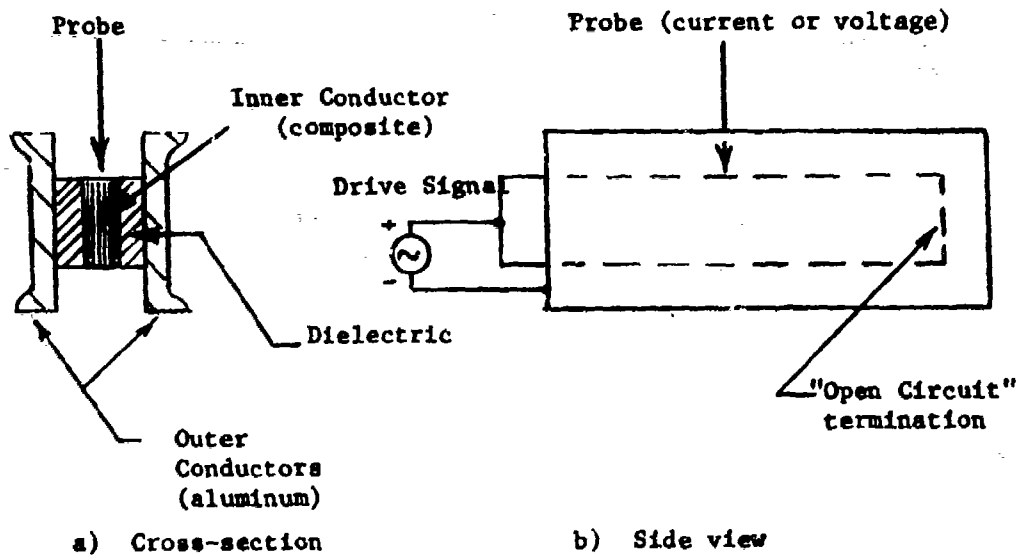


Figure 3-6 - Slotted Stripline

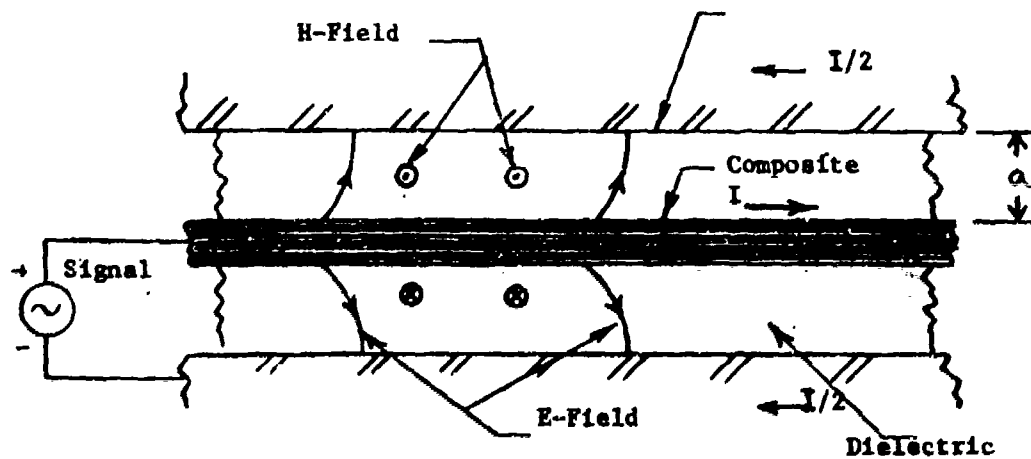


Figure 3-7 - Fields and Currents in the Stripline

the required relationships between propagation and lossy material characteristics which form the basis of the slotted stripline technique described here. The approach taken in Ramo, Whinnery and Van Duzer (3-2) will serve as a starting point for the development of the propagation characteristics of the slotted stripline.

Ramo, Whinnery, and Van Duzer define three propagation constants: γ , K_c and K_d which characterize sinusoidal field behavior in "Quasi-TEM" waves propagating between the plates shown in Figure 3-8 (b):

$\gamma = \alpha + j\beta$ = complex propagation factor in the direction parallel to the plates

$K_c^2 = \gamma^2 + \omega^2 \mu_0 \epsilon_c$ = (propagation factor)² in the lossy material in the direction normal to the plate surfaces

$K_d^2 = \gamma^2 + \omega^2 \mu_0 \epsilon_d$ = (propagation factor)² in the dielectric between the plates in a direction normal to the plate surfaces.

The parameters ϵ_c , ϵ_d , μ_0 and ω are:

ϵ_c = complex permittivity of the lossy material (F/m)

ϵ_d = permittivity of the dielectric (real) (F/m)

$\mu_0 = 4\pi \times 10^{-7}$ henries/meter

ω = radian frequency of the propagation wave.

Equation (7), p. 381 of Ramo, Whinnery and Van Duzer relates these parameters to the geometry of Figure 3-8 (b) as

$$\tan(k_d a) = j \frac{K_c \epsilon_d}{K_d \epsilon_c} \quad (3-A-1)$$

This equation results from matching boundary conditions on the E and H fields at the interface between the lossy plates and the dielectric. "a" is 1/2 the spacing between plates in Figure 3-8 (b) and equal to the spacing in Figure 3-8 (a) (and in the slotted line).

In the case of a lossy material such as the composites, the complex permittivity ϵ_c for the composite material can be expressed:

$$\epsilon_c = \epsilon_0 k'_c + \frac{\sigma_c}{j\omega} \quad (3-A-2)$$

where,

$$\epsilon_0 = 8.85 \times 10^{-12} \text{ farad/meter}$$

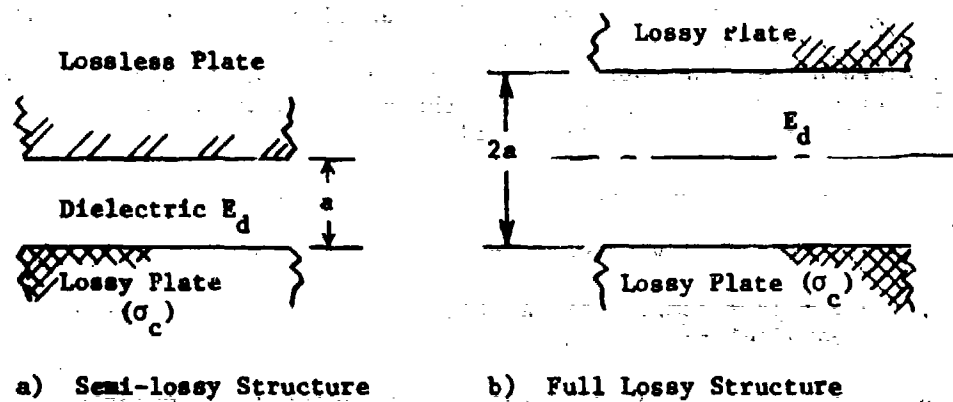


Figure 3-8 - Lossy Parallel Plate Guided Wave Structures

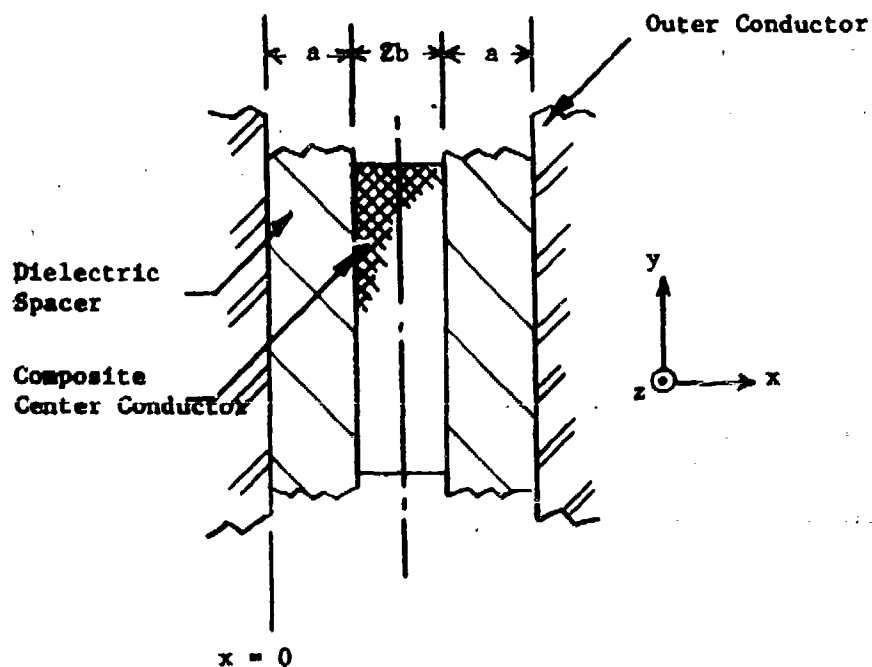


Figure 3-9 Transmission Line Cross Section

k'_c = real part of the composite material
dielectric constant (dimensionless)

σ_c = conductivity of the composite material
in the direction of propagation (mhos/m).

For graphite/epoxy and boron/epoxy with fibers running in the direction of propagation, it may be anticipated that the losses will be relatively low in the stripline so that γ^2 will be very nearly that for lossless boundaries. That is,

$$\gamma^2 \approx -\omega^2 \mu_0 \epsilon_d \quad (3-A-3)$$

Then since,

$$K_d^2 = \gamma^2 + \omega^2 \mu_0 \epsilon_d \quad (3-A-4)$$

it will be true that,

$$|K_d^2| \ll \omega^2 \mu_0 \epsilon_d \quad (3-A-5)$$

With a small spacing "a" between the plates, therefore, the term $(K_d a)$ will be much less than unity and the left hand side of equation (3-A-1) may be approximated by

$$\tan(K_d a) \approx K_d a \quad (3-A-6)$$

and there results,

$$K_d a \approx \frac{j K_c \epsilon_d}{K_d \epsilon_c} = \frac{-\omega \epsilon_d K_c}{j \omega \epsilon_c K_d} \quad (3-A-7)$$

or

$$K_d^2 a = \frac{-\omega \epsilon_d K_c}{j \omega \epsilon_c} \quad (3-A-8)$$

Recalling that ϵ_c is complex, the term $(j \omega \epsilon_c)$ is the "admittivity" of the composite material and may be written

$$j \omega \epsilon_c = (\sigma_c + j \omega \epsilon_0 k'_c)$$

Equation (3-A-8) then becomes,

$$K_d^2 a = \frac{-\omega \epsilon_d K_c}{(\sigma_c + j \omega \epsilon_0 k'_c)} \quad (3-A-9)$$

Now, recall that $K_c^2 = \gamma^2 + \omega^2 \mu_0 \epsilon_c = \gamma^2 - j\omega \mu_0 (\sigma_c + j\omega \epsilon_c k_c')$, so that even for $\sigma_c \approx 1$ mho/meter, $K_c^2 \approx -j\omega \mu_0 (\sigma_c + j\omega \epsilon_c k_c')$ for frequencies up through 10^{11} Hz. Using this approximation and squaring equation (3-A-9) yields,

$$K_d^4 a^2 = \frac{(-j\omega \mu_0) \omega^2 \epsilon_d^2}{(\sigma_c + j\omega \epsilon_c k_c')} \quad (3-A-10)$$

The term K_d^4 may be expressed in terms of the real and imaginary parts of the propagation factor, γ , where $\gamma = \alpha + j\beta$. That is,

$$K_d^2 = \gamma^2 + \omega^2 \mu_0 \epsilon_d = (\alpha^2 + \omega^2 \mu_0 \epsilon_d - \beta^2) + j2\alpha\beta. \quad (3-A-11)$$

Then the complex admittivity of the composite slab may be expressed as:

$$\hat{y}_c = (\sigma_c + j\omega \epsilon_c k_c') = \frac{(-j\omega \mu_0) \omega^2 \epsilon_d^2}{K_d^4 a^2} \quad (3-A-12)$$

Equations (3-A-11) and (3-A-12) form the basis of the use of the slotted stripline for the measurement of composite material admittivity. By measuring the lossy standing wave pattern along the line, the real (α) and imaginary (β) parts of the propagation factor, γ , may be determined, and these, together with a knowledge of the dielectric material (ϵ_d), and a , and the frequency, may be used in equations (3-A-11) and (3-A-12) to determine $(\sigma_c + j\omega \epsilon_c k_c')$.

In a practical example involving graphite/epoxy composites with unidirectional fibers running parallel to the direction of propagation, the following inequalities among α , β , and β_0 generally hold:

- a) β^2 is larger than β_0^2 but of the same order of magnitude
- b) $\beta_0^2 \gg \alpha^2$, where $\beta_0^2 = \omega^2 \mu_0 \epsilon_d$.

The result is that the angle of complex number K_d^4 in equation (3-A-12) is very sensitive to small percentage variations in the measurement of α or β . Correspondingly, the angle ascribed to $(\sigma_c + j\omega \epsilon_c k_c')$ by the measurement process may be questionable. However, the magnitude of the admittivity of the sample $|\sigma_c + j\omega \epsilon_c k_c'|$ will be given to about the same accuracy as the measurement accuracy of α and β individually.

Analysis for "Thick Skin-Depth"

The analysis above makes the tacit assumption that the conductivity of the composite-material center-conductor is sufficiently high so that

the skin-depth in the composite is much less than the actual thickness of the composite strip. This will be true at frequencies above 100 MHz for conductivities of 10^3 or more and composite strip thicknesses of 1.6×10^{-3} meters (1/16 inch) or more. If this is not the case, the analysis can be performed as follows.

Referring to Figure 3-9, and following a method similar to that above, one can postulate solutions in the composite conductor of the form:

$$E_{zc} = A \cos [K_c(x-a-b)], \text{ for } a < x < a + 2b$$

$$H_{yc} = \frac{-\hat{y}_c}{K_c^2} \frac{\partial E_{zc}}{\partial x} = \frac{A}{K_c} \hat{y}_c \sin [K_c(x-a-b)]. \quad (3-A-13)$$

In the dielectric spacer, let the fields be:

$$E_{zd} = B \sin (K_d x)$$

$$H_{yd} = \frac{-\hat{y}_d}{K_d^2} \frac{\partial E_{zd}}{\partial x} = \frac{-B \hat{y}_d}{K_d} \cos (K_d x). \quad (3-A-14)$$

The boundary conditions are:

a) At $x = 0$, $E_{zd} = 0$

(This is met by equation (14).)

b) At $x = a$, $E_{zc} = E_{zd}$, and $H_{yc} = H_{yd}$,

so that,

$$\frac{E_{zd}}{H_{yd}} = \frac{E_{zc}}{H_{yc}}.$$

This results in,

$$\frac{-K_d}{\hat{y}_d} \tan (K_d a) = \frac{-K_c}{\hat{y}_c} \cot (K_c b) \quad (3-A-15)$$

where,

$$K_d^2 = \gamma^2 + \omega^2 \mu_0 \epsilon_d$$

$$K_c^2 = \gamma^2 + j\omega\mu_0(\sigma_c + j\omega\epsilon_c)$$

$$\hat{\gamma}_c = \sigma_c + j\omega\epsilon_c \quad (3-A-16)$$

$$\gamma^2 = \alpha^2 + \beta^2$$

Equation (3-A-15) is a complex transcendental equation in the admittivity, $\hat{\gamma}$, of the composite strip and is more difficult to handle than equation (3-A-1). It may, however, be necessary to solve this for low conductivity composites.

Equation (3-A-15) may be solved numerically for $\hat{\gamma}$ as a function of γ using Newton-Raphson techniques. The starting value for this iterative method may be obtained from equation (3-A-12) for $\hat{\gamma}$ in Appendix 3-A. Another choice for a starting value is the DC conductivity of the sample. This numerical solution has been done.

3-B Computer Analysis of Measured Data

The slotted stripline method for parameter evaluation is described analytically in Appendix (3-A). The data derived from its use consists of measurements of the standing voltage (or current) wave resulting from the line geometry and the lossy composite center conductor. Figure 3-10 shows the situation schematically.

The standing wave phasor voltage $e(x)$ on a lossy terminated line will be:

$$e(x) = E_1 e^{+\gamma x} + E_r e^{-\gamma x} = E_1 [e^{\gamma x} (1 + \rho_L e^{-2\gamma x})] \quad (3-B-1)$$

Where:

E_1 = incident wave complex voltage

E_r = reflected wave complex voltage

$\gamma = \alpha + j\beta$ = complex propagation constant

$\rho_L = \frac{Z_L - Z_0}{Z_L + Z_0}$ = load reflection coefficient.

If the reflection coefficient, ρ_L , is represented in exponential form:

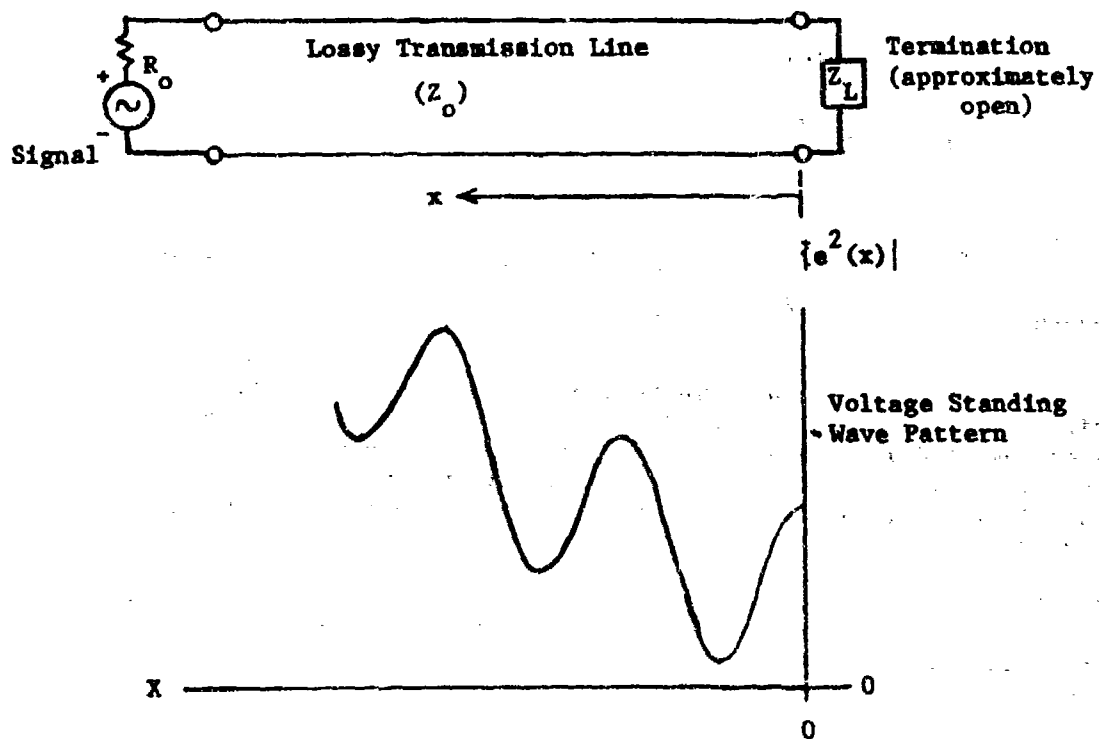


Figure 3-10 - Lossy Line Standing Waves

$$\rho_L = \epsilon^{-p} = \epsilon^{-2(u+j\phi)} \quad (3-B-2)$$

The voltage $e(x)$ is then,

$$e(x) = E_1 \epsilon^{-p/2} \left[\epsilon^{\left(\frac{p}{2} + \gamma x\right)} + \epsilon^{-\left(\frac{p}{2} + \gamma x\right)} \right]$$

or

$$e(x) = C \cosh [(u+\alpha x) + j(\phi+\beta x)], \quad (3-B-3)$$

where $C = E_1 \epsilon^{-p/2}$ = a complex constant.

Since standing wave measurements provide (usually) only the magnitude $|e(x)|$, it is convenient to work with $|e^2(x)|$ (i.e. the squared magnitude). The data taken from standing waves produced by a composite sample in the slotted stripline then form a table of values of $|e^2(x)|$ vs " x ", as measured by conventional standing wave measurement apparatus.

The function of the computer analysis to be described here is, primarily to identify the real (α) and the imaginary (β) components of the propagation constant, γ , from the squared standing-wave-voltage-record, $|e^2(x)|$.

By means of simple trigonometric and hyperbolic identities, equation (3-B-3) may be squared to produce,

$$|e^2(x)| = \frac{C^2}{2} \{ \cosh [2(u+\alpha x)] + \cos [2(\phi+\beta x)] \}. \quad (3-B-4)$$

The computer program produces a "minimum-mean-squared-error" fit of an expression such as that in the right hand side of (3-B-4) to the data record $|e^2(x)|$ by adjustment of the parameters: $|C^2/2|, \alpha, \beta, u$ and ϕ . If the data points are $\{y_n, x_n\} = \{|e^2(x_n)|, x_n\}$, and the test values of the "fitting function", $\{\hat{y}_n\}$ are:

$$\hat{y}_n = K \{ \cosh [2(u + \alpha x_n)] + \cos [2(\phi + \beta x_n)] \} \quad (3-B-5)$$

the error e_n at x_n will be:

$$e_n = y_n - \hat{y}_n \quad (3-B-6)$$

The sum-squared error ϵ , will then be

$$\epsilon = \sum_n e_n^2 = \sum_n (y_n - \hat{y}_n)^2 = \epsilon(K, \alpha, \beta, u, \phi) \quad (3-B-7)$$

The program then uses a "steepest descent" (i.e. gradient-directed) technique in $(K, \alpha, \beta, u, \phi)$ - space to successively adjust the parameters so as to minimize ϵ . Since the data $|e^2(x)|$ are subject to measurement error, the process is terminated when there is less than 1% change in ϵ over 30 successive adjustments of parameter values. The algorithms for the adjustment of parameter values are given below.

If $(K_m, \alpha_m, \beta_m, u_m, \phi_m)$ is the "mth" set of adjusted parameter values,

$$K_{m+1} = \frac{\sum_n y_n \{ \cosh [2(u_m + \alpha_m x_n)] + \cos [2(\phi_m + \beta_m x_n)] \}}{\sum_n \{ \cosh [2(u_m + \alpha_m x_n)] + \cos [2(\phi_m + \beta_m x_n)] \}^2}$$

$$\alpha_{m+1} = \alpha_m + \Delta K_{m+1} \sum_n e_n x_n \sinh [2(u_m + \alpha_m x_n)]$$

$$\beta_{m+1} = \beta_m - \Delta K_{m+1} \sum_n e_n x_n \sin [2(\phi_m + \beta_m x_n)] \quad (3-B-8)$$

$$u_{m+1} = u_m + \Delta K_{m+1} \sum_n e_n \sinh [2(u_m + \alpha_m x_n)]$$

$$\phi_{m+1} = \phi_m - \Delta K_{m+1} \sum_n e_n \sin [2(\phi_m + \beta_m x_n)]$$

where Δ = a gain factor controlling the step size.

Since the error is by no means a linear function of the adjustment parameters, the analytic determination of Δ to produce both rapid convergence and stability in the process is formidable, if not impracticable. It has instead been determined experimentally by exercising the program with a wide variety of representative data.

The program "EXTRACT" below accepts values of the squared magnitude $|e^2(x)|$ of the voltage $e(x)$ along the line together with the corresponding values of x (the distance from the "open" end of the line). It then estimates α and β from these values and computes $|V + j\omega L|$ from these estimates. The following table defines the various key parameters (i.e. input data) for the program.

$X(K)$ = distance, in meters, from the "open" end of the line at which values of $e(x)$ are measured

- Y(K) = $|e^2(x)|$ = squared magnitude of the line voltage measured at X(K)
- N = total number of data points taken
- ED = permittivity of the dielectric spacer used on the slotted line (e.g. $2.1 \times 8.85 \times 10^{-12}$ farads/meter for Teflon)
- UO = μ_0 = permeability of free space = $4\pi \times 10^{-7}$ henries per meter
- FFRQ = operating frequency in Hz
- SEP = dielectric spacer thickness in meters
- A(K) = a set of weighting coefficients for the data-smoothing function (e.g. 1,3,4,3,1). These coefficients "smooth" the input data points Y(K) to produce:

$$YS(K) = \frac{1}{12} \sum_{j=1}^5 Y(K + J - 3) A(J)$$

The process produces local weighted averaging without significantly disturbing the underlying standing wave pattern inherent in the data. (See lines 14.000 through 18.000 in the program).

The following quantities are output data from the program.

- T(I) = values of X(K) corresponding the maximum values of the smoothed data
- F(L) = maximum values of the smoothed data
- P(H) = values of X(V) corresponding to stationary values of the smoothed data (usually none)
- H(M) = stationary values of the smoothed data
- B(I) = values of X(K) corresponding to minimum values of the smoothed data
- E(I) = minimum values of the smoothed data
- AS = starting value of "a" (prior to the mean-square fit process)
- BS = starting value of "b" (prior to the mean-square fit process)
- CS = starting value of the constant "K" (see equation (3-b-5))

AM = mean-square estimate of " α "

BM = mean-square estimate of " β "

CM = mean-square estimate of K

UM = mean-square estimate of u (see equation (3-B-5))

RM = mean-square estimate of ϕ (see equation (3-B-5))

E(M) = ϵ = summed-squared error at the termination of the mean-square fit process

M = number of parameter adjustments necessary to meet the termination criterion.

```

1.000 C 'EXTRACT' - 'MEAN-SQUARE' ESTIMATION OF PROPAGATION FACTOR
1.100 C ENTRY OF DATA
1.500     REAL X(200),Y(200),YS(200),A(5),T(50),P(50),B(50)
2.000     REAL F(50),G(50),H(50),YM(200),EL(200),E(500)
3.000     READ(105,100)N
4.000     100 FORMAT(I3)
5.000     READ(105,110)ED
6.000     110 FORMAT(E12.5)
7.000     READ(105,120)UD
8.000     120 FORMAT(E12.5)
9.000     READ(105,125)FREQ
10.000    125 FORMAT(E10.3)
10.100    READ(105,130)SEP
10.200    130 FORMAT(E10.3)
11.000    READ(105,140)(A(K),K=1,5)
12.000    140 FORMAT(5F6.3)
12.100    READ(105,131)(X(K),K=1,N)
12.200    131 FORMAT(10F6.3)
12.300    READ(105,132)(Y(K),K=1,N)
12.350 C SMOOTHING OF DATA
12.400    132 FORMAT(10F6.3)
13.000    L=N-2
14.000    DO 142 J=3,L
15.000    YAM=0
16.000    DO 141 K=1,5
17.000    141 YAM=YAM+A(K)*Y(J-3+K)/12.
18.000    142 YS(J)=YAM
23.000    L=0
24.000    M=1
25.000    Z=0
26.000    J=N-3
27.000    DO 210 K=4,J
28.000    PROD=(YS(K+1)-YS(K))*(Y3(K)-YS(K-1))
29.000    IF (PROD)170,180,200
30.000    170 DIFF1=YS(K+1)-YS(K)

```

```

31.000      IF(DIFF1)171,171,172
32.000  171 L=L+1
33.000      T(L)=X(K)
34.000      F(L)=YS(K)
35.000      GO TO 210
36.000  172 I=I+1
37.000      B(I)=X(K)
38.000      G(I)=YS(K)
39.000      GO TO 210
40.000  180 DIFF2=YS(K)-YS(K-1)
41.000      IF(DIFF2)181,182,183
42.000  181 GO TO 210
43.000  182 DIFF1=YS(K+1)-YS(K)
44.000      IF(DIFF1)190,191,192
45.000  190 L=L+1
46.000      T(L)=X(K)
47.000      F(L)=YS(K)
48.000      GO TO 210
49.000  191 M=M+1
50.000      P(M)=X(K)
51.000      H(M)=YS(K)
52.000      GO TO 210
53.000  192 I=I+1
54.000      B(I)=X(K)
55.000      G(I)=YS(K)
56.000      GO TO 210
59.000  183 GO TO 210
60.000  200 GO TO 210
61.000  210 CONTINUE
62.000      WRITE(108,220)
63.000  220 FORMAT(4X,'T(L)',6X,'F(L)')
64.000      WRITE(108,230)(T(K),F(K),K=1,L)
65.000  230 FORMAT(2X,F6.3,4X,F6.3)
68.000      WRITE(108,240)
69.000  240 FORMAT(4X,'P(M)',6X,'H(M)')
70.000      WRITE(108,245)(P(K),H(K),K=1,M)
72.000  245 FORMAT(2X,F6.3,4X,F6.3)
73.000      WRITE(108,250)
74.000  250 FORMAT(4X,'B(I)',6X,'G(I)')
75.000      WRITE(108,255)(B(K),G(K),K=1,I)
76.000  255 FORMAT(2X,F6.3,4X,F6.3)
76.500 C CALCULATION OF STARTING VALUES:-AS,BB,CS
77.000      BB=6.2832*FREQ*(UD*ED)**0.5
78.000      LEM=L-2
79.000      IF (LEM) 270,260,260
80.000  260 AS=((F(2)-F(1))/(F(1)*T(2)**2.-F(2)*T(1)**2.))**0.5
81.000      CS=(F(2)/(1.+(T(2)*AS)**2.))/2.
92.000      GO TO 290
93.000  270 ITER=I-2
94.000      IF (ITER) 271,280,280
95.000  271 LEM=L-1

```

```

96.000      IF(LEM)272,273,273
97.000      272 XT=X(N-5)
98.000      YT=YS(N-5)
99.000      GO TO 274
100.000     273 XT=T(1)
101.000      YT=F(1)
102.000     274 X1=X(5)
103.000      Y1=YS(5)
104.000      AS=.0001
105.000      DELA=BS/10.
106.000     275 DTA=YT*(COSH(2.*AS*X1)+COS(2.*BS*X1))
106.100      DTB=Y1*(COSH(2.*AS*XT)+COS(2.*BS*XT))
106.200      DT=DTA-DTB
107.000      IF(DT)276,279,278
108.000     276 FRAC=DELA/AS-0.05
109.000      IF(FRAC)279,279,277
110.000     277 DELA=DELA/2.
111.000      AS=AS-DELA
112.000      GO TO 275
113.000     278 AS=AS+DELA
114.000      GO TO 275
115.000     279 CS=YT/(COSH(2.*AS*XT)+COS(2.*BS*XT))
116.000      GO TO 290
117.000     280 AS=(G(2)/(F(1)*B(2)**2.-G(2)*T(1)**2.))*0.5
118.000      CS=(F(1)*B(2)**2.-G(2)*T(1)**2.)/(2.*B(2)**2.)
119.000      GO TO 290
120.000     290 WRITE(108,295)AS,BS,CS
121.000     295 FORMAT(3X,'AS=',F6.3,3X,'BS=',F6.3,3X,'CS=',F6.3/)
122.000     C CALCULATION OF 'MEAN-SQUARE' FIT
123.000      DELTA=.01
124.000      UM=0
125.000      RM=0
126.000      AM=AS
127.000      BM=BS
128.000      CM=CS
129.000      M=1
130.000     296 DO 300 K=1,N
131.000      YM(K)=CM*(COSH(2.*(UM+AM*X(K)))+COS(2.*(RM+BM*X(K))))
132.000     300 EL(K)=Y(K)-YM(K)
133.000      E(M)=0
134.000     DO 310 K=1,N
135.000     310 E(M)=E(M)+EL(K)**2.
136.000      L=30
137.000      D=M-31
138.000      IF (D) 315,311,311
139.000     311 DEM=(E(M-L)-E(M))/E(M)
140.000      CHNG=.01-DEM
141.000      IF (CHNG) 315,340,340
142.000     315 TOP=500.-M
143.000      IF (TOP) 340,340,320
144.000     C ADJUSTMENT OF ALPHA BETA AND GAIN
145.000     320 CNUM=0
146.000

```

```

152.000      M=M+1
153.000      DO 325 J=1,N
154.000 325 CNUM=CNUM+Y(J)*(COSH(2.*(UM+AM*X(J)))+COS(2.*(RM+BM*X(J))
))
155.000      CDEN=0
156.000      DO 330 K=1,N
157.000 330 CDEN=CDEN+(COSH(2.*(UM+AM*X(K)))+COS(2.*(RM+BM*X(K))))**2
158.000      CM=(CNUM/CDEN)
159.000      DA=0
160.000      DO 331 K=1,N
161.000 331 DA=DA+EL(K)*CM*X(K)*SINH(2.*(UM+AM*X(K)))
162.000      AM=AM+DELTA*(DA/10.)
163.000 333 DB=0
164.000      DO 336 K=1,N
165.000 336 DB=DB+EL(K)*CM*X(K)*SIN(2.*(RM+BM*X(K)))
166.000      BM=BM-(DELTA*DB)
166.100      DUM=0
166.200      DO 337 K=1,N
166.300 337 DUM=DUM+EL(K)*CM*SINH(2.*(UM+AM*X(K)))
166.400      UM=UM+DELTA*(DUM/100.)
166.500      DRM=0
166.600      DO 338 K=1,N
166.700 338 DRM=DRM+EL(K)*CM*SIN(2.*(RM+BM*X(K)))
166.800      RM=RM-DELTA*(DRM/50.)
167.000      GO TO 296
168.000 C PRINT-OUT OF 'BEST-FIT' PARAMETERS
169.000 340 WRITE(108,341)AM,BM,CM
169.200 341 FORMAT('AM=',F6.3,2X,'BM=',F6.3,2X,'CM=',F6.3/)
169.400      WRITE(108,342)UM,RM
170.000 342 FORMAT('UM=',F6.4,2X,'RM=',F6.4/)
173.000      WRITE(108,355)E(M),M
174.000 355 FORMAT(3X,'E(M)=',F7.3,4X,'M=',I5//)
175.000      CD4=(AM**2.-BM**2.+BS**2.)*2.+4*(AM*BM)**2.
176.000      SIGMA=(6.2832*FREQ*ED*BS**2.)/(CD4*SEP**2.)
177.000      WRITE(108,360)SIGMA,FREQ
178.000 360 FORMAT(2X,'SIGMA=',E10.3,3X,'FREQUENCY=',E10.3)
179.000      STOP
180.000      END

```


3-C References:

- (1) C. Skouby, "Electromagnetic Effects of Advanced Composites", Final Report, (ONR), January 1975, Contract N00014-C-0200, McDonnell Aircraft Co.
- (2) S. Ramo, J. Whinnery, T. Van Duzer, "Fields and Waves in Communication Electronics", J. Wiley, 1965, pp 377-382.

4.0 ELECTROMAGNETIC SHIELDING EFFECTIVENESS OF ADVANCED COMPOSITE MATERIALS

4.1 INTRODUCTION

This section of the report presents results of a study of measurement and analytical technique to be used in the determination and interpretation of electromagnetic shielding effectiveness of advanced composite (e.g. fiber reinforced epoxy) materials. Most of the results are applicable to a wider range of materials including the usual metallic shields.

Advanced composite materials are inherently inhomogeneous and anisotropic from an electrical point of view. However, in many practical situations, particularly for multilayer shields at lower frequencies, the inhomogeneous, anisotropic character of the composite is relatively unimportant in determining its shielding properties. In such cases it is convenient to utilize "effective" or "averaged" electromagnetic material parameters to represent the composite. Section 4.3.4 of this report treats the measurement and interpretation of "effective" conductivity for multilayer composites. Section 4.4 presents a general method for dealing with the anisotropic effects in those cases where it becomes necessary.

Electromagnetic "shielding effectiveness" has historically [4-8] proven to be a deceptively illusive quantity to measure, to evaluate analytically or even to define unambiguously. Shielding depends not only on the intrinsic material parameters of the shield but also on shield geometry, properties of the impinging external signal (i.e., polarization, wave impedance, frequency, etc.) and properties of the output region. It is not uncommon for shielding numbers obtained on a given material from different measurement methods to differ by as much as 30 or 40 dB. Yet, aircraft design and evaluation clearly require accurate knowledge of the shielding capability of fabrication materials if threats from external electromagnetic signals to flight and mission critical systems are to be properly identified. The purpose of the current study is to examine techniques for measuring, interpreting and utilizing the shielding effectiveness data of advanced composite materials.

4.2 BACKGROUND

Shielding effectiveness (S.E.) is the insertion loss incurred by electromagnetic energy in passing from an input medium through a shield into an output medium. Both reflective and absorptive losses contribute to shielding effectiveness. Aircraft need substantial electromagnetic shielding to protect sensitive internal electronics from extraneous signals. Some vital areas particularly sensitive to inadequate shielding include low-level integrated circuit communication and navigation equipment, fly-by-wire systems, fire control systems, and electro-explosive devices.

In a typical situation the skin of the aircraft might be considered the shield with the air external to the vehicle as the input medium and a complex varying mixture of personnel, air, cables, electronic devices, fittings, etc. of the aircraft's interior as the output region. The

external electromagnetic field to be excluded from the interior of the shield might be produced by any of a variety of electromagnetic sources including a direct lightning strike to the aircraft, a nearby lightning strike, a nearby radar or other high powered transmitter, or perhaps by a nuclear detonation (EMP).

For a perfect shield the insertion loss (or shielding effectiveness) between input and output sides of the shield would be infinitely large. In practice, it is exceptional to find shields with greater than 100 dB shielding effectiveness; and for a metal aircraft with the usual apertures, seams and cracks, effective overall shielding of the order of 20 dB is common at UHF frequencies. Metals are in general good electromagnetic shields. Commonly used composite materials, composed typically of small, relatively poorly conducting fibers embedded in an insulating matrix, provide considerably less shielding particularly at lower frequencies. Metal matrix composite materials are being studied [4-3] but are still in an early stage of development and are not considered further in this report. From the point of view of electromagnetic shielding metal matrix composites would clearly be superior.

4.3 MEASUREMENT TECHNIQUES AND THEORY

Several measurement techniques that have been used in determining the shielding effectiveness of advanced composite materials are presented and mathematical approximations are introduced to provide analytical relationships between the methods. In some cases it is also possible to extract, rather simply, values of intrinsic parameters (particularly "effective" conductivity) from measured values of shielding. "Effective" implies that the pertinent parameter has been averaged to suppress anisotropic and/or inhomogeneous characteristics. Some discussion of advantages and limitations of various methods is also included.

4.3.1 Plane Wave Normally Incident on Infinite Flat Plate

This idealized configuration, shown in Figure 4-1, provides a useful "reference" standard as well as an approximate model of a number of more complex measurement configurations. In this preliminary work, it is assumed as a first step that the shield material is homogeneous and is isotropic in the plane of the shield. This hypothesis appears to include multilayer graphite epoxy laminates in which the layers are oriented at different angles (e.g. $0^\circ - 90^\circ - 0^\circ$, etc.). Unidirectional laminates and perhaps even multilayer mixed orientation boron require a different hypothesis taking into account the three-dimensional anisotropy effects. The less complex behavior of the multilayer, mixed-orientation graphite laminates arises from the fiber-to-fiber contact between layers observed in present materials. The more complex unidirectional layer model has also been studied and results are presented in Section 4.4 of this report.

Using the well-known transmission-line analogy [4-1] for plane wave propagation as shown schematically in Figure 4-1(a-c), the overall ABCD matrix for the shield with the effects of the output medium included is given by:

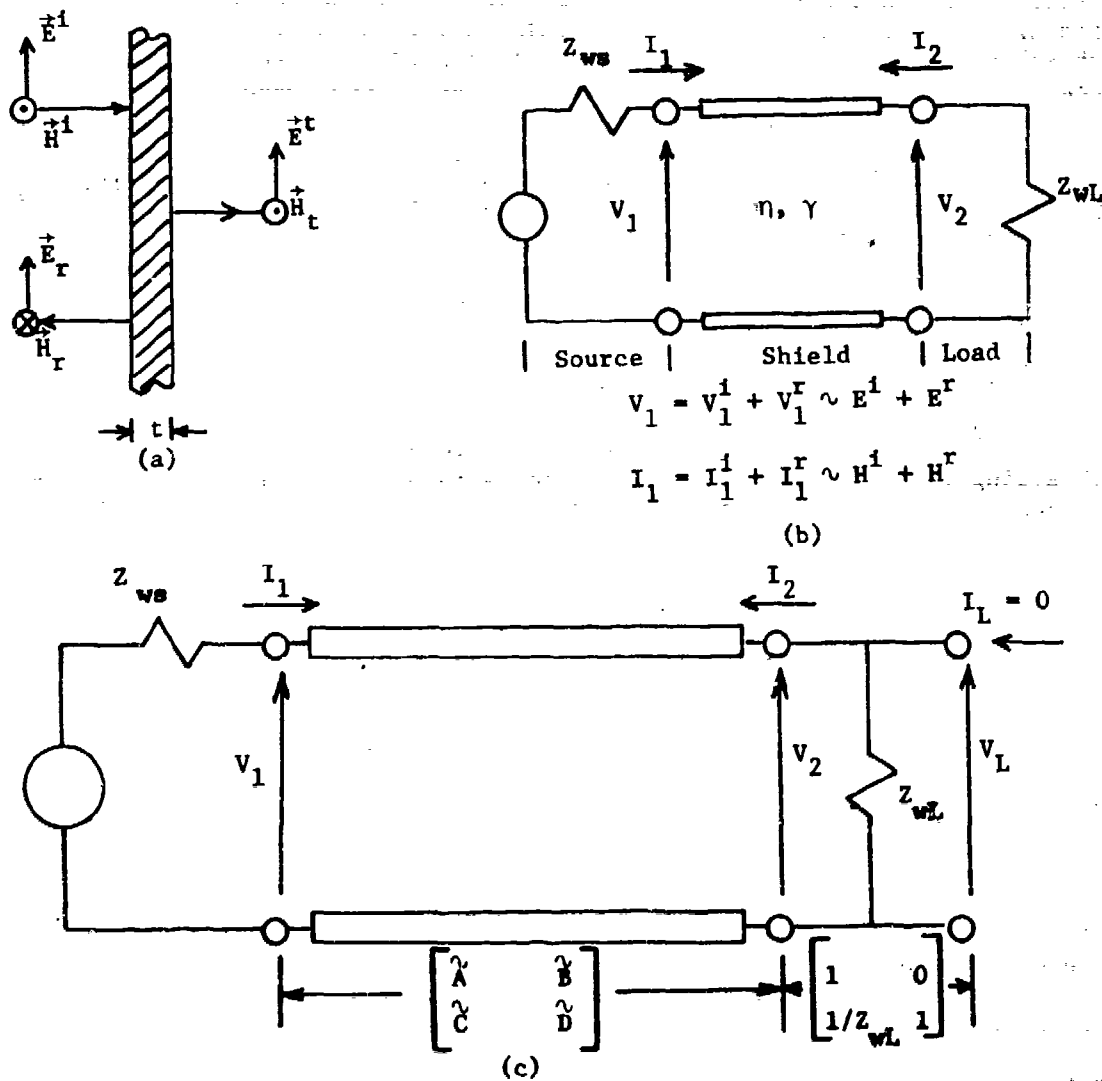


Figure 4-1. a) Elementary Plane Wave Shielding
b) Transmission Line Analogy
c) ABCD Parameter Representation

$$\begin{bmatrix} A_T & B_T \\ C_T & D_T \end{bmatrix} = \begin{bmatrix} \tilde{A} & \tilde{B} \\ \tilde{C} & \tilde{D} \end{bmatrix} \begin{bmatrix} 1 & 0 \\ \frac{1}{Z_{WL}} & 1 \end{bmatrix} = \begin{bmatrix} (\tilde{A} + \frac{\tilde{B}}{Z_{WL}}) & \tilde{B} \\ (\tilde{C} + \frac{\tilde{D}}{Z_{WL}}) & \tilde{D} \end{bmatrix} \quad (4-1)$$

where $\tilde{A} = \tilde{D} = \cosh \theta$

$$\tilde{B} = \eta \sinh \theta$$

$$\tilde{C} = 1/\eta \sinh \theta$$

Thus,

$$\begin{bmatrix} V_1 \\ I_1 \end{bmatrix} = \begin{bmatrix} A_T & B_T \\ C_T & D_T \end{bmatrix} \begin{bmatrix} V_L \\ -I_L \end{bmatrix} \quad \text{where } I_L = 0. \quad (4-2)$$

$$V_1 = V_1^i + V_1^r = V_1^i (1 + \rho_{in}) \quad (4-3)$$

$$I_1 = I_1^i + I_1^r = \frac{V_1^i}{Z_{ws}} (1 - \rho_{in})$$

$$\rho_{in} = \frac{Z_{in} - Z_{ws}}{Z_{in} + Z_{ws}} = \frac{\frac{V_1}{I_1} - Z_{ws}}{\frac{V_1}{I_1} + Z_{ws}} = \frac{A_T - Z_{ws} C_T}{A_T + Z_{ws} C_T} = \text{Input Reflection Coefficient}$$

where the circuit quantities are defined in Figure 4-1.

Substituting from equations (4-1) and (4-3) and (4-2) and solving for

$$\frac{V_1^i}{V_2} \text{ and } \frac{-I_1^i}{I_2} \text{ yields:}$$

$$\frac{V_1^i}{V_2} = \frac{1}{2} \left\{ \left[1 + \frac{Z_{ws}}{Z_{WL}} \right] \cosh \theta + \left[\frac{\eta}{Z_{WL}} + \frac{Z_{ws}}{\eta} \right] \sinh \theta \right\} \quad (4-4)$$

= Reciprocal of the electric shielding ratio

$$\frac{-I_1^i}{I_2} = \frac{1}{2} \left\{ \left[\frac{Z_{WL}}{Z_{ws}} + 1 \right] \cosh \theta + \left[\frac{\eta}{Z_{ws}} + \frac{Z_{WL}}{\eta} \right] \sinh \theta \right\} \quad (4-5)$$

= Reciprocal of the magnetic shielding ratio.

Then,

$$\text{Magnetic Shielding Effectiveness} = -20 \log_{10} \left| \frac{I_2}{-I_1} \right| \text{ and} \quad (4-6)$$

$$\text{Electric Shielding Effectiveness} = -20 \log_{10} \left| \frac{V_2}{V_1} \right|. \quad (4-7)$$

Notice that magnetic and electric shielding ratios are identical if $Z_{ws} = Z_{wL}$, i.e., for $Z_{wL} = Z_{ws} = Z_0$, the inverse ratios are

$$\frac{V_1}{V_2} = \frac{-I_1}{I_2} = \cosh \theta + \frac{1}{2} \left(\frac{\eta}{Z_0} + \frac{Z_0}{\eta} \right) \sinh \theta. \quad (4-8)$$

By proper choice of Z_{wL} and Z_{ws} to match the incident wave characteristics, it is possible to use equations (4-4), (4-5), and (4-8) as very good approximations to a number of other more complex shielding configurations. Physically this is true because the wavelength is typically much smaller within the shield material than outside, in most shield configurations shield thickness is small compared with shield radii of curvature, and to the characteristics of sources utilized in certain measurement structures.

The plane wave shielding given above is used as a "reference" throughout this report. Each new configuration is, where possible, mathematically related to the reference plane-wave configuration. For example, as will be shown, it is possible to relate both transfer impedance and two-loop/flat plate data to the above model.

The transmission-line model can be extended to handle plane waves incident at oblique angles [4-1]. The required modification is straight forward, and only the characteristic impedance and propagation factor must be changed.

4.3.2 Two-loop/Infinite Flat Plate Configuration

This configuration (Figure 4-2), with the two loops parallel to the flat plate having a common axis and spaced such that the flat plate lies in the near field of the loops, is closely related to several popular and useful configurations for measuring the shielding effectiveness to low-impedance waves. The low-impedance (magnetic field dominates) waves as viewed at the flat plate result from being in the near field of the loops. Note that the wave impedance of the impinging wave varies over the surface of the plate as a function of distance from the source. If the coil-to-plate spacing is a small fraction of a wave length, most of the energy is concentrated within a narrow zone under the coil so that in approximate representations a constant source wave impedance may be used with little error.

Shielding data from configurations of this type for fiber-reinforced laminates have simple interpretations only for materials which are essentially isotropic in the plane of the flat plate, e. g. for multi-layer,

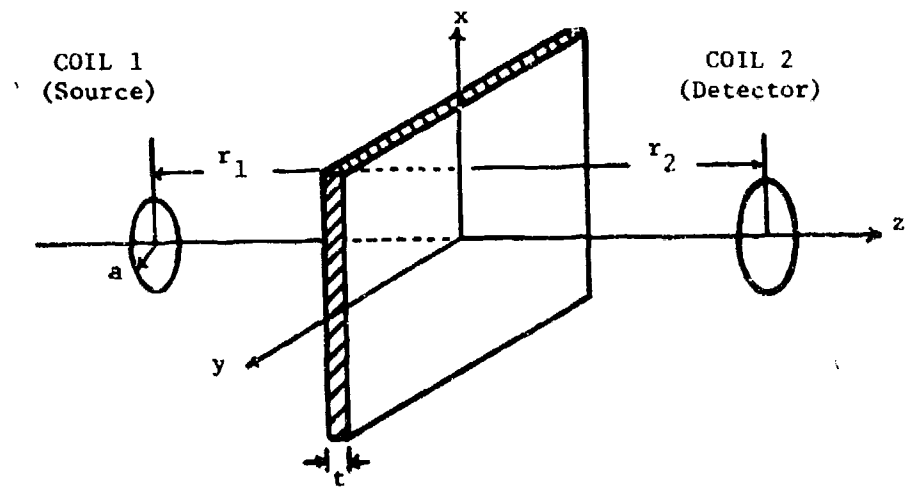


Figure 4-2. Two-loop/Infinite Flat Plate Configuration

mixed orientation graphite laminates but not for unidirectional samples. This restriction is a consequence of the need for roughly circular currents to flow in the plane of the flat plate if the incident magnetic field (which is largely perpendicular to the plate) is to be terminated.

Configurations for which the two-loop/infinite flat plate configuration serves as a useful approximate model include a variety of box-like structures [4-2] with the flat plate shield forming a partition and undesired leakage between loops inhibited by the enclosure. Such configurations are typically used at frequencies below 100 MHz. Care must be taken, however, since box resonances can obscure the shield's properties.

Mcser [4-3] and Bannister [4-4, 4-5] have provided an integral equation solution for the shielding effectiveness of the two-loop/infinite flat plate geometry assuming uniform current in the loops. It is assumed that the shield is a good enough conductor that displacement currents in the shield can be neglected. The complete expression for shielding effectiveness as given by Bannister is given in Appendix 4-A.

As shown in Appendix 4-A, if it is assumed that $r' < \frac{\lambda_{air}}{20}$, $\tau_r t > 2$, $\tau_r r' > 10$, $\frac{\tau_r r'}{\mu_r} > 10$, $z \gg t$ and $z \gg a$, where the quantities are defined in the appendix, then

$$S.E._{dB} \approx 8.686\sqrt{2} \tau_r t + 20 \log_{10} \left(\frac{\tau_r z}{8.485 \mu_r} \right) . \quad (4-9)$$

This equation can be shown to be of the same form as the plane wave shielding equation provided an appropriate near-field value is used for the source and load wave impedances. Equation (4-8) for plane wave shielding can be cast in the well-known Schelkunoff form [4-6] using the following parameter definitions:

$$\begin{aligned} k &= \frac{Z_0}{\eta} & q &= \left(\frac{k-1}{k+1} \right)^2 \\ p &= \frac{4k}{(k+1)^2} \end{aligned} \quad (4-10)$$

Using the above parameters equation (4-8) can be written as:

$$\frac{\text{Inverse Shielding}}{\text{Ratio}} = \frac{1}{p} (1 - q e^{-2\theta}) e^{\theta} . \quad (4-11)$$

Shielding effectiveness is then:

$$S.E._{dB} = 20 \log_{10} \left| \frac{1}{p} (1 - q e^{-2\theta}) e^{\theta} \right| . \quad (4-12)$$

For the present situation, using $Z_0 = j\omega \mu_0 r_1$ and recognizing $|k| \gg 1$, it follows that $q \approx 1$ and $\frac{1}{p} \approx k/4$. Furthermore, for $\tau_r t > 2$, the term $20 \log_{10} |1 - q e^{-2\theta}|$ is negligible. Thus, equation (4-12) becomes:

$$S. E._{dB} \approx 8.686\sqrt{2}\tau_r t + 20 \log_{10} \left(\frac{\tau_r r_1}{2.828\mu_r} \right) \quad (4-13)$$

Following Moser, to compensate for the fact that the near field characteristic wave impedance is actually not constant over the shield, let $r_1 = z/3$. Then equation (4-13) becomes identical with the simplified Moser formula of equation (4-9). This indicates that under a class of important measurement conditions the plane-wave shielding equations with appropriate source and load wave impedances yield excellent results. The transmission line analogy thus applies to the configurations discussed in Sections 4.3.1 and 4.3.2. Frequently a symmetric arrangement with $r_1 = r_2 = z/2$ is utilized in measurements.

4.3.3 Quasistatic Shielding Formulas for Electrically Thin-Shell Ellipsoids

The boundary value problems for certain ellipsoidal-shell shields geometries as shown in Figure 4-3 have been solved and the corresponding magnetic shielding effectiveness calculated [4-7]. Following King, formulas for each of the ellipsoidal and degenerate ellipsoidal shielding formulas can be obtained in the same form as the plane wave shielding equations. These formulas are useful in interpreting measured data from flat-plate and quadrax structures as well as spheres and closed cylinders. Using the notation developed for the plane wave shielding equations (4-4), (4-5) and (4-8), the King equations for shielding to low-impedance impinging waves can be placed in the form

$$\text{Inverse Magnetic Shielding Ratio} \approx \cosh \theta + \frac{Z_M}{2\eta} \sinh \theta \quad (4-14)$$

A similar relationship can be derived for high wave-impedance impinging signals. The equation is of the same form as the above case but with a different wave impedance for the impinging signal.

$$\text{Inverse Electric Shielding Ratio} \approx \cosh \theta + \frac{Z_E}{2\eta} \sinh \theta \quad (4-15)$$

Equation (4-15) is different from that given by Boeing [4-2] but reduces to the Boeing form as a special case.

4.3.4 Surface Transfer Impedance and Effective Conductivity

Surface transfer impedance has been used for many years as a measure of shielding effectiveness. Combined with other "two-port" parameters it can also be used to characterize shielding materials in computer-aided analysis programs for determining interior and scattered fields of complex geometrical structures [4-8]. For shields which are thin compared to the radii of curvature of the shield and for which wavelength within the shield is much smaller than that external to the shield, the electromagnetic behavior of the shield is essentially a local phenomena. Each local region may then be considered planar [4-6]. For a planar shield, the two-port parameters are given in Figure 4-4.

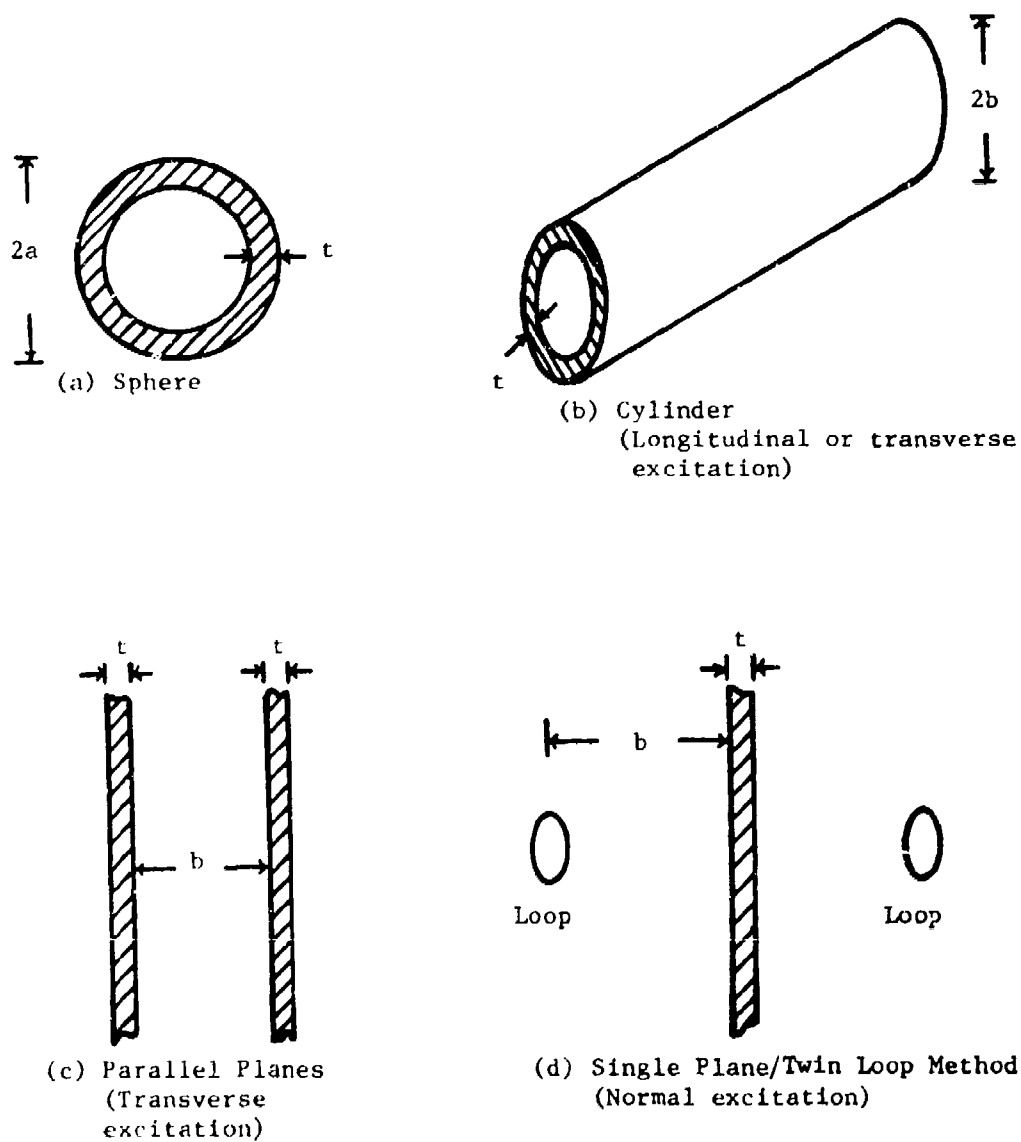
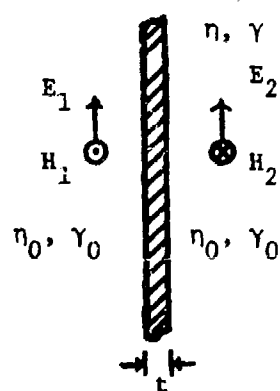


Figure 4-3. Quasistatic Ellipsoidal Shields.



$$E_1 = z_{11}H_1 + z_{12}H_2$$

$$E_2 = z_{21}H_1 + z_{22}H_2$$

$$\text{where } z_{11} = z_{22} = \eta \coth \phi$$

$$z_{12} = z_{21} = \eta \operatorname{csch} \phi$$

$$\theta = \gamma t$$

η = wave impedance of shield

γ = propagation factor of shield

Figure 4-4. Two-port Impedance Representation

The impedances Z_{12} and Z_{21} are known as surface transfer impedances since they relate field values at opposite interfaces of the shield. Surface transfer impedance is frequently measured using triaxial or quadraxial configurations [4-2] and the data are reduced using the Schelkunoff theory [4-6]. From Figure 4-4 surface transfer impedance written with the new symbol Z_s becomes:

$$Z_s = \eta \operatorname{csch} \theta \quad (4-16)$$

Surface transfer impedance can be related to the two-loop/flat-plate configuration through use of the approximations for Equation (4-9) or the equivalent Equation (4-14) as follows

$$\begin{array}{l} \text{Inverse Magnetic} \\ \text{Shielding Ratio} \end{array} = R \approx \cosh \theta + \frac{Z_M}{2\eta} \sinh \theta \quad (4-17)$$

Substituting $\frac{\sinh \theta}{\eta} = \frac{1}{\eta \operatorname{csch} \theta} = \frac{1}{Z_s}$ yields

$$R \approx \cosh \theta + \frac{Z_M}{2Z_s} \quad (4-18)$$

Thus,

$$Z_s \approx \frac{Z_M}{2(R - \cosh \theta)} \quad (4-19)$$

For good shields $\cosh \theta \approx 1$ at low frequencies where θ is small and at high frequencies R is much larger than $\cosh \theta$. Thus, for reasonably good shields Z_s can be written in terms of the shielding effectiveness measured in the two-loop/flat-plate configuration as

$$Z_s \approx \frac{Z_M}{2(R-1)} \quad (4-20)$$

where R is obtained from the shielding measurement as

$$R = 10^{\frac{SE_{dB}}{20}}$$

At frequencies where θ is sufficiently small such that $\sinh \theta$ can be replaced by θ , it is possible to determine an effective conductivity directly from Z_s in a very simple manner. Such scalar conductivity numbers, as mentioned earlier, seem meaningful for multi-ply, mixed orientation, graphite laminates, but not for unidirectional graphite laminates. Assuming a scalar effective conductivity σ_{eff} in the plane of the laminate and recognizing that for reasonably good conductors

$$\gamma = (1+j) \sqrt{\pi f \mu \sigma_{\text{eff}}} = \sigma_{\text{eff}} \eta,$$

then

$$Z_s = \frac{\eta}{\sinh \theta} = \frac{(1+j) \sqrt{\frac{\pi f \mu}{\sigma_{\text{eff}}}}}{\sinh[(1+j)t \sqrt{\pi f \mu \sigma_{\text{eff}}}]}$$
 (4-21)

For small θ , $\sinh \theta \approx \theta$, so that

$$Z_s \approx \frac{(1+j) \sqrt{\frac{\pi f \mu}{\sigma_{\text{eff}}}}}{t(1+j) \sqrt{\pi f \mu \sigma_{\text{eff}}}} = \frac{1}{\sigma_{\text{eff}} t}$$
 (4-22)

Thus, for small θ

$$\sigma_{\text{eff}} \approx \frac{1}{t Z_s}$$
 (4-23)

For larger θ , σ can be obtained by solving the transcendental equation

$$Z_s \sinh \theta - \eta = 0$$
 (4-24)

The phase of Z_s has not been measured in past experiments, but would clearly be needed if Z_s were to be used to characterize a material in system analysis programs.

The form of the approximation given in Equation (4-23) is in excellent agreement with measured data given by Boeing [4-2] with varying thickness. Calculated conductivities seem to be in agreement with results from on-going measurements by other techniques discussed in Sections 2.0 and 3.0.

As an example of the correspondance between two-loop/flat-plate measurements and surface transfer impedance measurements, consider the 24-ply T-300/5208 graphite samples measured by Boeing [4-2]. The samples were cross-ply layups (0°/45°/90°).

At 1 MHz the measured magnetic shielding from the two-loop/flat-plate configuration is M.S.E. = 16 dB. Thus, $R = 10^{0.8} = 6.31$ and for a loop-to-plate spacing of 1 inch and $|Z_M| = |j\omega \mu_0 b| = 0.201$ ohm.

$$\text{Then } |Z_s| \approx \frac{Z_M}{2(R-1)} = \frac{0.201}{2(5.31)} \approx 1.9 \times 10^{-2} \text{ ohm}$$

as calculated from the two-loop/flat-plate measurement data. The corresponding 1 MHz direct measured value of surface transfer impedance is

$$|Z_s| \approx 1.8 \times 10^{-2} \text{ ohm}$$

as measured in the quadrx configuration. The agreement is excellent.

For the same material at 1 MHz

$$\sigma_{\text{eff}} \approx \frac{1}{|Z_s|t} = \frac{1}{(1.8 \times 10^{-2})(24 \times 5.25 \times 10^{-3} \times 2.54 \times 10^{-2})} \approx 1.73 \times 10^4 \text{ mhos/m}$$

for T-300/5208 Cross-ply layup at 1 MHz.

Similar calculations for 12-ply HTS/5208 graphite show excellent agreement between flat-plate and quadrx data and indicate

$$\sigma_{\text{eff}} \approx 1.5 \times 10^4 \text{ mhos/m}$$

for HTS/5208 cross-ply layup at 1 MHz.

4.3.5 Transverse Flat Plate Samples in Waveguide and Transmission Line Structures

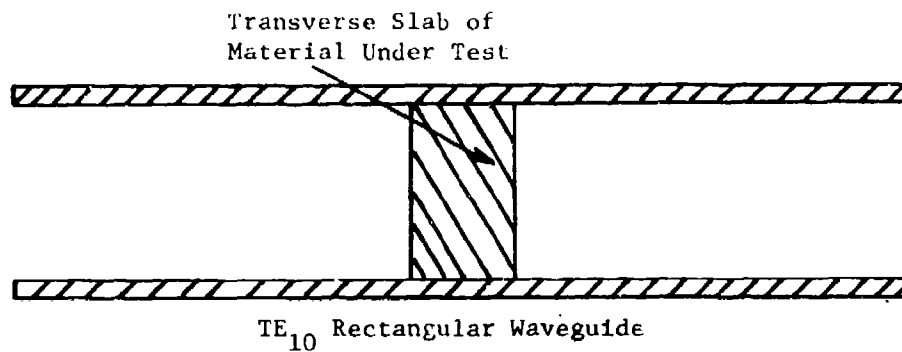
Transmission loss and phase measurements on a flat plate sample completely filling the transverse section of a waveguide or transmission line structure can be utilized to characterize a material electromagnetically [4-10]. Provided the reflections from the sample are not too large, conductivity and permittivity can be determined analytically from the measured insertion loss and phase. Reference [4-10] provides a complete discussion on limitations of the solution procedure. Typical arrangements for rectangular waveguide and coaxial line structures are shown in Figure 4-5. The analysis of these and other structures can be carried out simultaneously through the use of the generalized transmission line analogy [4-6].

4.3.5.1 General Case

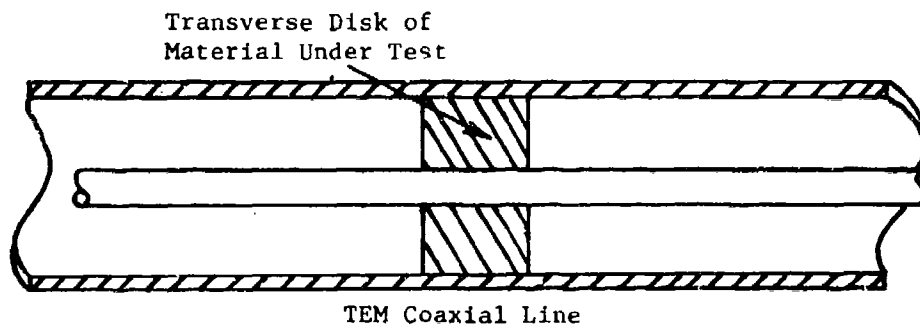
Following Schelkunoff's procedure [4-6], let each section of the measurement structure be represented by a section of generalized transmission line. The geometry being discussed is shown in Figure 4-6. The characteristic impedances of the equivalent transmission lines are interpreted as the wave impedance of the actual structure. Equivalent transmission line propagation factors are equal to the corresponding factor of the real structure.

From Figure 4-6,

$$\begin{bmatrix} V_P \\ I_P \end{bmatrix} = \begin{bmatrix} \tilde{A} & \tilde{R} \\ \tilde{C} & \tilde{D} \end{bmatrix} \begin{bmatrix} V_Q \\ I_Q \end{bmatrix} \quad (4-25)$$



(a)



(b)

Figure 4-5. Two Types of Measurement Structures Included in the Generalized Analysis

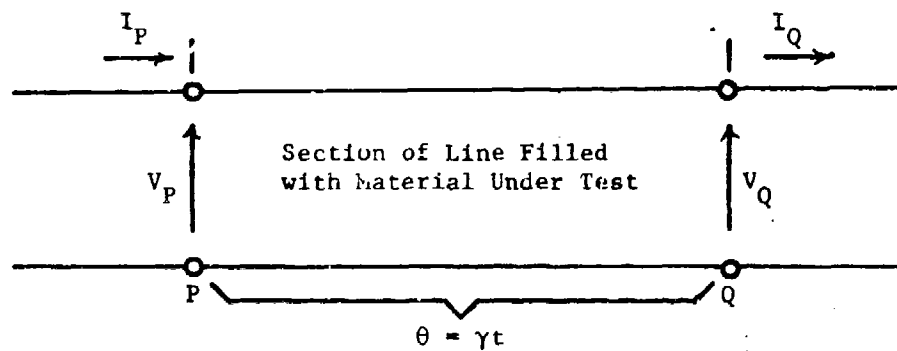


Figure 4-6. Generalized Transmission Line Model for Measurement Structure. Note:

$$V_P = V_i + V_r, I_P = I_i + I_r$$

where

$$\begin{aligned} I_Q &= V_Q / Z_{03} & \theta &= \gamma t \\ \tilde{A} &= \cosh \theta & \tilde{B} &= Z_{02} \sinh \theta \\ \tilde{C} &= \frac{\sinh \theta}{Z_{02}} & \tilde{D} &= \cosh \theta \end{aligned}$$

From equations (4-25), it can be shown that

$$\frac{I_Q}{I_P} = \frac{Z_{02}}{Z_{02} \cosh \theta + Z_{03} \sinh \theta} \quad (4-26)$$

$$\frac{V_Q}{V_P} = \frac{Z_{03}}{Z_{03} \cosh \theta + Z_{02} \sinh \theta} \quad (4-27)$$

Let the total impedance at P looking toward Q be equal to Z_P (note, Z_P includes effects of both interfaces). Then,

$$V_P = \tau_V V_1 = \frac{2 Z_P}{Z_{01} + Z_P} V_1 \quad (4-28)$$

$$I_P = \tau_I I_1 = \frac{2 Z_{01}}{Z_{01} + Z_P} I_1 \quad (4-29)$$

where V_1 , I_1 are the incident voltage and current, respectively, and

$$Z_P = Z_{02} \left[\frac{Z_{03} \cosh \theta + Z_{02} \sinh \theta}{Z_{02} \cosh \theta + Z_{03} \sinh \theta} \right] = \frac{V_P}{I_P} \quad (4-30)$$

Replacing $\cosh \theta$ and $\sinh \theta$ by their exponential equivalents and substituting from equations (4-26) to (4-30) into equation (4-25), the following result is obtained (after considerable algebra).

$$\tau_I = \frac{I_Q}{I_1} = \frac{(1 + \rho_{V,P})(1 - \rho_{V,Q}) e^{-\theta}}{1 - \rho_{V,P} \rho_{V,Q} e^{-2\theta}} \quad (4-31)$$

where T_I = Overall current transmission coefficient across the section PQ

$$\rho_{v,P} = \frac{Z_{01} - Z_{02}}{Z_{01} + Z_{02}} = \text{Interface voltage reflection coefficient at P}$$

$$\rho_{v,Q} = \frac{Z_{03} - Z_{02}}{Z_{03} + Z_{02}} = \text{Interface voltage reflection coefficient at Q.}$$

It can be shown that the overall voltage transmission coefficient across the section PQ is

$$T_V = \frac{V_Q}{V_1} = \frac{Z_{03}}{Z_{01}} T_I. \quad (4-32)$$

If structures 1 and 3 are identical then

$$T = T_I = T_V = \frac{(1 - \rho_v^2) \epsilon^{-\theta}}{1 - \rho_v^2 \epsilon^{-2\theta}} \quad (4-33)$$

$$\text{where } \rho_v = \frac{Z_{01} - Z_{02}}{Z_{01} + Z_{02}}.$$

Insertion loss is thus

$$I.L. = -20 \log_{10} |T| \quad (4-34)$$

and the insertion phase is

$$\Delta\phi = \angle T = \text{Angle of Transmission Coefficient.}$$

Given measured values of insertion loss and insertion phase for a specified structure equation (4-33) can be solved for the conductivity and the real part of the permittivity of the material under test. This procedure is demonstrated in Section 4.3.5.2 for a rectangular waveguide measurement system.

4.3.5.2 Rectangular Waveguide

As a particular case of the preceeding analysis, let the transmission structure be TE_{10} rectangular waveguide with region 2 consisting of a section of guide of width "a", height "b" and length "t", totally filled with the material under test. Further assume that the material can be represented as a lossy dielectric with $\mu = \mu_0$, $\epsilon = \epsilon_0 \epsilon' (1 - j \tan \delta)$. $\tan \delta$ is the loss tangent of the material and ϵ' is the real part of the permittivity. Regions 1 and 3 are air-filled and have the same width and height as section 2.

$$Z_{TE}^1 = \frac{\eta_0}{\sqrt{1 - \left(\frac{\lambda_0}{\lambda_c}\right)^2}} = \text{Wave impedance of regions 1 and 3} \quad (4-36)$$

$$Z_{TE}^2 = \frac{\eta_2}{\sqrt{1 - \left(\frac{\lambda_2}{\lambda_c}\right)^2}} = \frac{1}{\sqrt{\epsilon_r}} \frac{\eta_0}{\sqrt{1 - \left(\frac{\lambda_0}{\sqrt{\epsilon_r} \lambda_c}\right)^2}} = \text{Wave impedance of region 2} \quad (4-37)$$

$$\text{where } \eta_0 = \sqrt{\frac{\mu_0}{\epsilon_0}} \quad \eta_2 = \sqrt{\frac{\mu_0}{\epsilon_2}}$$

$$\epsilon_r = \epsilon'_r (1 - j \tan \delta) \quad \lambda_2 = \frac{\lambda_0}{\sqrt{\epsilon_r}}$$

λ_0 = wavelength in freespace at measurement frequency

λ_c = cutoff wavelength (e.g. $2a$ in air-filled waveguide)

Also,

$$\rho_v = \frac{Z_{TE}^1 - Z_{TE}^2}{Z_{TE}^1 + Z_{TE}^2} \quad (4-38)$$

$$\Theta = \gamma t = j\omega \sqrt{\mu_0 \epsilon_0} \sqrt{\epsilon_r - \left(\frac{\lambda_0}{\lambda_c}\right)^2} t, \quad (4-39)$$

Substitution into equation (4-33) yields the desired result.

Given measured values of insertion loss and phase, equation (4-33) can now be solved for ϵ'_r and $\tan \delta$. The conductivity, σ , is related to the loss tangent, $\tan \delta$, by $\sigma = \omega \epsilon'_r \epsilon_0 \tan \delta$. An iterative numerical procedure [4-11] is used to solve equation (4-33). For relatively high conductivity materials such as graphite epoxy, insertion loss and phase are quite insensitive to variations in ϵ'_r , as shown in Figure 4-7. It is then exceptionally difficult to determine accurate values of ϵ'_r from measured insertion loss and phase by solving equation (4-33). If ϵ'_r is independently known, accurate conductivity values can be obtained.

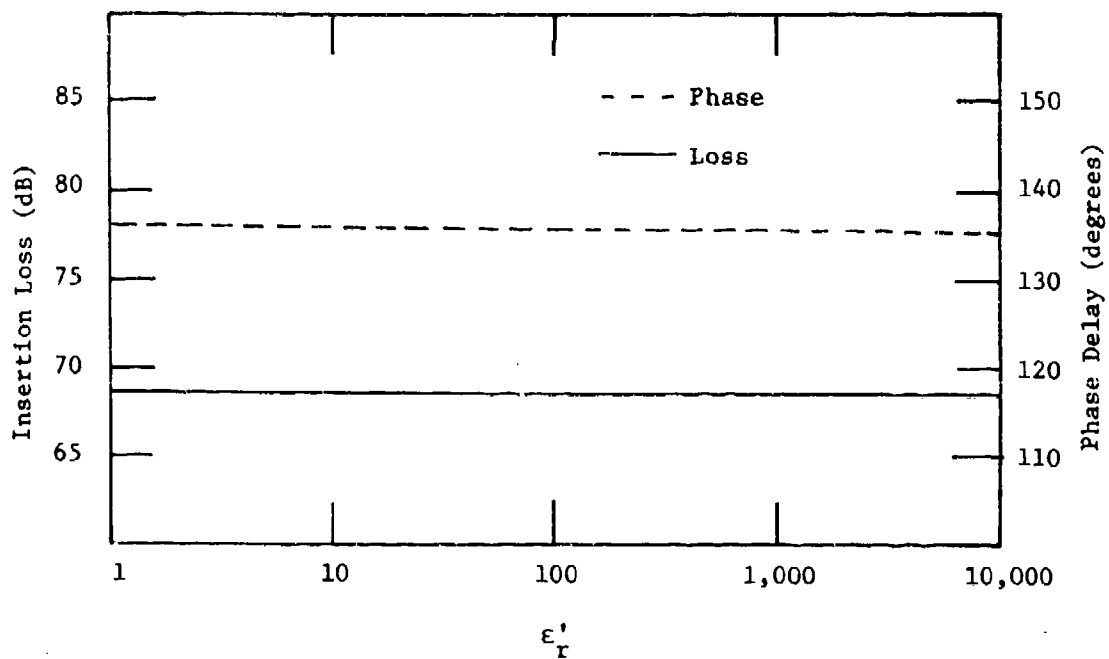


Figure 4-7. Insertion loss and phase delay for a lossy transverse slab in L-band rectangular waveguide, $t = 0.02$ inches, $\sigma = 10^4$ mhos/m. Loss and phase are both essentially independent of ϵ'_r .

4.4 AN ANISOTROPIC MODEL FOR PLANE WAVE PROPAGATION THROUGH SINGLE AND MULTILAYER ADVANCED COMPOSITES

As discussed in Section 2.0, advanced composite materials are laminates made up of a number of individual layers bonded together. Each layer consists of a unidirectional array of long fibers embedded in, and firmly bonded to a matrix. The basic building blocks of any specific composite are the types of fibers and matrix involved. Some fiber/matrix systems are: boron/epoxy, graphite/epoxy, Kevlar/epoxy, graphite/polyimide and graphite/thermoplastic.

The purpose of this section is to describe a macroscopic electromagnetic model for plane wave propagation through fiber-reinforced materials. It is convenient to distinguish between "ply" and "layer". A ply is the basic composite material unit. A layer is made up of plies with uniform fiber orientation. Thus, both plies and layers are unidirectional but a layer may consist of more than one ply. In a multilayer structure, fibers in adjacent layers have different orientations. A multilayer flat panel with arbitrarily polarized incident plane waves is considered. The fibers in each layer may be oriented in any desired direction permitting both unidirectional and mixed-orientation samples to be considered.

On a microscopic basis advanced composites are clearly both inhomogeneous and anisotropic. From a macroscopic point of view, the fiber spacings are sufficiently close that over a wide frequency range (perhaps dc - 18 GHz) it appears that the inhomogeneities can be averaged out, at least to first order. The anisotropic nature, however, of a unidirectional sample must be taken into account. For mixed orientation, multilayer samples the anisotropic effects are important unless the layers are so thin electrically that considerable layer-to-layer averaging occurs.

Based on the above discussion, it appears reasonable to model each layer as a "quasi-homogeneous" anisotropic material. Both fiber and matrix materials currently under consideration are nonmagnetic so that the permeability of these composite materials can be taken to be essentially μ_0 . Both permittivity and conductivity parameters may be anisotropic. It is assumed that the principal axes of the permittivity and conductivity properties are the same so that both the permittivity and conductivity tensors may be diagonalized simultaneously. As a labor saving device the usual combination of conductivity and permittivity into a single complex permittivity tensor is assumed. Two sets of coordinates are utilized as shown in Figure 4-8. The x, y, z coordinates are the "propagation coordinates", and all the final equations are expressed in terms of xyz-components. The $\zeta_1, \zeta_2, \zeta_3$ coordinates are called "material coordinates". The material coordinate axes are aligned with the principal directions of the composite material.

Analytically it is possible that the "material axes" $\zeta_1, \zeta_2, \zeta_3$ within each layer be skewed with respect to each of the "propagation coordinate" axes x, y, z. Physically, however, a laminate is made up of

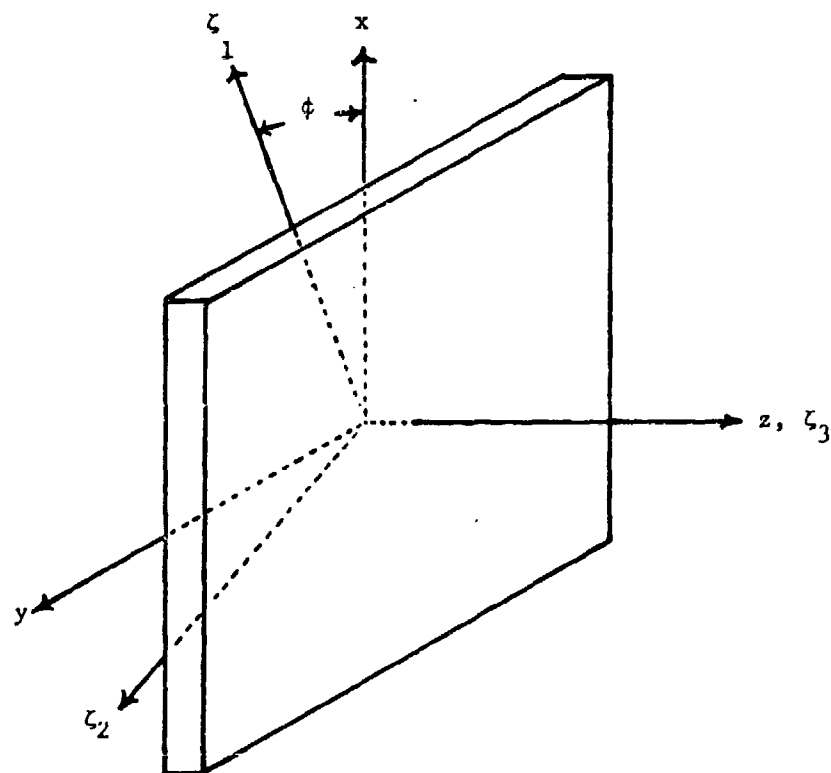


Figure 4-8. Propagation (x, y, z) and Material ($\zeta_1, \zeta_2, \zeta_3$) Coordinates for Treating Anisotropic Material with "OpticAxis" in z Direction..

parallel layers with the fibers of adjacent layers lying in parallel planes but having different fiber orientation within the plane, i.e., the material coordinate ζ_3 will usually coincide with z in every layer of a multilayer sample, while the direction of ζ_1, ζ_2 with respect to x, y varies from layer to layer.

4.4.1 Unidirectional Samples

Consider a unidirectional flat plate of advanced composite material. The principal directions (along the fibers, perpendicular to the fibers but parallel to the plane of the layer, and perpendicular to both the fiber direction and the plane of the layer) are used to define "material" coordinates. Let ζ_1 be parallel to the fibers, ζ_2 perpendicular to the fibers but parallel to the plane, ζ_3 perpendicular to both fibers and the plane of the layer. In these coordinates the complex permittivity matrix is diagonal with each of the three components, in general, different.

$$\vec{\epsilon}^+ = \begin{matrix} & \begin{matrix} \zeta_1 & \zeta_2 & \zeta_3 \end{matrix} \\ \begin{matrix} \zeta_1 \\ \zeta_2 \\ \zeta_3 \end{matrix} & \begin{bmatrix} \hat{\epsilon}_{11} & 0 & 0 \\ 0 & \hat{\epsilon}_{22} & 0 \\ 0 & 0 & \hat{\epsilon}_{33} \end{bmatrix} \end{matrix} \quad (4-40)$$

where $\hat{\epsilon}_{11} = \epsilon_{11} - j \frac{\sigma_{11}}{\omega}$.

In terms of $\zeta_1, \zeta_2, \zeta_3$ the complex permittivity tensor $\vec{\epsilon}^+$ is diagonal. The individual elements of $\vec{\epsilon}^+$, namely $\hat{\epsilon}_{11} = \epsilon_{11} - j \frac{\sigma_{11}}{\omega}$, can be measured or calculated for a single unidirectional sample of each fiber/matrix combination. The matrix in each case is normally a good dielectric while the fibers vary from modest conductors (graphite) to poor dielectrics (boron) to good dielectrics (Kevlar). Thus, the relative importance of ϵ_{11} and σ_{11} in the complex permittivity $\hat{\epsilon}_{11}$ is a function of the fiber/matrix combination and frequency.

4.4.2 Unidirectional Sample with Normally Incident, Arbitrarily Polarized Plane Wave

Assume an infinite plane sheet of unidirectional material of thickness t oriented perpendicular to the z -direction. Fibers are oriented in the ζ_1 -direction as shown in Figure 4-8. The ζ_3 and z axes are aligned. The direction of propagation of the incident plane wave is $+z$. The permeability μ is essentially equal to μ_0 . Permittivity and conductivity are combined in the complex permittivity tensor given by equations (4-40). In material coordinates there are two possible normal modes for propagation in each direction, $+z$ and $-z$. These modes are not coupled to one another and correspond to polarization perpendicular and parallel to the fiber direction, respectively. Using the transmission line analogy [4-6] the response to the normal modes can be written in material coordinates as follows.

For \vec{E} parallel to the fiber direction (ζ_1)

$$\begin{bmatrix} E_{\zeta_1}(\zeta_3) \\ H_{\zeta_2}(\zeta_3) \end{bmatrix} = \begin{bmatrix} \cosh\theta_1 & \eta_1 \sinh\theta_1 \\ \frac{1}{\eta_1} \sinh\theta_1 & \cosh\theta_1 \end{bmatrix} \begin{bmatrix} E_{\zeta_1}(\zeta_3 + t) \\ H_{\zeta_2}(\zeta_3 + t) \end{bmatrix} \quad (4-41)$$

where

$$\theta_1 = \omega \sqrt{\mu_0 \hat{\epsilon}_{11}} t = k_1 t$$

$$\eta_1 = \sqrt{\frac{\mu_0}{\hat{\epsilon}_{11}}}$$

For \vec{E} perpendicular to the fiber direction but parallel to the plane of the sample (ζ_2)

$$\begin{bmatrix} E_{\zeta_2}(\zeta_3) \\ -H_{\zeta_1}(\zeta_3) \end{bmatrix} = \begin{bmatrix} \cosh\theta_2 & \eta_2 \sinh\theta_2 \\ \frac{1}{\eta_2} \sinh\theta_2 & \cosh\theta_2 \end{bmatrix} \begin{bmatrix} E_{\zeta_2}(\zeta_3 + d) \\ -H_{\zeta_1}(\zeta_3 + d) \end{bmatrix}$$

where $\theta_2 = \omega \sqrt{\mu_0 \hat{\epsilon}_{22}} t = k_2 t$

$$\eta_2 = \sqrt{\frac{\mu_0}{\hat{\epsilon}_{22}}}$$

E_{ζ_1} , H_{ζ_2} , E_{ζ_2} , H_{ζ_1} are components of a single arbitrarily polarized plane wave. It is convenient to collect these terms into a single 4-port matrix equation relating tangential fields at input and output interfaces. E and H terms are slightly rearranged in the new matrix. Note, there is no coupling between the ζ_1 and ζ_2 polarizations.

$$\begin{bmatrix} E_{\zeta_1}(\zeta_3) \\ E_{\zeta_2}(\zeta_3) \\ H_{\zeta_2}(\zeta_3) \\ -H_{\zeta_1}(\zeta_3) \end{bmatrix} = \begin{bmatrix} \cosh\theta_1 & 0 & \eta_1 \sinh\theta_1 & 0 \\ 0 & \cosh\theta_2 & 0 & \eta_2 \sinh\theta_2 \\ \frac{1}{\eta_1} \sinh\theta_1 & 0 & \cosh\theta_1 & 0 \\ 0 & \frac{1}{\eta_2} \sinh\theta_2 & 0 & \cosh\theta_2 \end{bmatrix} \begin{bmatrix} E_{\zeta_1}(\zeta_3 + t) \\ E_{\zeta_2}(\zeta_3 + t) \\ H_{\zeta_2}(\zeta_3 + t) \\ -H_{\zeta_1}(\zeta_3 + t) \end{bmatrix} \quad (4-43)$$

To transform from components expressed in material coordinates to those in propagation coordinates, it can be seen from the geometry of Figure 4-8 that

$$\begin{aligned} A_{\zeta_1} &= A_x \cos\phi + A_y \sin\phi \\ A_{\zeta_2} &= -A_x \sin\phi + A_y \cos\phi \end{aligned} \quad (4-44)$$

where A represents either an electric or magnetic field component. Substituting from equation (4-44) into equation (4-43) yields the following equation:

$$\begin{bmatrix} E_{11} \\ E_{12} \\ H_{11} \\ H_{12} \end{bmatrix} = \begin{bmatrix} \cosh\theta_1 & 0 & \eta_1 \sinh\theta_1 & 0 \\ 0 & \cosh\theta_2 & 0 & \eta_2 \sinh\theta_2 \\ \frac{\sinh\theta_1}{\eta_1} & 0 & \cosh\theta_1 & 0 \\ 0 & \frac{\sinh\theta_2}{\eta_2} & 0 & \cosh\theta_2 \end{bmatrix} \begin{bmatrix} E_{o1} \\ E_{o2} \\ H_{o1} \\ H_{o2} \end{bmatrix} \quad (4-45)$$

where

$$\begin{aligned} E_{11} &= E_x(z) \cos\phi + E_y(z) \sin\phi \\ E_{12} &= -E_x(z) \sin\phi + E_y(z) \cos\phi \\ H_{11} &= -H_x(z) \sin\phi + H_y(z) \cos\phi \\ H_{12} &= -H_x(z) \cos\phi - H_y(z) \sin\phi \\ E_{o1} &= E_x(z+t) \cos\phi + E_y(z+t) \sin\phi \\ E_{o2} &= -E_x(z+t) \sin\phi + E_y(z+t) \cos\phi \\ H_{o1} &= -H_x(z+t) \sin\phi + H_y(z+t) \cos\phi \\ H_{o2} &= -H_x(z+t) \cos\phi - H_y(z+t) \sin\phi. \end{aligned}$$

Algebraically manipulating equation (4-45) leads to equation 4-46 given below.

$$\begin{bmatrix} E_x(z) \\ E_y(z) \\ H_y(z) \\ -H_x(z) \end{bmatrix} = \begin{bmatrix} A_{11} & A_{12} & B_{11} & B_{12} \\ A_{21} & A_{22} & B_{21} & B_{22} \\ C_{11} & C_{12} & D_{11} & D_{12} \\ C_{21} & C_{22} & D_{21} & D_{22} \end{bmatrix} \begin{bmatrix} E_x(z+t) \\ E_y(z+t) \\ H_y(z+t) \\ -H_x(z+t) \end{bmatrix} \quad (4-46)$$

where

$$\begin{aligned}
 A_{11} &= D_{11} = \cosh\theta_1 \cos^2\phi + \cosh\theta_2 \sin^2\phi \\
 A_{22} &= D_{22} = \cosh\theta_1 \sin^2\phi + \cosh\theta_2 \cos^2\phi \\
 A_{12} &= A_{21} = D_{12} = D_{21} = \sin\phi \cos\phi (\cosh\theta_1 - \cosh\theta_2) \\
 B_{11} &= \eta_1 \sinh\theta_1 \cos^2\phi + \eta_2 \sinh\theta_2 \sin^2\phi \\
 B_{22} &= \eta_1 \sinh\theta_1 \sin^2\phi + \eta_2 \sinh\theta_2 \cos^2\phi \\
 C_{11} &= \frac{1}{\eta_1} \sinh\theta_1 \cos^2\phi + \frac{1}{\eta_2} \sinh\theta_2 \sin^2\phi \\
 C_{22} &= \frac{1}{\eta_1} \sinh\theta_1 \sin^2\phi + \frac{1}{\eta_2} \sinh\theta_2 \cos^2\phi \\
 B_{12} &= B_{21} = \sin\phi \cos\phi (\eta_1 \sinh\theta_1 - \eta_2 \sinh\theta_2) \\
 C_{12} &= C_{21} = \sin\phi \cos\phi \left(\frac{1}{\eta_1} \sinh\theta_1 - \frac{1}{\eta_2} \sinh\theta_2 \right).
 \end{aligned}$$

Other quantities have been defined earlier. Notice that x and y polarizations are coupled unless $\phi = 0^\circ$ or 90° . Thus, except for these two special cases an x-polarized incident wave will produce both x and y polarized reflected and transmitted waves.

A still more condensed equation results if matrix notation is further exploited.

$$\begin{bmatrix} \vec{E}_t(z) \\ \vec{H}_t(z) \end{bmatrix} = \begin{bmatrix} \vec{A} & \vec{B} \\ \vec{C} & \vec{D} \end{bmatrix} \begin{bmatrix} \vec{E}_t(z+t) \\ \vec{H}_t(z+t) \end{bmatrix} \quad (4-47)$$

where

$$\vec{E}_t(\cdot) = \begin{bmatrix} E_x(\cdot) \\ E_y(\cdot) \end{bmatrix} = \begin{array}{l} \text{Transverse} \\ \text{Components of } \vec{E} \text{ at} \\ \text{either } z \text{ or } z+t \end{array}$$

$$\vec{H}_t(\cdot) = \begin{bmatrix} H_y(\cdot) \\ -H_x(\cdot) \end{bmatrix} = \begin{array}{l} \text{Transverse} \\ \text{Components of } H \text{ at} \\ \text{either } z \text{ or } z+t \end{array}$$

$$\begin{aligned}
 \text{and } \vec{A} &= \begin{bmatrix} A_{11} & A_{12} \\ A_{21} & A_{22} \end{bmatrix} \\
 \vec{B} &= \begin{bmatrix} B_{11} & B_{12} \\ B_{21} & B_{22} \end{bmatrix}, \text{ etc.}
 \end{aligned}$$

and $A_{ij}, B_{ij}, C_{ij}, D_{ij}$; coefficients were defined above.

4.4.3 Multilayer Samples with Normally Incident, Arbitrarily Polarized Plane Waves

To analyze multilayer structures, construct $\begin{bmatrix} \vec{A} & \vec{B} \\ \vec{C} & \vec{D} \end{bmatrix}$ for each layer taking

into account the different ϕ and \vec{E} for each layer. Obtain the overall ABCD matrix as the product of the matrices for the individual layers. Thus, for a 90° , 45° , 90° multilayer sample

$$\begin{bmatrix} \vec{A} & \vec{B} \\ \vec{C} & \vec{D} \end{bmatrix} = \begin{bmatrix} \vec{A}_{90^\circ} & \vec{B}_{90^\circ} \\ \vec{C}_{90^\circ} & \vec{D}_{90^\circ} \end{bmatrix} \begin{bmatrix} \vec{A}_{45^\circ} & \vec{B}_{45^\circ} \\ \vec{C}_{45^\circ} & \vec{D}_{45^\circ} \end{bmatrix} \begin{bmatrix} \vec{A}_{90^\circ} & \vec{B}_{90^\circ} \\ \vec{C}_{90^\circ} & \vec{D}_{90^\circ} \end{bmatrix}. \quad (4-48)$$

The resulting ABCD matrix relates the "total" (i.e., sum of incident and reflected) fields at the input side of the sample to the corresponding quantities on the output side. Most often the desired end result of such analysis is various ratios of traveling wave (not "total") fields. To facilitate calculations such as determining power reflected, power transmitted, power converted from one polarization to another, etc., it is convenient after the overall ABCD matrix is computed to convert to scattering parameters [4-12]. Scattering parameters provide direct relationships between the traveling wave quantities. Clearly, scattering parameters or their transmission counterpart could be used to describe each layer and then combined to provide the overall multilayer matrix. However, the determination of the overall ABCD matrix and then its conversion to scattering parameters is computationally much more efficient in the class of problems being considered.

4.4.4 Scattering Matrix for a Multilayer Composite Structure with Normally Incident, Arbitrarily Polarized Plane Waves

Either normalized or unnormalized scattering parameters [4-12] may be used. In many cases normalized parameters are a distinct advantage. At this point there is little advantage to be gained from normalization and some danger of confusion arising from the normalization process. Therefore, unnormalized scattering parameters are used.

Let the fields on the input side of the sample be expressed as follows:

$$\left\{ \begin{array}{l} E_x(z) = E_{x1}(z) + E_{xr}(z) \\ E_y(z) = E_{y1}(z) + E_{yr}(z) \\ H_y(z) = H_{y1}(z) + H_{yr}(z) = \frac{1}{\eta_0} [E_{x1}(z) - E_{xr}(z)] \\ -H_x(z) = -[H_{x1}(z) + H_{xr}(z)] = \frac{-1}{\eta_0} [E_{y1}(z) - E_{yr}(z)] \end{array} \right. \quad (4-49)$$

where η_s = intrinsic impedance of input medium and the subscript i refers to incident traveling wave components while r refers to reflected or reverse traveling wave components.

Similarly, fields on the output side of the sample are given in equation (4-50). Note, as is conventional in scattering analysis "incident waves" travel towards the sample while "scattered or reflected waves" travel away from the sample. This means that incident waves on opposite sides of the sample travel in opposite directions.

$$\left\{ \begin{array}{l} E_x(z+t) = E_{x1}(z+t) + E_{xr}(z+t) \\ E_y(z+t) = E_{y1}(z+t) + E_{yr}(z+t) \\ H_y(z+t) = H_{y1}(z+t) + H_{yr}(z+t) = \frac{-1}{\eta_3} [E_{x1}(z+t) - E_{xr}(z+t)] \\ -H_x(z+t) = -[H_{x1}(z+t) + H_{xr}(z+t)] = \frac{1}{\eta_3} [E_{y1}(z+t) - E_{yr}(z+t)] \end{array} \right. \quad (4-50)$$

where η_3 = intrinsic impedance of output medium.

If there are no sources on the output side of the sample the incident signals from that side will be zero, i.e., $E_{y1}(z+t) = E_{x1}(z+t) = 0$. It is assumed that this is true in the following analysis. Substituting equations (4-49) and (4-50) into equation (4-47) and solving for the scattered or reflected components in terms of the nonzero incident components yields the following relationship. Note that since $E_{y1}(z+t) = E_{x1}(z+t) = 0$, only the first two columns of the scattering matrix are required for this analysis.

$$\begin{bmatrix} E_{xr}(z) \\ E_{yr}(z) \\ E_{xr}(z+t) \\ E_{yr}(z+t) \end{bmatrix} = \begin{bmatrix} S_{11} & S_{12} & S_{13} & S_{14} \\ S_{21} & S_{22} & S_{23} & S_{24} \\ S_{31} & S_{32} & S_{33} & S_{34} \\ S_{41} & S_{42} & S_{43} & S_{44} \end{bmatrix} \begin{bmatrix} E_{x1}(z) \\ E_{y1}(z) \\ 0 \\ 0 \end{bmatrix} \quad (4-51)$$

where

$$S_{41} = \frac{2}{\Delta} \left[A_{21} + \frac{B_{21}}{\eta_3} + \eta_s C_{21} + \frac{\eta_s}{\eta_3} D_{21} \right]$$

$$S_{42} = \frac{-2}{\Delta} \left[A_{11} + \frac{B_{11}}{\eta_3} + \eta_s C_{11} + \frac{\eta_s}{\eta_3} D_{11} \right]$$

$$\begin{aligned}
S_{31} &= \frac{-2}{\Delta} \left[A_{22} + \frac{B_{22}}{\eta_3} + \eta_s C_{22} + \frac{\eta_s}{3} D_{22} \right] \\
S_{32} &= \frac{2}{\Delta} \left[A_{12} + \frac{B_{12}}{\eta_3} + \eta_s C_{12} + \frac{\eta_s}{2} D_{12} \right] \\
S_{21} &= \left[\left(A_{21} + \frac{B_{21}}{\eta_3} \right) S_{31} + \left(A_{22} + \frac{B_{22}}{\eta_3} \right) S_{41} \right] \\
S_{22} &= \left[-1 + \left(A_{21} + \frac{B_{21}}{\eta_3} \right) S_{32} + \left(A_{22} + \frac{B_{22}}{\eta_3} \right) S_{42} \right] \\
S_{11} &= \left[-1 + \left(A_{11} + \frac{B_{11}}{\eta_3} \right) S_{31} + \left(A_{12} + \frac{B_{12}}{\eta_3} \right) S_{41} \right] \\
S_{12} &= \left[\left(A_{11} + \frac{B_{11}}{\eta_3} \right) S_{32} + \left(A_{12} + \frac{B_{12}}{\eta_3} \right) S_{42} \right] \\
\Delta &= \left[\left(A_{12} + \frac{B_{12}}{\eta_3} + \eta_s C_{12} + \frac{\eta_s}{3} D_{12} \right) \left(A_{21} + \frac{B_{21}}{\eta_3} + \eta_s C_{21} + \frac{\eta_s}{3} D_{21} \right) \right. \\
&\quad \left. - \left(A_{11} + \frac{B_{11}}{\eta_3} + \eta_s C_{11} + \frac{\eta_s}{3} D_{11} \right) \left(A_{22} + \frac{B_{22}}{\eta_3} + \eta_s C_{22} + \frac{\eta_s}{3} D_{22} \right) \right] .
\end{aligned}$$

Equation (4-51) can be used to calculate the quantities of interest in electromagnetic shielding problems. The procedure is to first calculate the total 4-port ABCD parameters for the multilayer sample, as indicated in Section 4.4.3. The values of A_{ij} , B_{ij} , C_{ij} , D_{ij} obtained are used in equation (4-51) to determine the overall scattering parameters for the multilayer sample. Figure 4-9 and 4-10 illustrate shielding effectiveness calculated for some single-layer and multilayer graphite epoxy shields. The value of ϵ' is not critical for the values of conductivity utilized. Indeed varying ϵ'_r from 1 to about 100 has no noticeable effect on the shielding effectiveness. Figure 4-9 illustrates the effect on shielding effectiveness of varying polarization of the wave incident on a single anisotropic layer. Data is plotted for polarization parallel to the fiber direction ($\phi=0^\circ$), perpendicular to the fiber direction ($\phi=90^\circ$) and inclined at 45° to the fiber direction ($\phi=45^\circ$). As would be expected, much larger attenuation is experienced when the wave is polarized parallel to the fibers. Figure 4-10 illustrates shielding effectiveness for 4-layer (0° , $+45^\circ$, 90°) and 7-layer (0° , $+45^\circ$, 90° , $+45^\circ$, 0°) structures. The incident wave in each case is polarized parallel to the fiber direction of the first layer.

4.4.5 Extension to Oblique Angles of Incidence

The analysis of multilayer anisotropic composite structures with the plane waves incident at oblique angles can be handled in a very similar fashion. This procedure is currently being developed and the results will be presented in a future report.

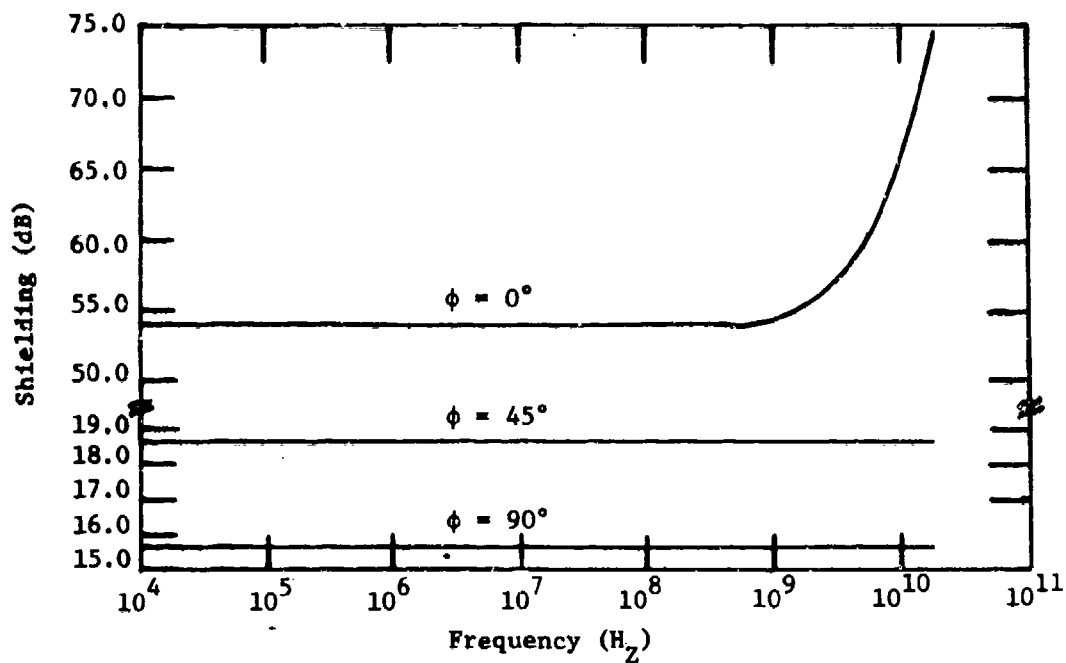


Figure 4-9. Shielding effectiveness of a single layer anisotropic shield for various fiber orientations. A plane wave polarized in the $\phi = 0^\circ$ direction is normally incident on the input side of the shield, shield parameters are $\tau = .00525$ inches, $\sigma = 2 \times 10^4$ mhos/m, $\sigma_2 = 2 \times 10^2$ mhos/m, $\epsilon_{r1} = \epsilon_{r2} = 3$.

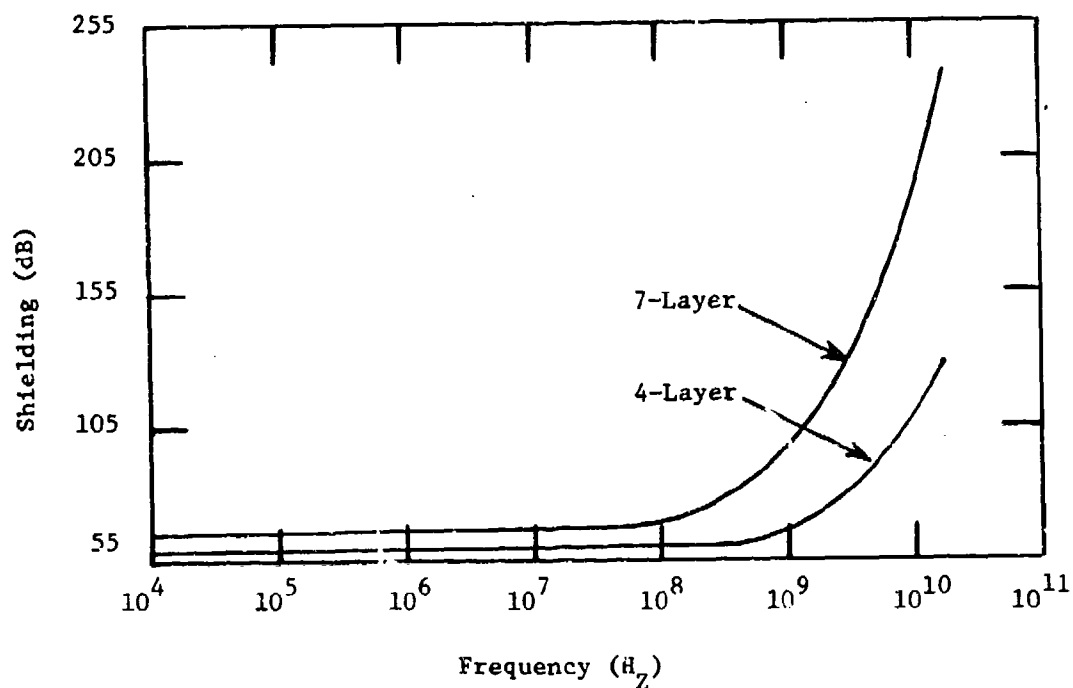


Figure 4-1C. Shielding effectiveness of 4-layer and 7-layer anisotropic shields. Fiber orientations for 4-layer shield are $(0^\circ, \pm 45^\circ, 90^\circ)$; for 7-layer shield are $(0^\circ, \pm 45^\circ, 90^\circ, \pm 45^\circ, 0^\circ)$. Each layer has $t = .00525$ inches, $\sigma_1 = 2 \times 10^4$ mhos/m, $\sigma_2 = 2 \times 10^2$ mhos/m, $\epsilon_{r1} = \epsilon_{r2} = 3$.

APPENDIX 4-A

DERIVATION OF EQUATION (4-9)

Moser [4-3] and Bannister [4-4, 4-5] have provided an integral equation solution for the shielding effectiveness of the two-loop/infinite flat plate geometry assuming uniform current in the loops. It is assumed that the shield is a good enough conductor that displacement currents in the shield can be neglected. The complete expression for the shielding effectiveness as given by Bannister is shown in equation (4-A-1).

$$S. E._{dB} = 20 \log_{10} \frac{1}{4\mu_r} \left| \frac{\int_0^\infty \frac{\lambda^2}{\tau_0} J_1(\lambda a) e^{-\tau_0 z} d\lambda}{\int_0^\infty \frac{C\lambda^2 \tau}{\tau_0^2} J_1(\lambda a) e^{-\tau_0 z - t(\tau - \tau_0)} d\lambda} \right| \quad (4-A-1)$$

where

$$C = [(\tau/\tau_0 + \mu_r)^2 - (\tau/\tau_0 - \mu_r)^2 e^{-2t\tau}]^{-1}$$

$$\tau = (\lambda^2 + \gamma^2)^{1/2}$$

$$\tau_0 = (\lambda^2 + \gamma_0^2)^{1/2}$$

$$\gamma_0 = \frac{j2\pi}{\lambda_{air}} = \text{free-space propagation factor}$$

$$\gamma = (j\omega\mu_0\mu_r\sigma)^{1/2} = \text{propagation constant in the shield (displacement currents are neglected)}$$

$$\tau_r = \frac{|Y|}{\sqrt{2}} = (\omega\mu_0\mu_r\sigma/2)^{1/2} = \frac{1}{\delta}$$

$$\delta = (2/\omega\mu_0\mu_r\sigma)^{1/2} = \text{skin depth in the shield}$$

$$\mu_r = \text{relative permeability of the shield}$$

$$t = \text{shield thickness}$$

$$\sigma = \text{shield conductivity}$$

$$z = r_1 + r_2 = \text{center-to-center separation of the two loops}$$

$$J_1(\lambda a) = \text{Bessel function of order one and argument } (\lambda a).$$

$$a = \text{loop radius}$$

$$\lambda = \text{dummy variable of integration}$$

$$r = \sqrt{a^2 + z^2}$$

$$\lambda_{air} = \text{wavelength in air}$$

Simplified approximate forms of Moser's formula can be derived under certain conditions [4-3, 4-4]. Let $r' = [a^2 + (z-t)^2]^{1/2}$ be termed the measurement distance. Then for conditions such that $r' < \frac{\lambda_{air}}{20}$, $\tau_r t > 2$, $\tau_r r' > 10$ and $\frac{\tau_r}{\mu_r} > 10$ are satisfied, the shielding equation takes on the much simpler form given below.

$$S. E._{dB} \approx 8.686 \sqrt{2} \tau_r t + 20 \log_{10} \left| \left(\frac{\tau_r r'}{8.485 \mu_r} \right) \left(\frac{r'}{z-t} \right) \left(\frac{r'}{r} \right)^3 \right| . \quad (4-A-2)$$

If, as is usually the case, $z \gg t$, then:

$$S. E._{dB} \approx 8.686 \sqrt{2} \tau_r t + 20 \log_{10} \left| \frac{\tau_r z}{8.485 \mu_r} \left(\frac{r}{z} \right)^2 \right| . \quad (4-A-3)$$

If in addition $z \gg a$, then:

$$S. E._{dB} \approx 8.686 \sqrt{2} \tau_r t + 20 \log_{10} \left(\frac{\tau_r z}{8.485 \mu_r} \right) . \quad (4-A-4)$$

SYMBOLS USED IN SECTION 4

A_T, B_T, C_T, D_T = Elements of total ABCD matrix for a cascade of shield sections

$\bar{A}, \bar{B}, \bar{C}, \bar{D}$ = Elements of ABCD matrix for individual shield section

$\overleftrightarrow{A}, \overleftrightarrow{B}, \overleftrightarrow{C}, \overleftrightarrow{D}$ = Matrix components of 4-port ABCD matrix

f = Frequency (Hertz)

$j = \sqrt{-1}$

r_1 = Distance from source loop to shield (meters)

r_2 = Distance from detector loop to shield (meters)

S_{ij} = Components of scattering matrix

t = Thickness of shield (meters)

$\tan \delta = \epsilon''/\epsilon' = \text{loss tangent}$

$z = r_1 + r_2$

$Z_E = \frac{1}{j\omega\epsilon_0 b}$, where b is defined in Figure 4-3

Z_0 = Characteristic wave impedance (ohms)

$Z_m = j\omega\mu_0 b$, where b is defined in Figure 4-3

Z_s = Surface transfer impedance (ohms)

Z_{WL} = Wave impedance of output signal (ohms)

Z_{WS} = Wave impedance of input signal (ohms)

Z_{01}, Z_{02}, Z_{03} = Transmission line characteristic impedances

α = Attenuation factor (nepers/meter)

β = Phase factor (radians/meter)

γ = Propagation factor = $\alpha + j\beta$

δ see $\tan \delta$

$\epsilon = \epsilon' - j\epsilon'' = \epsilon_0(\epsilon'_r - j\epsilon''_r) = \text{permittivity}$

ϵ_0 = Permittivity of free space = 8.854×10^{-12} (farad/meter)

ϵ_r = Relative permittivity

$\overleftrightarrow{\epsilon}$ = Complex permittivity matrix

$\hat{\epsilon}_{ij}$ = Element of complex permittivity matrix

ζ_1

η

θ

λ

λ_0

λ_c

μ_0

μ_r

ρ_{in}

σ

σ_{ef}

τ_r

ω

SYMBOLS USED IN SECTION 4 (cont'd.)

shield

$\zeta_1, \zeta_2, \zeta_3$ = Material coordinate axes

on

η = Intrinsic wave impedance of shield (ohms)

$\theta = \gamma t$

λ = Dummy variable of integration in Appendix 4-8

λ_0 = Wavelength in free space (meters)

λ_c = Cutoff wavelength in waveguide (meters)

μ_0 = Permeability of free space = 1.257×10^{-6} (henry/meter)

μ_r = Relative permeability of shield

ρ_{in} = Input reflection coefficient

σ = Conductivity (mhos/meter)

σ_{eff} = Scalar effective conductivity of the shield (mhos/meter)

$\tau_r = |\gamma| / \sqrt{2}$

ω = Radian frequency

REFERENCES

- 4-1. S. Ramo, J. R. Whinnery, and T. van Duzer, Fields and Waves in Communication Electronics, John Wiley and Sons (1967).
- 4-2. D. Strawe, L. Piszker, "Interaction of Advanced Composites with Electromagnetic Pulse (EMP) Environment," AFML-TR-75-141, September 1975, (AD-B011927).
- 4-3. J. Moser, "Low-frequency Shielding of a Circular Loop Electromagnetic Field," IEEE Trans. on EMC, Vol. EMC-9, pp. 6-18, March 1967.
- 4-4. P. Bannister, "New Theoretical Expressions for Predicting Shielding Effectiveness for the Plane Shield Case," IEEE Trans. on EMC, Vol. EMC-10, pp. 2-7, March 1968.
- 4-5. P. Bannister, "Further Notes for Predicting Shielding Effectiveness for the Plane Shield Case," IEEE Trans. on EMC, Vol. EMC-11, pp. 50-53, May 1969.
- 4-6. S. A. Schelkunoff, Electromagnetic Waves, D. van Nostrand (1943).
- 4-7. L. V. King, "Electromagnetic Shielding at Radio Frequencies," Phil. Mag. J. Sci., Vol. 15, pp. 201-223, February 1933.
- 4-8. A Technology Plan for Electromagnetic Characteristics of Advanced Composites, RADC-TR-76-206, July 1976.
- 4-9. W. C. Harrigan, Jr. and D. M. Goddard, "Aluminum Graphite Composites: Effect of Processing on Mechanical Properties", Journal of Metals, May 1975, p. 20-25.
- 4-10. Technique of Microwave Measurements, Edited by C. G. Montgomery, Vol. VI, Radiation Laboratory Series, Chapter 10, McGraw-Hill (1947).
- 4-11. M. G. Salvadori and M. L. Baron, Numerical Methods in Engineering, Prentice-Hall, Inc. (1961).
- 4-12. H. J. Carlin and A. B. Giordano, Network Theory: An Introduction to Reciprocal and Nonreciprocal Circuits, Prentice-Hall, Inc. (1964).

5.0 NUMERICAL TECHNIQUES FOR THE ANALYSIS OF COMPOSITE MATERIALS

The use of advanced composite materials in aircraft structures poses some new electromagnetic problems, some of which can be treated by extension of previous methods and some of which require the introduction of new methods. A recent report [5-1] summarizes the present state-of-the-art with respect to advanced composites.

The basic electromagnetic problems confronting the user are outlined and basic methods for treating them are discussed in section 5.1. Then one of the most direct methods, that of loading for thin-wire and surface codes, is covered in more detail in section 5.2.

5.1 BASIC PROBLEMS AND TECHNIQUES

5.1.1 The Electromagnetic Problem

What are some of the basic problems which arise in the use of composite materials? Composite materials are considered here to be dissipative materials characterized by conductivity σ and complex permittivity ϵ .^{*} The basic change in electromagnetic analysis is thus the shift from lossless to dissipative materials.

Some of the basic operational problems which arise are described below. First, consider an aircraft constructed of composite materials in the presence of electromagnetic fields. One is interested in the energy coupled to the aircraft interior. This may occur by means of penetration through the composite skin of the aircraft, through apertures in the aircraft structure, and through antennas and transmission lines connected

^{*}Composites may also be non-linear, inhomogeneous, and anisotropic. These aspects are neglected in the present treatment. A consideration of permeability is also omitted since $\mu \approx \mu_0$ for composites.

directly to the interior. In addition, one is interested in the radar cross section and other scattering properties of the composite aircraft.

Fig. 5.1 shows the basic electromagnetic scattering problems thus posed. As noted, there are three mechanisms for coupling energy to the interior; (a) penetration through the skin, (b) coupling through apertures, and (c) direct coupling by antennas and transmission lines as indicated in Figs. 5-1a, b, c, respectively. In a given situation, all three types of coupling may be present. In Fig. 5-1 the incident field \underline{E}^{inc} may represent plane waves or any other specified incident fields. The composite material is characterized by its permittivity ϵ , conductivity σ , and thickness t . The coupling problems outlined above represent the solutions to the interior problems. The radar cross section and other scattering characteristics may be determined from the solution of the exterior problems.

Now consider a composite aircraft structure with antennas. One is interested in the radiating and terminal properties of the individual antennas and in the coupling characteristics between different antennas. The basic electromagnetic problems posed are shown in Fig. 5-2. Fig. 5-2a shows an antenna mounted over a composite structure, with terminals a-b. The impedance at terminals a-b and the radiated near and far fields are of interest. Fig. 5-2b shows two coupled antennas mounted over a composite structure. One is interested in the two-port parameters which determine the coupling between antennas and the input impedance of each in the presence of the other. In the problems of Fig. 5-2, the exterior fields are probably of primary concern. The interior fields, which may be considerably larger in magnitude than for the corresponding metal-skinned structure, may also be of interest. The interior problem is that of Fig. 5-1c.

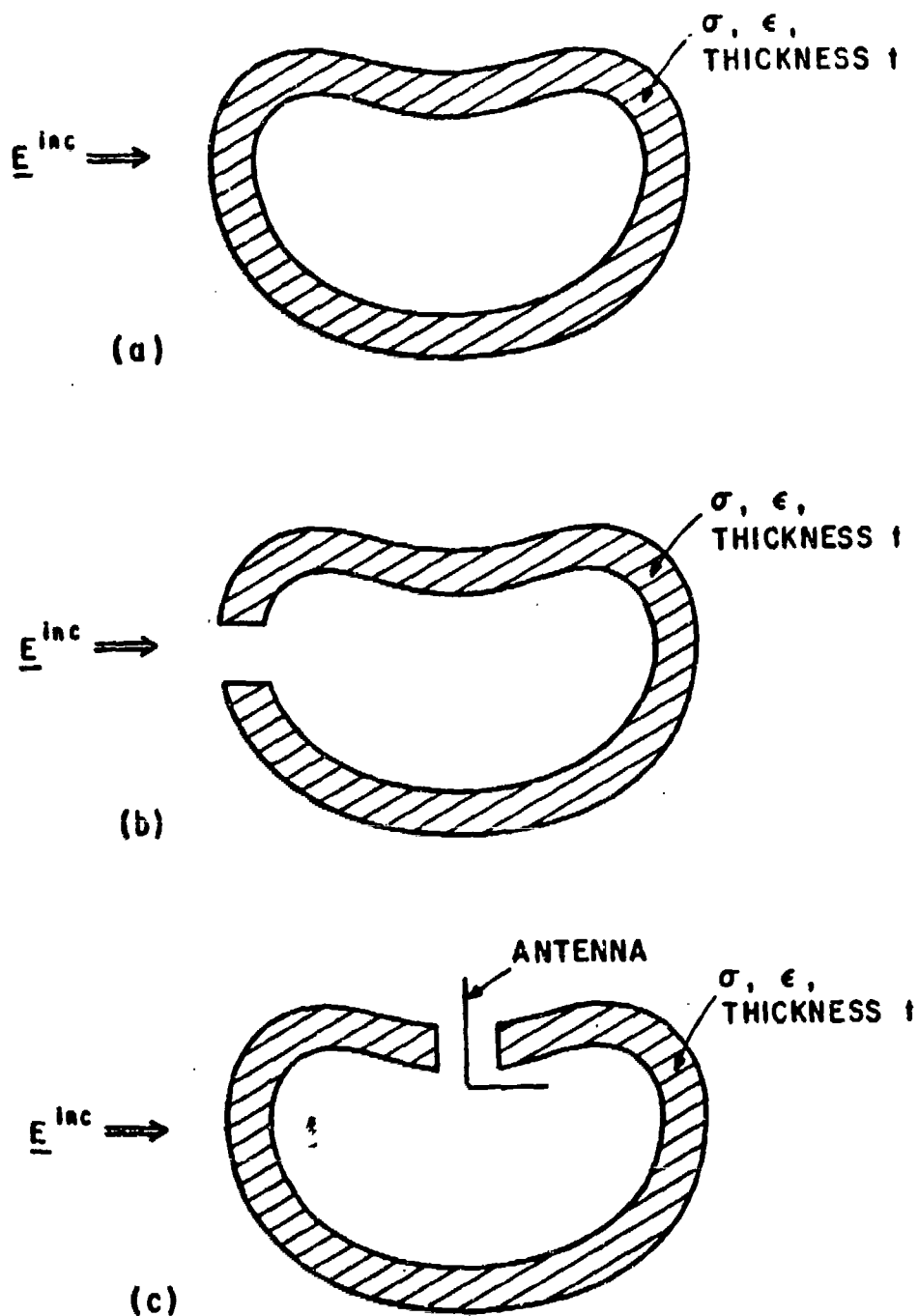
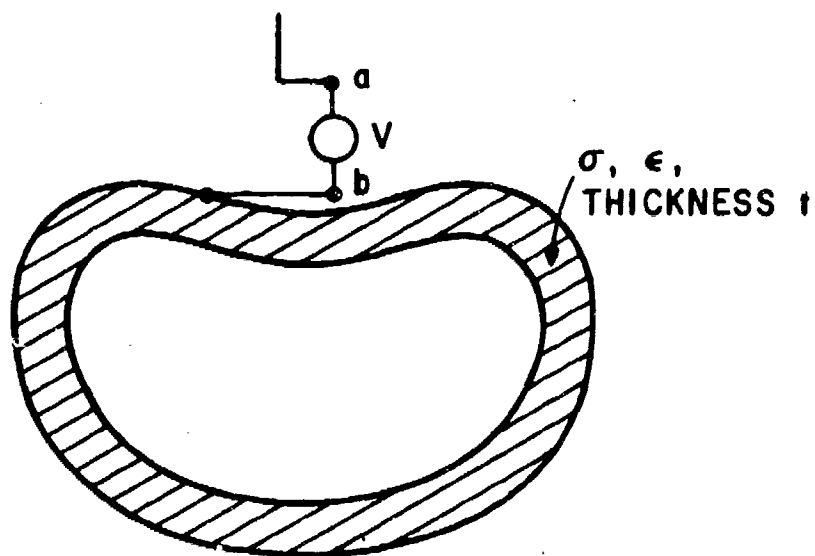
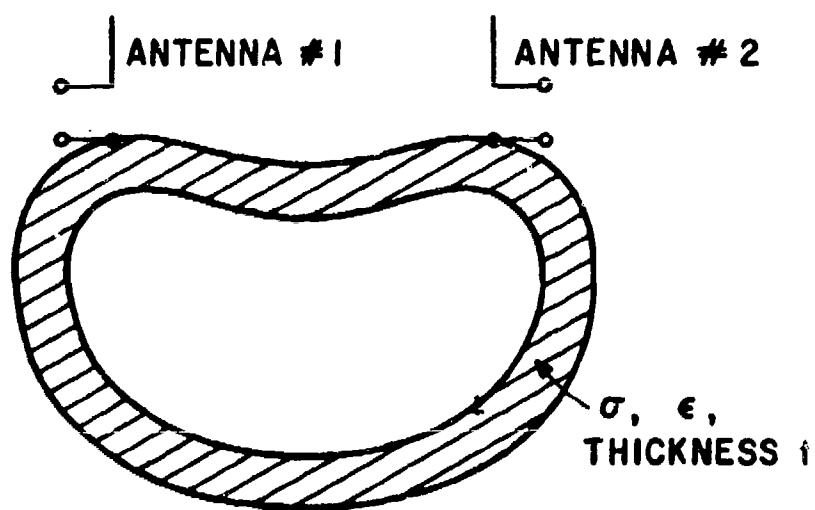


Figure 5-1. Basic electromagnetic scattering problems for composites.
 (a) the shielding problem, (b) aperture coupling,
 (c) direct coupling.



(a)



(b)

Figure 5-2. Basic electromagnetic radiation problems for composites. (a) antenna over a composite structure, (b) coupled antennas over a composite structure.

5.1.2 Characteristics of Advanced Composites

Some of the typical characteristics of advanced composites should be briefly noted here. Typical measurements of conductivity as given in section 2.5.5 for the longitudinal direction are:

$$\sigma \approx 2 \times 10^4 \text{ mho/meters for graphite/epoxy}$$

$$\sigma \approx 10 \text{ to } 100 \text{ mho/meters for boron/epoxy}$$

Typical relative permittivity is estimated to be about three ($\epsilon \approx 3\epsilon_0$)[5-1].

Typical composite material thickness t is expected to be .16 cm (1/16") to .48 cm (3/16"). Skin depth is defined as follows:

$$\text{skin depth} = \sqrt{\frac{2}{\omega \mu \sigma}}$$

If one assumes $\sigma = 2 \times 10^4$, $\mu = \mu_0$, then a 1/16" sheet of composite graphite material has a thickness t corresponding to 45, 4.5, 0.45 skin depths at 10,000 MHz, 100 MHz, 1 MHz respectively. Electromagnetic problems thus range from those with "thick" sheets to those with "thin" sheets of composite material.

In sections 5.0 through 5.1.2 some of the basic concepts and problems relating to composite materials have been discussed. Basic methods for treating these problems are covered in sections 5.1.3 and 5.1.4.

5.1.3 Available Numerical Techniques

The present state-of-the-art with respect to numerical techniques for the method of moments should be briefly noted here. The computer codes available have been described in [5-1]. At present, there are many well-documented programs for thin wires. Some of these include the most general orientation (arbitrarily skewed wires) and take junctions into account.

Codes available for surfaces include [5-2,3] which permits the treatment of combinations of flat plates and [5-4,5] for bodies of revolution. The treatment of bodies of revolution involves several codes, including those which take into account loading and the presence of thin wires.

5.1.4 Basic Methods for Analysis of Composite Materials

5.1.4.1 The Polarization Current Method

A general method of treating magnetic and dielectric materials is to replace the material with total volume current density \underline{J}_{TOTAL} (in free space), which represents the sum of conduction, polarization and magnetization volume current densities [5-6,7]

$$\underline{J}_{TOTAL} = \underline{J}_C + \frac{\partial \underline{P}}{\partial t} + \nabla \times \underline{M} \quad (5-1)$$

where

\underline{J}_C is volume conduction current density (due to motion of free charges)

$\frac{\partial \underline{P}}{\partial t}$ represents volume polarization current density (due to motion of bound charges, i.e. dipoles)

$\nabla \times \underline{M}$ represents volume magnetization current density (due to Amperian bound currents of magnetization).

This point of view recognizes the fact that currents of all types contribute to radiation. For composite materials, permeable effects are negligible ($\underline{M} = 0$) and Eq. (5-1) becomes in the time-harmonic case*:

$$\underline{J}_{TOTAL} = \underline{J}_C + j\omega \underline{P} = [\sigma + j\omega(\epsilon - \epsilon_0)]\underline{E} \quad (5-2)$$

* Identical symbols are used for the general and time-harmonic cases. This does not lead to confusion since time derivatives are always present in the general case.

Different types of current have the same effect, as far as external fields are concerned. The electromagnetic effects of composites may thus be treated by considering conduction and polarization currents. For typical values of σ and ϵ as noted previously, the conduction current is much larger in magnitude than the polarization current, even at frequencies as high as 20 GHz.

In the method-of-moments formulation [5-8,9] one can always replace the volume of the composite material with currents \underline{J}_{TOTAL} acting in free space, with \underline{J}_{TOTAL} related to electric field \underline{E} as Eq. (5-2).

Consider fields incident upon a volume of composite material, as in Fig. 5-1a. The volume current density \underline{J}_{TOTAL} is expressed in terms of approximate expansion functions, the vector and scalar potentials \underline{A} and ϕ are determined from \underline{J}_{TOTAL} as in [5-8,9] except that \underline{J} is replaced everywhere with \underline{J}_{TOTAL} in Eq. (5-2). Appropriate weighting functions are applied. The result (see Appendix 5-A) is a matrix equation of the form:

$$[-v^{inc}] = [[z] + [z_\ell]][1] \quad (5-3)$$

where $[-v^{inc}]$ represents a weighted integral of incident fields, $[1]$ represents the unknown total currents, $[z]$ represents the generalized impedance matrix (voltage at one location due to unit current at another), and $[z_\ell]$ represents a generalized load matrix expressing the relationship between total current and total electric field; its characteristics are determined by eq. (5-2) and the particular geometry. The result is analogous to that for loaded wires; the net effect is that a load matrix is added to the generalized impedance matrix.

The method described briefly here is one of the most basic. It can be

used immediately for inhomogeneous problems where σ and ϵ are functions of position. The only effect is that eq. (5-2) is a function of position also, and the elements of $[z_\ell]$ vary according to the positions of corresponding currents [1].*

The basic limitation of the method is that the number of unknowns increases very rapidly with the electric size of the composite material. The number of unknowns is proportional to the volume of the composite material. Generalized impedance functions $[z]$ have been developed for certain specialized cases [5-10,11] involving impulsive expansion and weighting functions. For thin shells, the above formulation is simplified considerably, since the volume distribution of currents approaches a single sheet of surface current. The current and fields are again directly related as in eq. (5-2). The formulation for thin dielectric sheets is given in [5-12].

5.1.4.2 The Equivalent Surface Current Method

For homogeneous materials, the equivalent surface current method may always be applied. Each surface of the material is covered with sheets of electric and magnetic surface currents. Then the fields within each region are represented by some linear combination of these current sheets acting in an unbounded homogeneous region. Boundary conditions are then enforced at the surfaces and the unknown surface currents are obtained.

Fig. 5-1a shows a typical problem with fields incident upon a shell of homogeneous composite material of permittivity ϵ and conductivity σ . Fig. 5-3a shows a set of electric and magnetic surface currents spread over each

* Unimoment Techniques [5-13,14,15] can also be used for inhomogeneous problems.

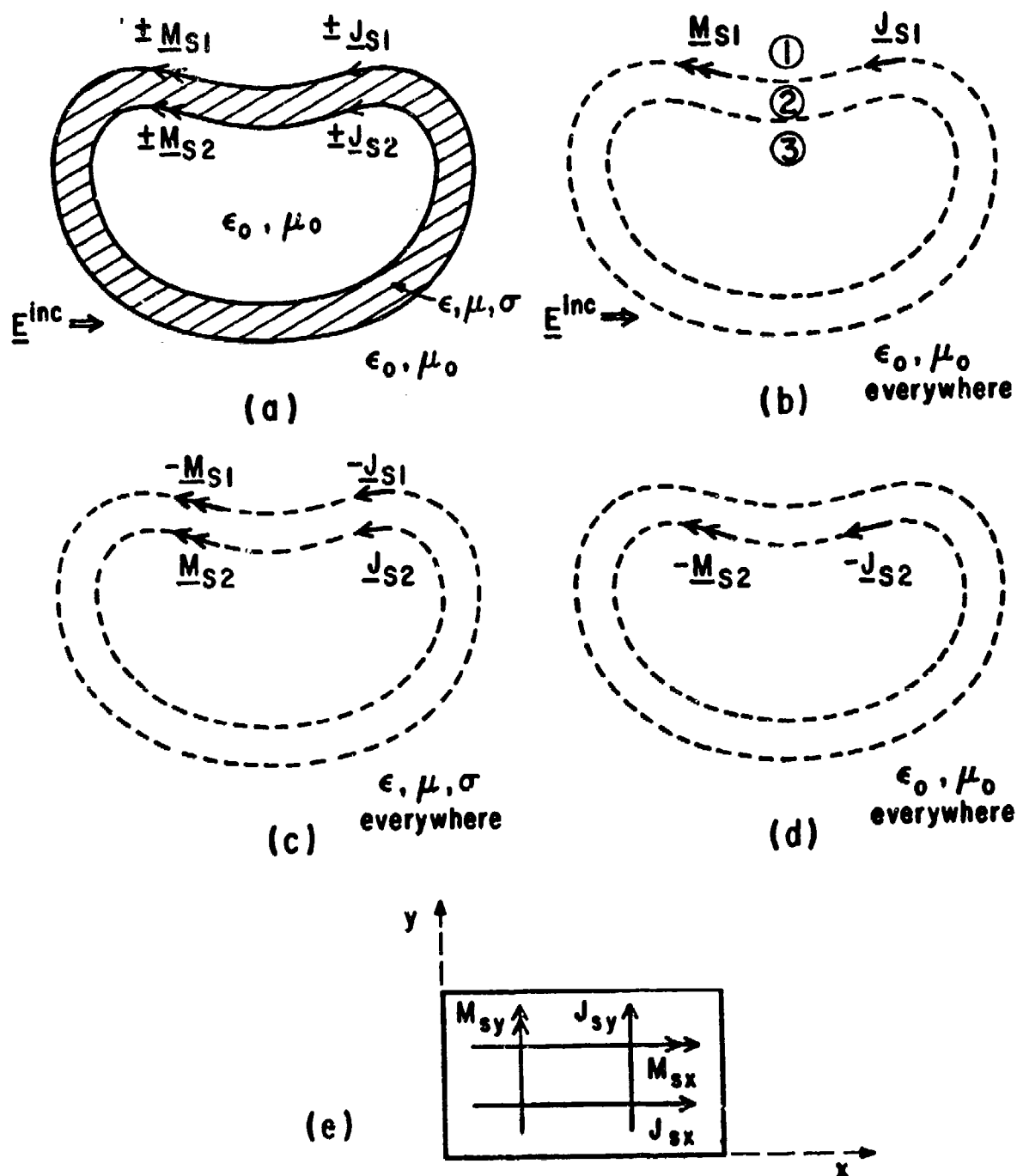


Figure 5-3. The equivalent surface current method.
 (a) equivalent currents, (b) fields in region 1, (c) in region 2, (d) in region 3, (e) patch representation.

surface, where

$$\underline{J}_{s1} = \underline{n} \times \underline{H}_1 \quad (5-4a)$$

$$\underline{M}_{s1} = \underline{E}_1 \times \underline{n} \quad \text{and } \underline{n} \text{ represents outward normals} \quad (5-4b)$$

$$\underline{J}_{s2} = \underline{n} \times \underline{H}_2 \quad \text{to the respective surfaces.} \quad (5-4c)$$

$$\underline{M}_{s2} = \underline{E}_2 \times \underline{n} \quad (5-4d)$$

The outer and inner surfaces are called surfaces 1, 2 respectively. The three regions of the problem are labelled regions 1, 2, 3 respectively from exterior to interior. $(\underline{E}_1, \underline{H}_1)$ and $(\underline{E}_2, \underline{H}_2)$ in eq. (5-4) above represent electric and magnetic fields at surfaces 1 and 2 respectively.

Through the use of the equivalence principle [5-16], the fields in regions 1, 2, 3 may be represented by the source distributions shown in Figs. 5-3b,c,d, respectively. Figs. 5-3b and d involve sources in free space, and Fig. 5-3c involves sources in a homogeneous dissipative space of permittivity ϵ and conductivity σ . Fig. 5-3b involves the incident fields \underline{E}^{inc} , whereas Figs. 5-3c and d do not.

Each set of currents may then be expressed in terms of appropriate expansion functions. Suppose that the surfaces 1 and 2 are subdivided into $m + n$ subareas and that one expansion function is used per subarea for each component of electric and magnetic current. Fig. 5-3e shows such a subarea (a patch) with four expansion functions, one for each component of electric and magnetic current. There are the four unknowns for each subarea and four boundary conditions to be applied at each subarea (continuity of E_x, E_y, H_x, H_y for the patch of Fig. 5-3e). Weighting functions are then chosen, and the application of boundary conditions results in $4(n + m)$ equations in $4(n + m)$ unknowns.

The number of unknowns for this method will in general be smaller than that required for the polarization current method. Also, the number of unknowns will not increase as shell thickness t increases. However, the equivalent surface current method is limited to homogeneous problems.

As noted previously, Fig. 5-3c involves the computation of fields within a homogeneous, dissipative region. This necessitates the determination of corresponding impedance functions within a dissipative medium. Actually, this type of computation should be somewhat simpler than the computation of the corresponding free space impedance functions since the contributions of the fields at a point are more localized; the contribution of nearest current elements will dominate, and the contribution of more distant elements will be accompanied by an exponential decay with distance. Since the formulation of Fig. 5-3c applies only in region 2, one does not necessarily encounter a far-field region.

Several possible simplifications should be noted. For a thick conductor with thick composite "windows", only electric currents need be used and the number of unknowns over the composite surfaces is halved. For a "thin" composite material, only electric currents need to be used over a single surface [5-12]; thus the number of unknowns is one-fourth of that for a thick sheet.

5.1.4.3 Wire-Grid Loading Techniques

Several thin-wire codes have been developed [5-1]. In addition to treating thin-wire geometries, these codes are also capable of approximately treating metallic surfaces, which are modeled as wire-grid structures [5-17-20]. The wire-grid representation has proven useful in the computation

of beam patterns and scattering characteristics. Numerous geometries have been treated by the wire-grid technique. The wire-grid method has its limitations; one would not expect to obtain accurate near fields or interior fields from this representation.

The thin-wire codes can be extended by lumped loading techniques to approximately treat some problems involving composites; for instance, radiation patterns for antennas over a composite surface and scattering from a composite surface.

Consider a thin rectangular composite which can be represented by surface currents (I_x , I_y of Fig. 5-10). Fig. 5-4a indicates a portion of a wire-gridded representation of such a composite surface, with wire currents flowing in the x and y directions. Suppose that each wire section has a finite resistance to approximate the resistance of a portion of the composite surface. In the thin-wire methods, this can be accomplished by opening up each wire section and adding a lumped or distributed load. This is equivalent to open-circuiting all wires which are thus represented by sets of terminals, one at each junction, as shown in Fig. 5-4a. Then loads are placed across each pair of horizontal (x) and vertical (y) terminals. The terminals may be loaded with an impedance associated with the surface current model of Fig. 5-10. The pair of terminals a-b, for instance, may be loaded with the impedance of an area (the shaded area-patch #1 of Fig. 5-4a) from the surface model of Fig. 5-10. Terminals c-d are loaded with an impedance associated with patch #2, etc. The impedance would be computed assuming distributed current flow over the particular patch (section of composite). Computations of the value of the complex impedance load would be carried

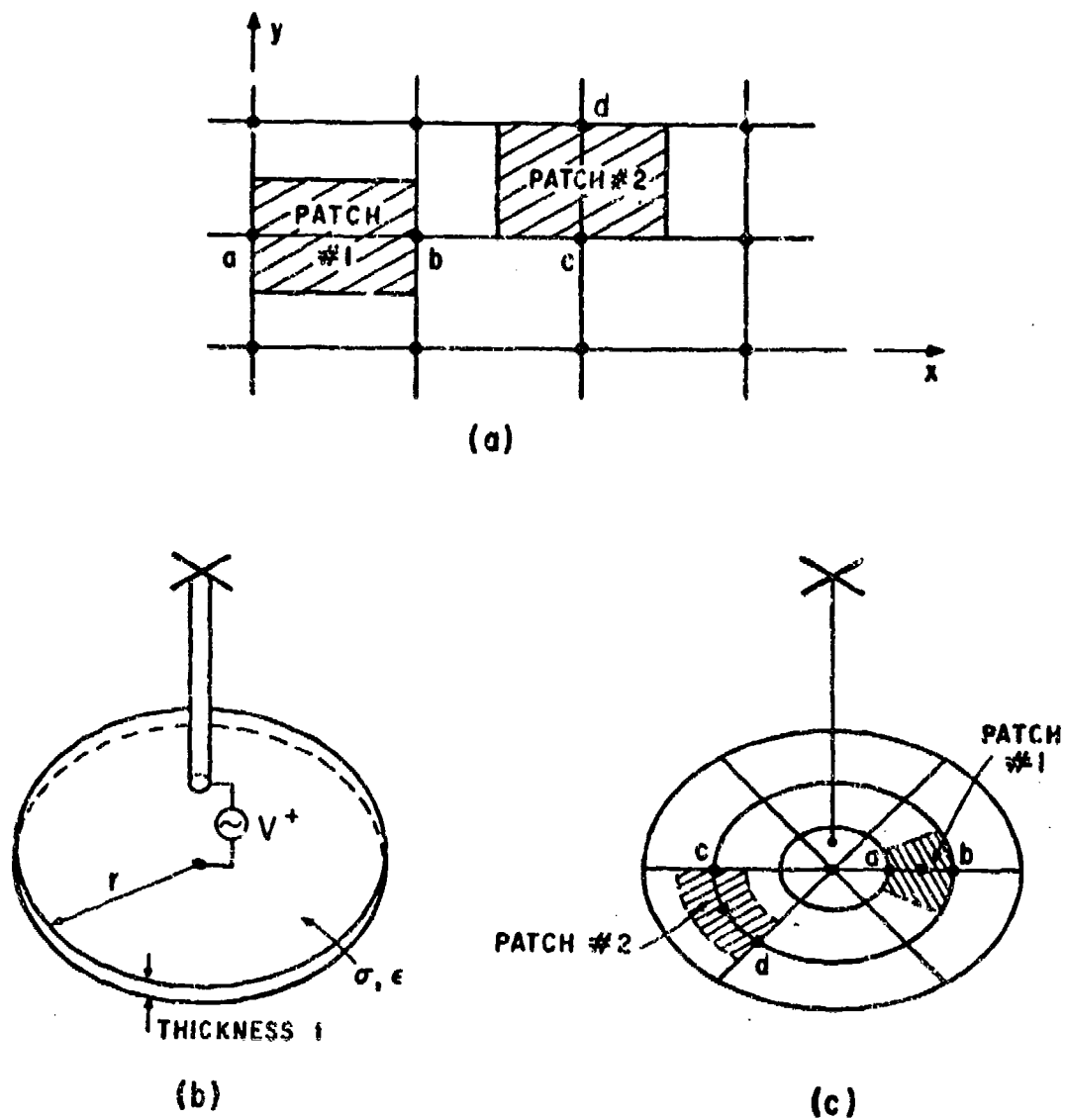


Figure 5-4. Wire-grid method for composite problems.
 (a) wire-grid model for scattering from a composite structure
 (b) radiation from a top-loaded antenna over a composite ground plane, (c) Wire-grid model of Fig. 5-4b.

out by static and quasi-static methods. One must consider carefully the relationship between the two-current models (the thin-wire model and the distributed model) in computing the load impedance elements. Special treatment of impedance elements is required at edges.

The matrix equations for radiation and scattering problems with loading are as follows [5-9]:

Scattering:

$$-[v^1] = [[z] + [z_\ell]][i] \quad (5-5)$$

Radiation:

$$[v'] = [[z] + [z_\ell]][i] \quad (5-6)$$

where $[v^1]$ is an incident matrix, $[v']$ is an applied voltage matrix, $[z]$ is the generalized impedance matrix, $[z_\ell]$ is a load matrix containing the load impedance elements, and $[i]$ represents the unknown currents.

The thin-wire model is taken into account in the generalized impedance $[z]$. The thin wire term z_{ii} represents the voltage across subsection i due to current flow across subsection i through the thin wire of finite radius. The term z_{ii} as used in connection with Figure 5-4a includes all electromagnetic effects due to current flow in the i -th wire subsection. It thus includes the self reactance of the thin wire. One must then consider whether there is a correction required for the self-reactance of a subsection due to the fact that the current is actually spread out over a sheet rather than passing through a thin wire. The resistance of the patch would be computed by straightforward static computations.

Fig. 5-4b shows an example of a radiation problem; i.e., a top-loaded antenna over a composite circular ground plane of radius r , permittivity ϵ ,

conductivity σ , and thickness t . The composite ground plane is replaced with a grid of circumferential and radial wires as shown in Fig. 5-4c. Wires are open-circuited and represented by a set of terminals, one at each junction, as before. Then loads are placed across each pair of circumferential and radial terminals; for instance, loads representing the impedance of patches #1, 2 are placed across terminals a-b, c-d respectively. Special treatment is again required at the edges and origin.

Currently available thin-wire codes which have junction and load capabilities can be directly modified to represent composite surfaces in the manner described above.

5.1.4.4 Surface Loading Techniques

Recently a surface code [5-3] has become available. This code uses pulse expansion and impulsive weighting functions. The pulse expansion functions require a fairly large number of unknowns. This code appears to be thoroughly tested and well-documented. The addition of a load routine to this code would permit the treatment of thin composite material shapes consisting of combinations, including junctions, or rectangular plates.

5.1.4.5 Body of Revolution Methods

Many of the structures which one encounters in practice (such as the fuselage of an aircraft or the body of a missile) can be approximately modeled as bodies of revolution. For this class of problems, several computer codes [5-4,5] are available which permit one to take thin shells of composite material directly into account by loading techniques.

5.1.4.6 Aperture Coupling Methods

Aperture coupling represents an important class of problems for

composite analysis, depicted by Fig. 5-1b. In general, one would want to consider a shell consisting of both conductor and composite, with apertures present. Harrington and Mautz [5-21] have recently completed a general formulation for this type of problem which splits the problem into two mutually exclusive parts and thus permits an analysis in terms of canonical problems. The technique can also be extended to treat bodies constructed of sheets of composite and is thus a completely general method. The general formulation is complete; specific algorithms and codes need to be developed for particular classes of problems.

5.1.5 Special Problems in Composites

There are a number of special problems in composites which can be treated by special methods or extensions of present techniques. Some of these problems can be treated quite simply; others require extensive analysis.

The coupling of energy through a long slot in a ground plane has been treated by the method of moments [5-22,23]. This work could readily be extended to treat long slots covered with a composite material.

The analysis of wire antennas located on or near spherical or cylindrical shells of composite material can be treated by classical methods in conjunction with the method of moments. These geometries might represent antennas on a composite satellite or aircraft fuselage, respectively.

The analysis of antennas over an infinite slab of composite material would be of interest. Considerable effort has been devoted to the related problem of antennas over an imperfect half-space and techniques are available [5-24] for the treatment of some of the improper integrals which result.

For large problems, iterative techniques [5-15] may be useful. These methods are most useful for long, thin objects. Significant reduction in computer time is obtained in some cases.

5.2 LOAD TECHNIQUES FOR THIN WIRES AND SURFACES

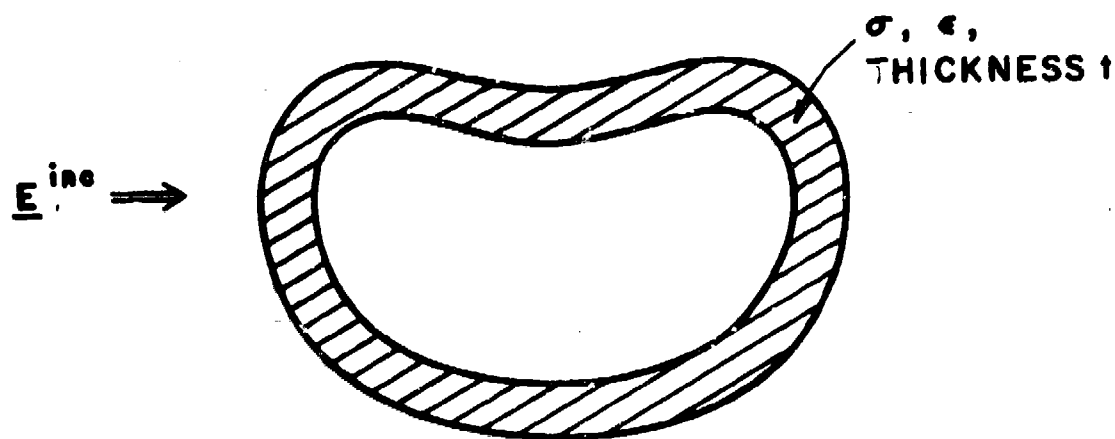
In sections 5.2.1 to 5.2.3, the application of loading and thin-wire techniques is discussed, as related to the analysis of certain problems involving composite materials. In particular, the methods would appear to be useful for problems such as (1) far-field scattering properties (for instance the back-scattering cross section) of composite structures (Fig. 5-5a), and (2) far-field beam patterns of wire antennas in the presence of composite structures (Fig. 5-5b).

5.2.1 Loading Techniques for Thin Wires

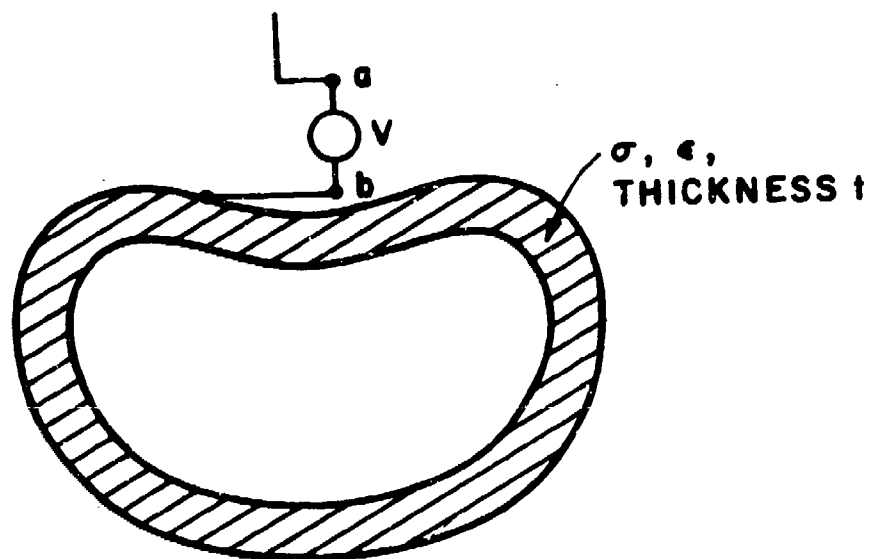
Consider the loading techniques, first as applied to thin-wire geometries, and later as applied to surfaces. Fig. 5-6a shows a collection of thin-wire antennas, for which $L \gg a$, $a \ll \lambda$, where L and a are antenna length and radius, respectively. The antennas are represented by filamentary currents*, subsectioned as shown in Fig. 5-6b. It is assumed that subsection lengths are small electrically, but large compared to antenna radius. The current is expressed in terms of a series of expansion functions [5-8,9], and it is assumed that there are a total expansion functions and N sources and/or loads, as in Fig. 5-6.

Fig. 5-7 shows typical pulse, triangular and sinusoidal expansion functions for a single wire. The typical two-terminal pair, or port of the

* Antenna radius is taken into account by applying boundary conditions at the wire surface.

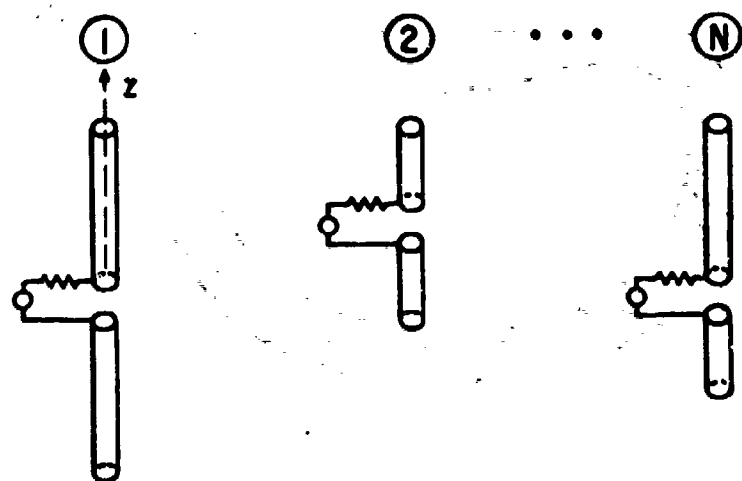


(a)

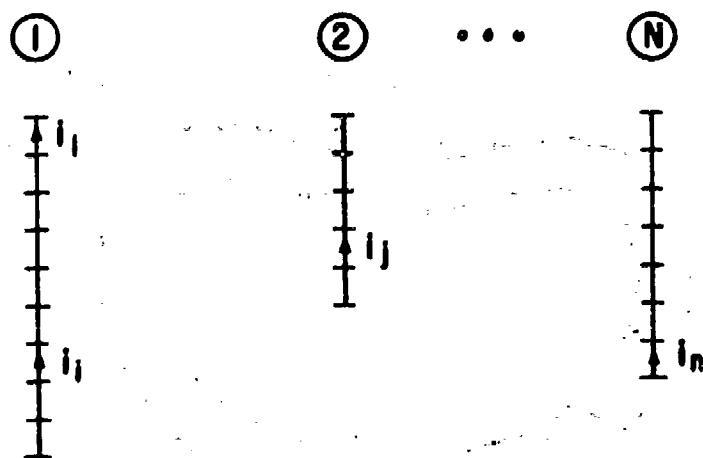


(b)

Fig. 5-5. Composite problems.
(a) far-field scattering properties, (b) far-field radiation properties.



(a)



(b)

Figure 5-6. Thin-wire Antennas

(a) a collection of straight, parallel, thin-wire antennas
 (b) filamentary, subsection model of antennas.

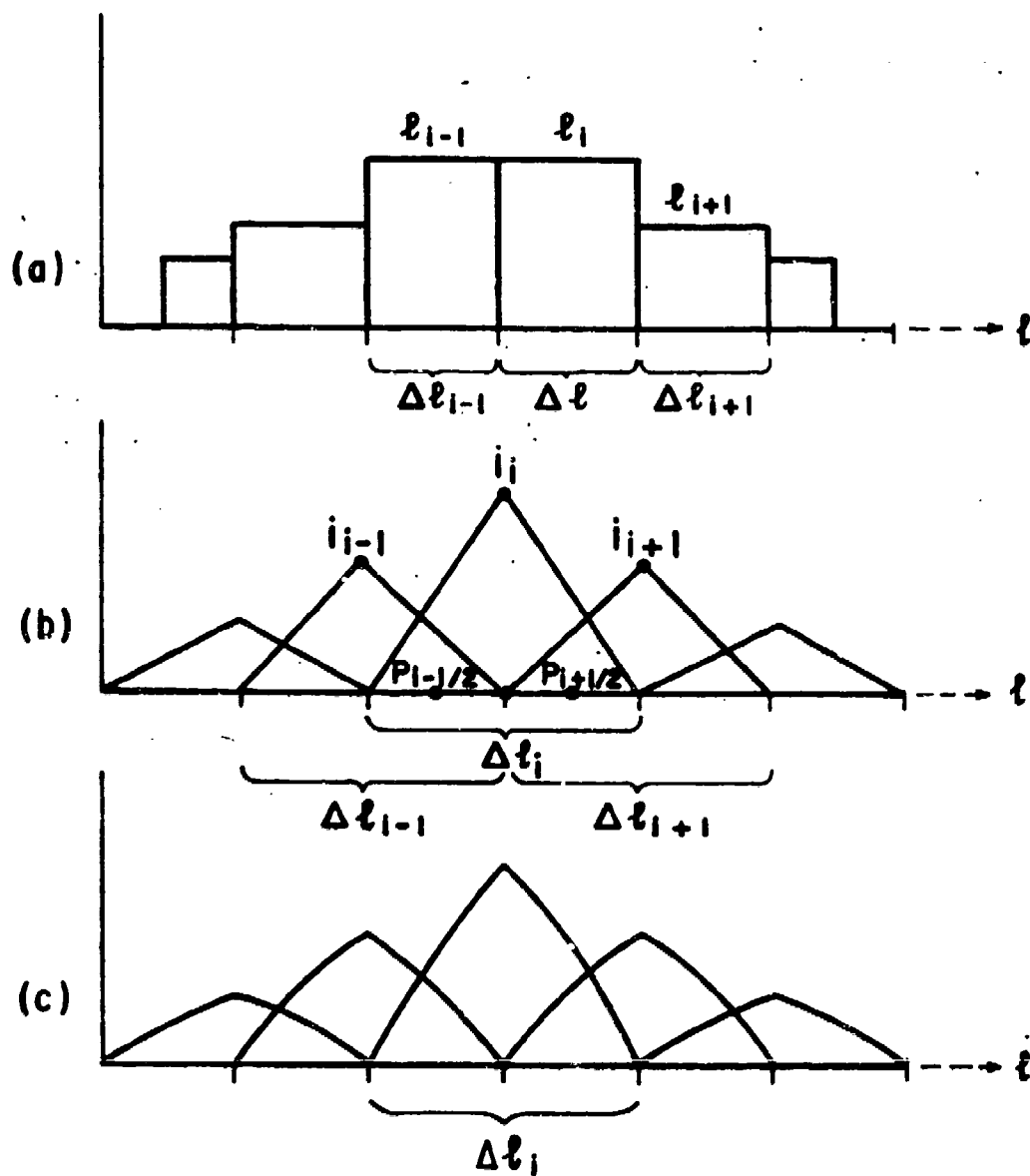


Figure 5-7. Typical expansion functions
 (a) Pulse (b) Triangular (c) Sinusoidal

system, will be represented by a group of subsections, of total length Δl_1 at which the i th expansion function is non-zero. For pulse functions, there is a one-to-one correspondence between subsections and ports; whereas, for triangular and sinusoidal expansion functions, each expansion function spans two subsections and the numbers of subsections and expansion functions for a single wire differ by unity.

To explain this further, assume that weighting and expansion functions are identical. There are n unknowns, one associated with each expansion function. Each expansion function is non-zero over a group of subsections. For instance, let the i th expansion function be non-zero over a group of subsections Δl_1 . A variational expression is obtained if constraints are imposed on the voltage (weighted integral of the electric field) over the same group of subsections Δl_1 . Thus it becomes natural to consider the voltages across groups of subsections Δl_1 as shown in Fig. 5-8.

Fig. 5-8 shows a typical subsection group 1, of length Δl_1 , driven with an applied voltage v_1' and loaded with a lumped impedance element z_{l1} . The v_1' and z_{l1} represent the Thevenin's equivalent circuit of the devices and loads attached to subsection group 1.* Since the subsections are small electrically, the response of the system of antennas to the excitation and loading does not depend on the fine details of the generator and load construction, but only on the values of the applied voltage v_1' and load z_{l1} . As far as terminal behavior is concerned, the electromagnetic problem becomes a network problem. A weighting function is used, and the application

* z_{l1} may thus include internal generator impedance.

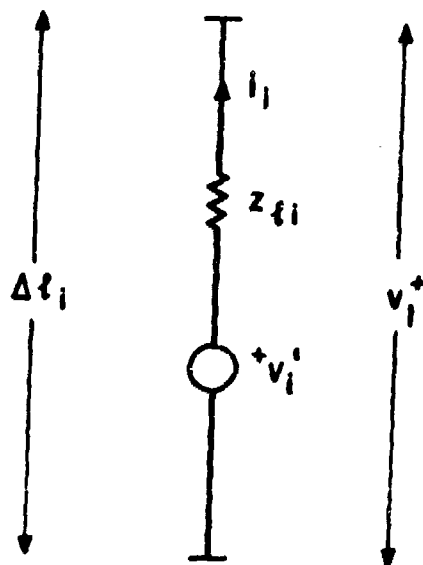


Figure 5-8. A typical driven, loaded group of subsections.

of boundary conditions leads to the matrix equation

$$[v] = [z][i] \quad (5-7)$$

and the equations of constraint

$$[v] = [v'] - [z_\ell][i] \quad (5-8)$$

where

$$[v] = \begin{bmatrix} v_1 \\ \vdots \\ v_n \end{bmatrix}, [v'] = \begin{bmatrix} v'_1 \\ \vdots \\ v'_n \end{bmatrix}, [i] = \begin{bmatrix} i_1 \\ \vdots \\ i_n \end{bmatrix}$$

$$[z] = \begin{bmatrix} z_{11} & \cdots & z_{1n} \\ \vdots & & \vdots \\ \vdots & & \vdots \\ z_{n1} & \cdots & z_{nn} \end{bmatrix} \quad \text{and} \quad [z_\ell] = \begin{bmatrix} z_{\ell 1} & \bigcirc & \vdots \\ \vdots & \bigcirc & \vdots \\ \bigcirc & \vdots & \ddots \\ \vdots & \vdots & \vdots & z_{\ell n} \end{bmatrix}$$

Combining (5-7) and (5-8) yields

$$[v] = \begin{bmatrix} v'_1 - z_{\ell 1} & i_1 \\ v'_2 - z_{\ell 2} & i_2 \\ \vdots & \vdots \\ v'_n - z_{\ell n} & i_n \end{bmatrix} = \begin{bmatrix} z_{11} & \cdots & z_{1n} \\ \vdots & & \vdots \\ \vdots & & \vdots \\ z_{n1} & \cdots & z_{nn} \end{bmatrix} \begin{bmatrix} i_1 \\ \vdots \\ i_n \end{bmatrix} \quad (5-9)$$

Transposing terms $-z_{\ell k} i_k$ yields

$$\begin{bmatrix} v'_1 \\ v'_2 \\ \vdots \\ v'_n \end{bmatrix} = \begin{bmatrix} (z_{11} + z_{\ell 1}) & z_{12} & \cdots & z_{1n} \\ z_{21} & (z_{22} + z_{\ell 2}) & & \vdots \\ \vdots & \vdots & \ddots & \vdots \\ z_{n1} & \cdots & \cdots & (z_{nn} + z_{\ell n}) \end{bmatrix} \begin{bmatrix} i_1 \\ \vdots \\ \vdots \\ i_n \end{bmatrix}$$

or

$$[v'] = [[z] + [z_\ell]][i] . \quad (5-10)$$

Solving for the currents yields

$$[i] = [[z] + [z_\ell]]^{-1}[v'] . \quad (5-11)$$

The total voltages $[v]$ may be determined by Eq. (5-9). Note that the effect of loading is merely to replace the matrix $[z]$ with $[[z] + [z_\ell]]$ and $[v]$ with $[v']$.

In Eq. (5-8), zeros occur on the left-hand side if the total voltage across a subsection is zero. In Eq. (5-10), zeros occur on the left-hand side only if the applied voltage is zero. Thus, if a subsection is loaded but not driven, a zero would occur in the appropriate element of $[v']$. Problems involving loading and excitation may be treated by the above formulation. In some cases in which terminal behavior alone is sought, a simpler equation with N unknowns may be used as explained in [5-9].

The load impedance $[z_\ell]$ may contain some off-diagonal terms in the general case. To show this, consider the current $I(\ell)$ which is represented by a series of expansion functions as follows:

$$I(\ell) = \sum_{j=1}^n i_j f_j(\ell) \quad (5-12)$$

where $I(\ell)$ represents the total current at a point ℓ , ℓ is a coordinate which spans the filaments of Fig. 5-6b, i_j are complex numbers (representing, for instance, pulse heights and triangle peaks in Figs. 5-7a, and b, respectively), and $f_j(\ell)$ are the expansion functions (for instance, the triangle functions of Fig. 5-7c).

The typical voltage v_i is defined in terms of a weighted integral of the

tangential electric field over the i th group of subsections:

$$v_i = - \int_{\Delta l_i} E_\ell(\ell) v_i(\ell) d\ell \quad (5-13)$$

where $E_\ell(\ell)$ is the tangential electric field (parallel to the coordinate ℓ) and $v_i(\ell)$ is an arbitrary weighting function.*

Now consider the i th group of subsections over which the i th expansion function is non-zero. Assume that this group is loaded but not driven ($v_i' = 0$) as shown in Fig. 5-9a. Now write the i th equation of (5-9):

$$v_i = -z_{li} i_i = z_{i1} i_1 + z_{i2} i_2 + \dots + z_{ii} i_i + \dots + z_{in} i_n \quad (5-14)$$

For off-center lumped loading (load not located at center of subsection group i) or for distributed loading, the term $-z_{li} i_i$ on the left-hand side of equation (5-14) may be altered. Terms involving i_{i+1} , i_{i-1} , etc., may be required, as shown by the following discussion. For instance, consider off-center lumped loading with triangular expansion functions. Locate a lumped load z_{li} at some point in Δl_i (subsection group i). The total current at the load point ℓ is

$$I(\ell) = \sum_j i_j f_j(\ell) \quad (5-15)$$

which reduces to

$$I(\ell) = i_{i-1} f_{i-1}(\ell) + i_i f_i(\ell) + i_{i+1} f_{i+1}(\ell) \quad (5-15)$$

(since f_{i-1} , f_i , f_{i+1} are the only expansion functions which are non-zero on Δl_i).

*For a Galerkin (variational) solution, weighting and expansion functions are identical.

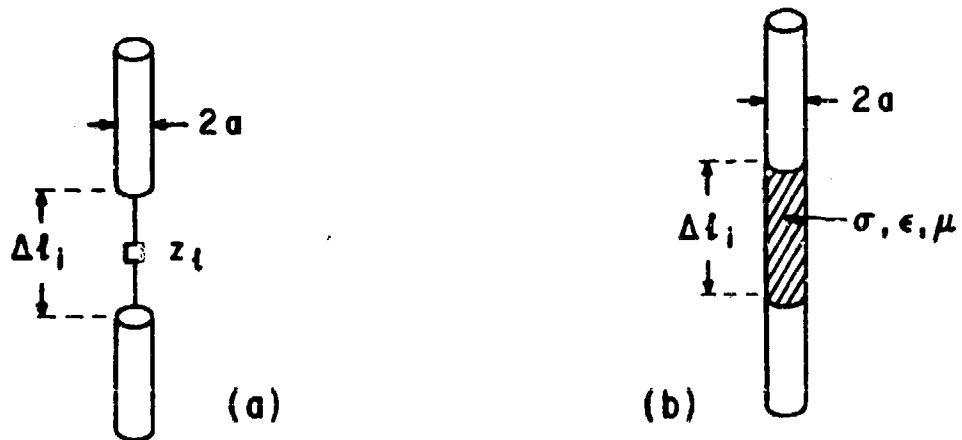


Figure 5-9. Thin-wire loading.
(a) lumped (b) distributed

For lumped loading at particular points $P_{i-1/2}$, P_i , $P_{i+1/2}$ (shown in Fig. 5-7), the total current reduces to

$$\left(\frac{i_{i-1}}{2} + \frac{i_i}{2}\right), \quad (i_i), \quad \text{and} \quad \left(-\frac{i_i}{2} + \frac{i_{i+1}}{2}\right),$$

respectively. This total current replaces I_i in eq. (5-14) which leads to a tridiagonal form for $[z_\ell]$, since three expansion functions are non-zero on $\Delta\ell_i$.

5.2.2 Loading Techniques for Surfaces

Now consider the application of loading techniques to surfaces. Fig. 5-10 shows a rectangular section of composite material which might be a portion of a composite scatterer (Fig. 5-5a). Surface currents on the scatterer are represented as follows:

$$\begin{aligned} \underline{J}_s &= J_{sx}\hat{x} + J_{sy}\hat{y} \\ &= \sum_{j=1}^n I_{xj} f_{xj}(x,y)\hat{x} + \sum_{j=1}^n I_{yj} f_{yj}(x,y)\hat{y} \end{aligned} \quad (5-17)$$

where $f_{xj}(x,y)$, $f_{yj}(x,y)$ are expansion functions, I_{xj} , I_{yj} are complex numbers and \hat{x} , \hat{y} are unit vectors. Using weighting functions $w_{x1}(x,y)$, $w_{y1}(x,y)$ and applying boundary conditions (see Appendix 5-A), one obtains the matrix equation

$$\begin{bmatrix} v_{x1} \\ \vdots \\ v_{xn} \\ v_{y1} \\ \vdots \\ v_{yn} \end{bmatrix} = \begin{bmatrix} z_{xx} & z_{xy} \\ \vdots & \vdots \\ z_{yx} & z_{yy} \end{bmatrix} + \begin{bmatrix} z_{\ell 1} & z_{\ell 2} & \cdots \\ \vdots & \vdots & \ddots \\ \vdots & \vdots & \vdots & z_{\ell 2n} \end{bmatrix} \begin{bmatrix} I_{x1} \\ \vdots \\ I_{xn} \\ I_{y1} \\ \vdots \\ I_{yn} \end{bmatrix} \quad (5-18)$$

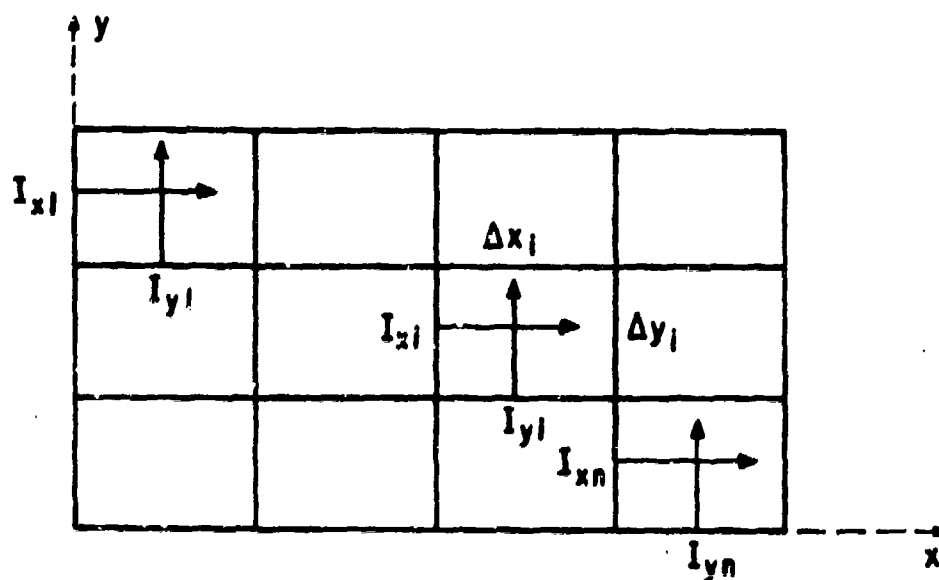


Figure 5-10. A rectangular section of a composite structure.

which is of the form

$$[v] = [[z] + [z_l]][I] \quad (5-19)$$

as before in Eq. 5-10.

The matrix $[v]$ is the negative of the specified incident fields as in [5-9]. The first matrix $[z]$ on the right-hand side of (5-19) represents the generalized impedance matrix and the second matrix $[z_l]$ represents the load matrix. As shown in section 5.2.1, $[z_l]$ is diagonal for pulse functions and may be slightly more complex for triangular and sinusoidal expansion functions.

5.2.3 Application of the Load Techniques

Both the thin-wire and surface loading techniques have applications to electromagnetic problems involving composites. For composite geometries consisting of flat plates, the surface code available [5-3] can be applied directly once a load routine is added. For bodies of revolution, there is a code available which can take thin composites into account [5-4]. For more general surface geometries, these can be approximated by loaded flat plates [5-3] or by loaded thin wires.

Appendix 5A. The Polarization Method and Surface Loading

Consider the situation shown in Fig. 5-1a, with electric fields \underline{E}^{inc} incident upon a volume of composite material. The volume current density \underline{J} induced in the material may be expressed in terms of expansion functions:

$$\underline{J}(\underline{r}) = \sum_j^{3n} J_{j-f}(\underline{r}') \quad (5-20)$$

$$= \sum_{j=1}^n J_{xj} f_{xj}(\underline{r}') \hat{x} + \sum_{j=n+1}^{2n} J_{yj} f_{yj}(\underline{r}') \hat{y} + \sum_{j=2n+1}^{3n} J_{zj} f_{zj}(\underline{r}') \hat{z} \quad (5-21)$$

where J_{xj} , etc. are unknown constants, and f_{xj} , etc. are known expansion functions. The vector potential \underline{A} is defined as follows:

$$\underline{A} = \frac{\mu}{4\pi} \iiint \frac{\underline{J}(\underline{r}') e^{-jk|\underline{r}-\underline{r}'|}}{|\underline{r}-\underline{r}'|} dv' \quad (5-22)$$

The scattered field \underline{E}^s due to induced current \underline{J} is

$$\underline{E}^s = \frac{\nabla \times \nabla \times \underline{A}}{j\omega\epsilon u} - \frac{\underline{J}}{j\omega\epsilon} \quad (5-23)$$

The total electric field \underline{E} is the sum of incident and scattered fields

$$\underline{E} = \underline{E}^{inc} + \underline{E}^s \quad (5-24)$$

Generalized voltages are obtained by multiplying Eq. (5-24) by weighting functions w_i and integrating over the i th group of subsections (The i th expansion function is non-zero only over volume Δv_i consisting of subsection group i . The subsections represent volume elements.). The result is

$$[v] = [v^{inc}] + [v^s] \quad (5-25)$$

where typical elements of $[v]$, $[v^s]$, $[v^{inc}]$ are

$$\begin{aligned} v_{x1} &= \int_{\Delta v_1} E_x(\underline{r}) w_1(\underline{r}) dv \\ v_{x1}^s &= \int_{\Delta v_1} E_x^s(\underline{r}) w_1(\underline{r}) dv \\ v_x^{inc} &= \int_{\Delta v_1} E_x^{inc}(\underline{r}) w_1(\underline{r}) dv \end{aligned} \quad (5-26)$$

Combining equation (5-21), (5-22), (5-23) and (5-26) a linear relationship is obtained between currents $[i]$ and scattered voltages $[v^s]$:

$$[v^s] = [z][i] \quad (5-27)$$

where $[z]$ represents a generalized impedance matrix.

Electric fields and induced currents at a given field point (\underline{r}) are proportional:

$$\underline{J} = [\sigma + j\omega(\epsilon - \epsilon_0)] \underline{E}$$

or

$$\underline{E} = \frac{1}{\sigma + j\omega(\epsilon - \epsilon_0)} \underline{J} \quad (5-28)$$

Integrating and multiplying both sides of eq. (5-28) by weighting function $w_1(\underline{r})$ and integrating over Δv_1 , a linear relationship between voltages $[v]$ and currents $[i]$ is obtained,

$$[v] = -[z_\lambda][i] \quad (5-29)$$

since voltages are weighted integrals of the fields. $[z_\lambda]$ is a diagonal matrix for pulse functions and a multi-diagonal one for triangles, etc. as

explained in section 5.2.1 for the wire loading case. $[z_0]$ is determined by eq. (5-28) which related currents and fields at a point. Then

$$[-v^{inc}] = [[z] + [z_0]][1] \quad (5-30)$$

as in eq. (5-3).

For surface loading, the formulation is quite similar. The surface currents \underline{J}_s are expressed in terms of expansion functions:

$$\begin{aligned} \underline{J}_s &= \sum_{j=1}^n J_{sj} f_j(x, y) \\ &= \sum_{j=1}^n I_{xj} f_{xj}(x, y) \hat{x} + \sum_{j=1}^n I_{yj} f_{yj}(x, y) \hat{y} \end{aligned} \quad (5-31)$$

The total field is expressed as a sum of incident and scattered fields as in (5-24). The scattered fields are proportional to induced surface currents as in (5-27), and the fields on the composite may be related to currents and impedance, as in (5-29), where

$$[I] = \begin{bmatrix} I_{x1} \\ \vdots \\ I_{xn} \\ - \\ I_{y1} \\ \vdots \\ I_{yn} \end{bmatrix}$$

Combining (5-27) and (5-29) yields (5-30) as before.

SYMBOLS USED IN SECTION 5

a = antenna radius

\underline{A} = vector magnetic potential

\underline{E} = electric field intensity

$\underline{E}^{\text{inc}}$ = incident electric field vector

$f_j(\ell)$ = expansion function

$[i]$ = current matrix

$I(\ell)$ = total current at a point

$j = \sqrt{-1}$

\underline{J}_c = volume conduction current density

\underline{J}_s = electric surface current

$\underline{J}_{\text{TOTAL}}$ = equivalent total volume current density

L = antenna length

\underline{M}_s = magnetic surface current

\underline{n} = normal to a surface

P = polarization

t = thickness

$[v^i]$ = incident voltage matrix

$[v']$ = applied voltage matrix

$w_1(\ell)$ = weighting function

$[Z]$ = generalized impedance matrix

$[Z_\ell]$ = diagonal load matrix

δ = skin depth

ϵ = permittivity

ϵ_0 = permittivity of free space = 8.85×10^{-12} farad/meter

λ = wavelength

μ = permeability

μ_0 = permeability of free space = 1.257×10^{-6} henry/meter

σ = conductivity

ϕ = scalar potential

ω = radian frequency

The rationalized MKS system is used throughout.

REFERENCES

- [5-1] J. Allen et al., "A Technology Plan for Electromagnetic Characteristics of Advanced Composites," RADC TR-76-206, July 1976, AD# A030507.
- [5-2] J.R. Mautz and R.F. Harrington, "Electromagnetic Transmission Through a Rectangular Aperture in a Perfectly Conducting Plane," TR-76-1, Feb. 1976, Dept. of Electrical and Computer Engineering, Syracuse University, Syracuse, NY 13210.
- [5-3] D.R. Wilton, A.W. Glisson, and C.M. Butler, "Numerical Solutions for Scattering by Rectangular Bent Plate Structures," Dept. of Electrical Engineering, Univ. of Mississippi, Oct. 1976, Report on Contract No. N00123-75-C-1372.
- [5-4] R.F. Harrington and J.R. Mautz, "Radiation and Scattering from Loaded Bodies of Revolution," Radio Science, Applied Scientific Research, Vol. 26, June 1971, pp. 209-217. See also computer program description, IEEE Trans. on Antennas and Propagation, Vol. AP-23, No. 4, p. 594, July 1975.
- [5-5] R.F. Harrington and J.R. Mautz, "Green's Functions for Surfaces of Revolution," Radio Science, Vol. 27, No. 5, May 1972, pp. 603-611.
- [5-6] W.K.H. Panofsky and M. Phillips, Classical Electricity and Magnetism. Addison-Wesley Publishing Company, Reading, Mass., 1st ed., p. 121.
- [5-7] A.T. Adams, "Equivalent Sources," Internal Memorandum, Dept. of Electrical and Computer Engineering, Syracuse University, March 1977.
- [5-8] R.F. Harrington, Field Computation by Moment Methods. Macmillan Company, New York, 1968, Chapter 4.
- [5-9] A.T. Adams, "An Introduction to the Method of Moments," RADC Method of Moments Applications, Vol. 1, RADC-TR-73-217, November 1974, Chapters 1 and 2, AD# A002820.
- [5-10] J.H. Richmond, "Scattering by a Dielectric Cylinder of Arbitrary Cross Section," IEEE Trans. on Antennas and Propagation, Vol. AP-13, No. 3, May 1965, pp. 334-342.
- [5-11] J.H. Richmond, "TE Scattering by a Dielectric Cylinder of Arbitrary Cross Section Shape," IEEE Trans. on Antennas and Propagation, Vol. AP-14, No. 4, July 1966, pp. 460-465.
- [5-12] R.F. Harrington and J.R. Mautz, "An Impedance Sheet Approximation for Thin Dielectric Shells," IEEE Trans. on Antennas and Propagation, pp. 531-534, July 1975.

- [5-13] K.K. Mei, "Unimoment Method of Solving Antenna and Scattering Problems," IEEE Trans. on Antennas and Propagation, Vol. AP-22, No. 6, November 1974, pp. 760-766.
- [5-14] R.E. Stovall and K.K. Mei, "Application of a Unimoment Technique to a Biconical Antenna with Inhomogeneous Dielectric Loading," IEEE Trans. on Antennas and Propagation, Vol. AP-23, No. 3, May 1975, pp. 335-342.
- [5-15] S.K. Chang and K.K. Mei, "Application of the Unimoment Method to Electromagnetic Scattering of Dielectric Cylinders," IEEE Trans. on Antennas and Propagation, Vol. AP-24, No. 1, January 1976.
- [5-16] R.F. Harrington, Time-Harmonic Electromagnetic Fields. McGraw-Hill, New York, 1961, Chapter three.
- [5-17] J.H. Richmond, "A Wire-Grid Model for Scattering by Conducting Bodies," IEEE Trans. on Antennas and Propagation, Vol. AP-14, Nov. 1966, pp. 782-785.
- [5-18] R. Mittra, Editor, Numerical and Asymptotic Techniques in Electromagnetics. Springer-Verlag, N.Y., 1975, Chapter Four, pp. 118-121.
- [5-19] S. Gee, E.K. Miller, A.J. Poggio, E.S. Selden, G.J. Burke, "Computer Techniques for Electromagnetic and Radiation Analysis," IEEE-EMC Symposium Record, Philadelphia, PA, 1971.
- [5-20] Antenna Modeling Program: Engineering Manual (Report IS-R-72-10, July 1972), User Manual (Report IS-R-72/15, July 1975), Systems Manual (Report IS-R-72/10, April 1973), Information Systems Division of MB Associates, Menlo Park, CA.
- [5-21] R.F. Harrington and J.R. Mautz, "A Generalized Network Formulation for Aperture Problems," TR-75-13, Nov. 1975, Dept. of Electrical and Computer Engineering, Syracuse University, Syracuse, NY 13210.
- [5-22] Jason Chou and A.T. Adams, "Aperture Coupling Through Large Slots," RADC Method of Moments Applications, Vol. VII, RADC-TR-73-217, December 1975, AD# A019771.
- [5-23] D.T. Auckland, "Electromagnetic Transmission Through a Slit in a Perfectly Conducting Plane," Technical Report TR-76-9, Sept. 1976, Dept. of Electrical & Computer Engineering, Syracuse University, Syracuse, NY.
- [5-24] Tapan K. Sarkar and Bradley J. Strait, "Analysis of Arbitrarily Oriented Thin Wire Antenna Arrays over Imperfect Ground Planes," Technical Report TR-75-15, Dec. 1975, Dept. of Electrical and Computer Engineering, Syracuse University, Syracuse, NY 13210.
- [5-25] R.J. Balestri, T.R. Ferguson and E.R. Anderson, "General Electromagnetic Model for the Analysis of Complex Systems," Vol. I (User's Manual) and Vol. II (Engineering Manual). The BDM Corp., Final Technical Report on Contract No. F30602-74-C-0182, April 1977.

6.0 ANTENNA CHARACTERISTICS

The increasing use of composite materials has prompted several studies of antennas with a composite ground plane, but most of these have been published in limited distribution reports.

This section presents measurements made for several antennas mounted first on a metal ground plane and then on a graphite/epoxy ground plane. A more complete account of these measurements will be presented in a report to be issued by the USAF Academy (6-1).

6.1 THE GROUND PLANE

Both the aluminum and the graphite/epoxy ground planes are 5 feet square. The aluminum ground plane is approximately 1/8 inch thick. The graphite/epoxy ground plane is approximately 1/4 inch thick, constructed of 50 plies of graphite/epoxy cloth made by Fiberite (Fiberite number HMF-133/34). The graphite/epoxy ground plane was constructed at the Composites Laboratory of the Air Force Flight Dynamics Laboratory at Wright-Patterson AFB, OH.

The antennas were mounted in the center of the ground plane.

6.2 INPUT IMPEDANCE

The input impedance of the two monopole antennas was measured using the slotted line technique.

The input impedance of a monopole antenna 18.7 cm long was measured between 260 and 430 MHz. The results are given in Figure 6-1. The input impedance of a second monopole antenna 8.7 cm long was measured between 780 and 900 MHz. The results are given in Figure 6-2.

6.3 ANTENNA PATTERNS

Antenna patterns were measured on the antenna range on top of the Radio Frequency Systems Laboratory at the USAF Academy, CO. In all cases the pattern was measured with the antenna on the ground plane as the receiver. The pattern was measured for both the aluminum and the graphite/epoxy ground plane. Unfortunately the power was not constant so the comparison of antenna patterns is for SHAPE ONLY. A comparison of the absolute gain of an antenna over the two ground planes is not possible.

The antenna patterns are plotted on a logarithmic scale and the noise of the measurements was averaged out by the draftsman.

6.3.1 Monopole Antennas

The antenna patterns for the monopole antennas of section 6.2 were measured. The results for the 18.7 cm antenna at 370 MHz are given in Figures 6-4 and 6-5. The results for the 8.7 cm antenna at 837 MHz are given in Figures 6-6 and 6-7. The coordinate system is shown in Figure 6-3a.

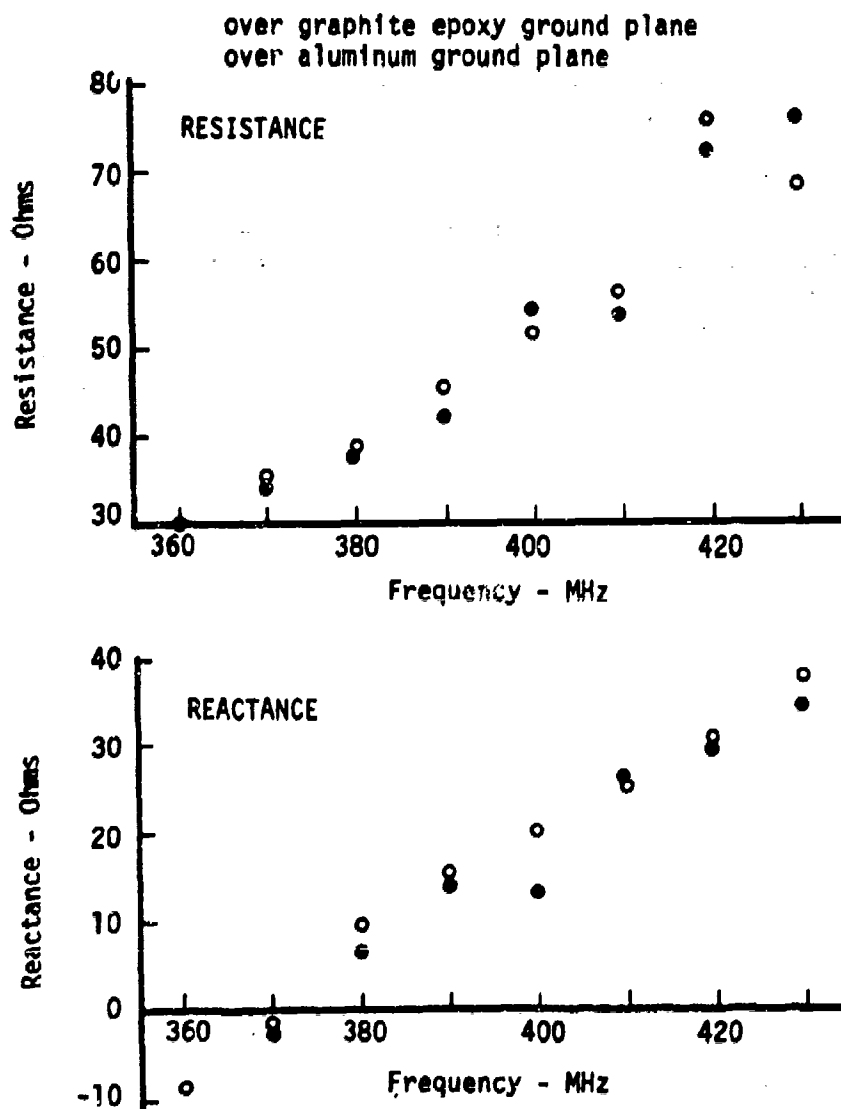


Figure 6-1 Impedance of a Monopole Antenna
(360 - 430 MHz)

over graphite epoxy ground plane
over aluminum ground plane

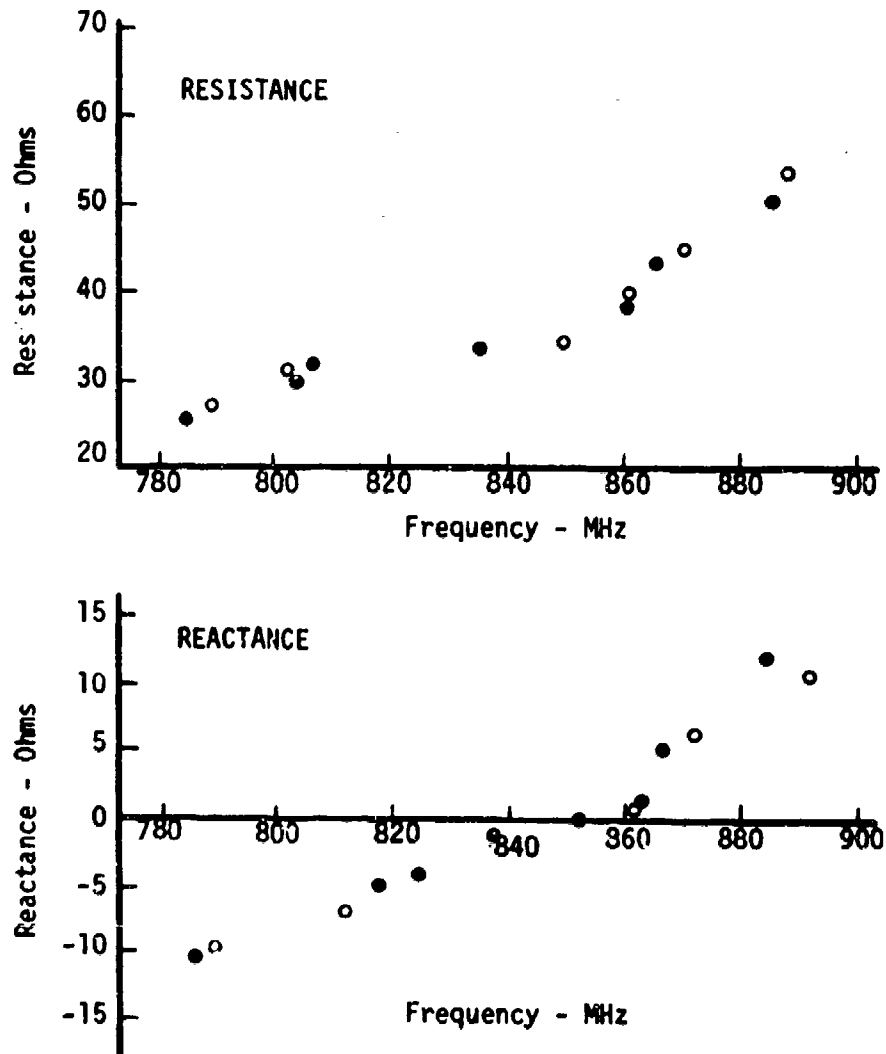


Figure 6-2 Impedance of a Monopole Antenna
(780 - 900 MHz)

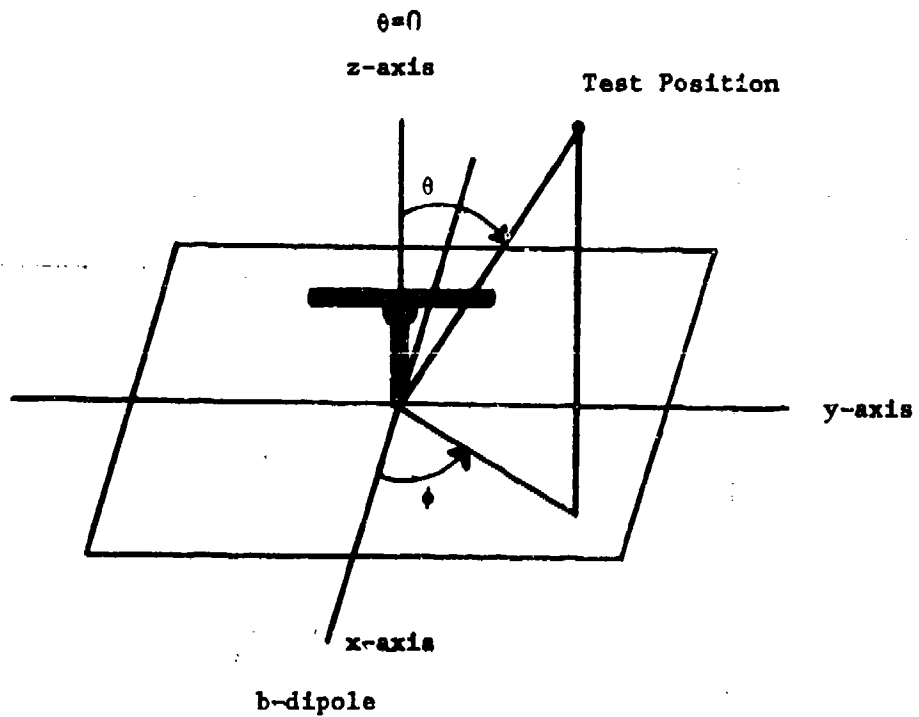
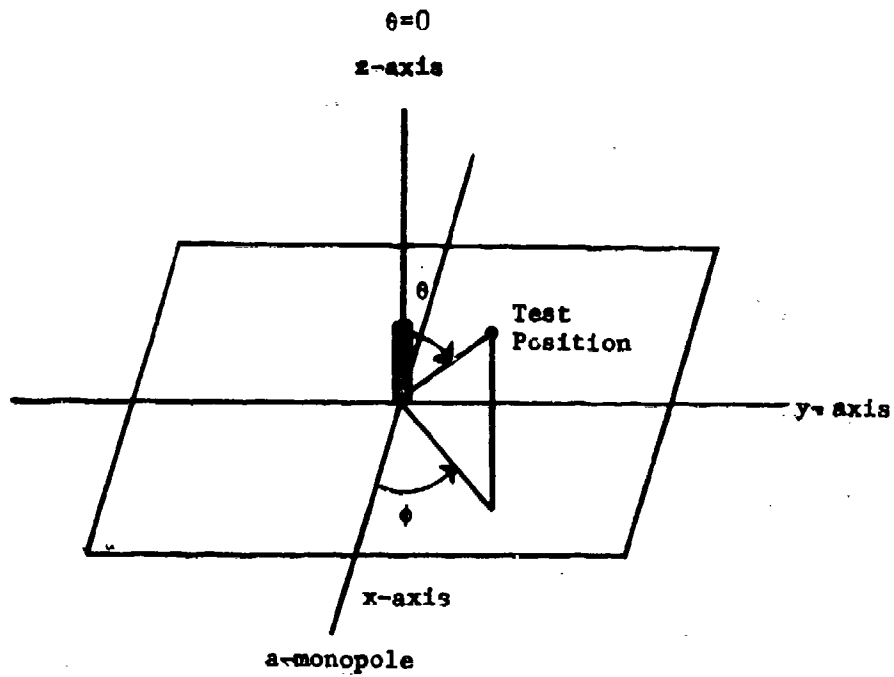


Figure 6-3 The coordinate systems used for the antenna patterns: a. monopole; b. dipole.

NOTE POWER LEVEL DIFFERENT FOR THESE TWO PATTERNS

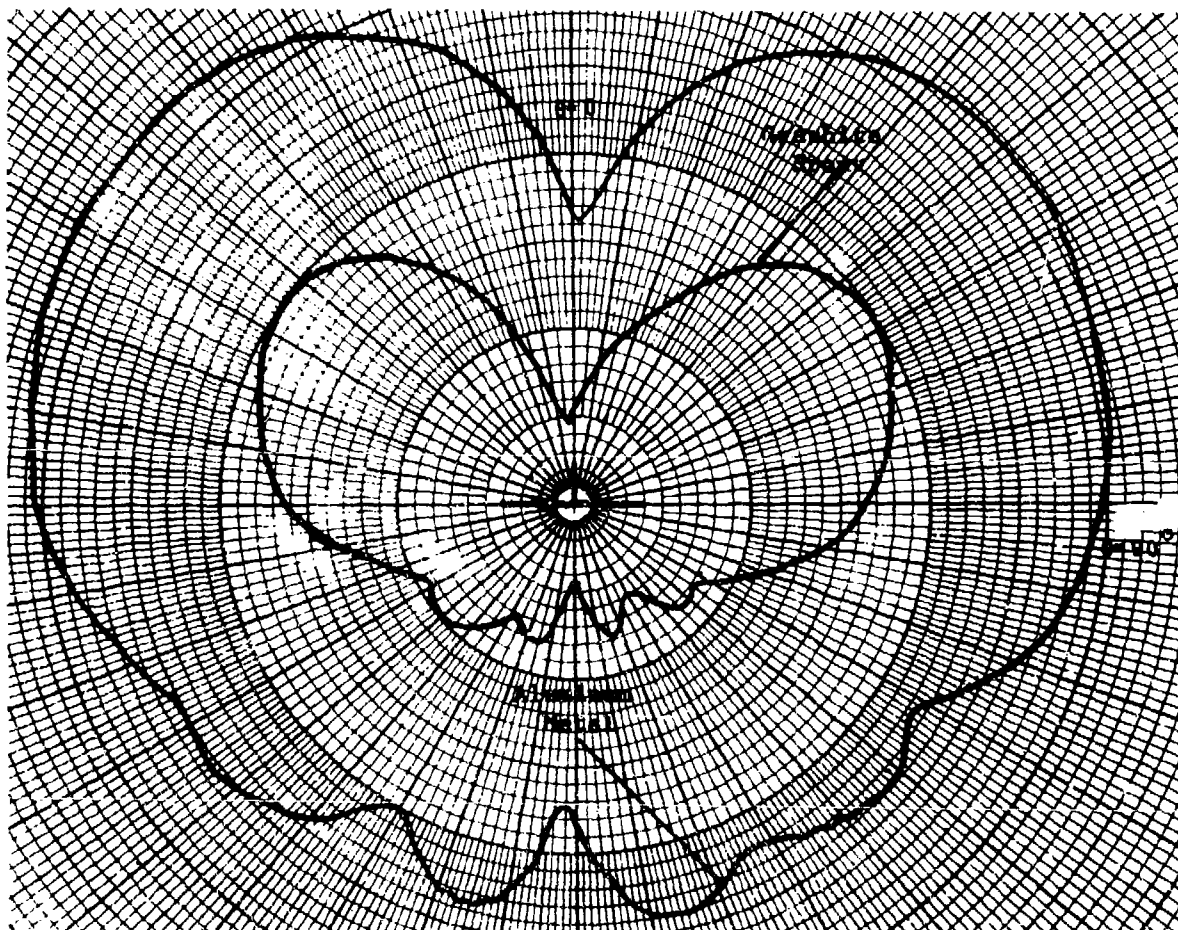


Figure 6-4 Monopole antenna at 370 MHz
Antenna pattern in the $\phi=0$ plane

NOTE POWER LEVEL DIFFERENT FOR THESE TWO PATTERNS

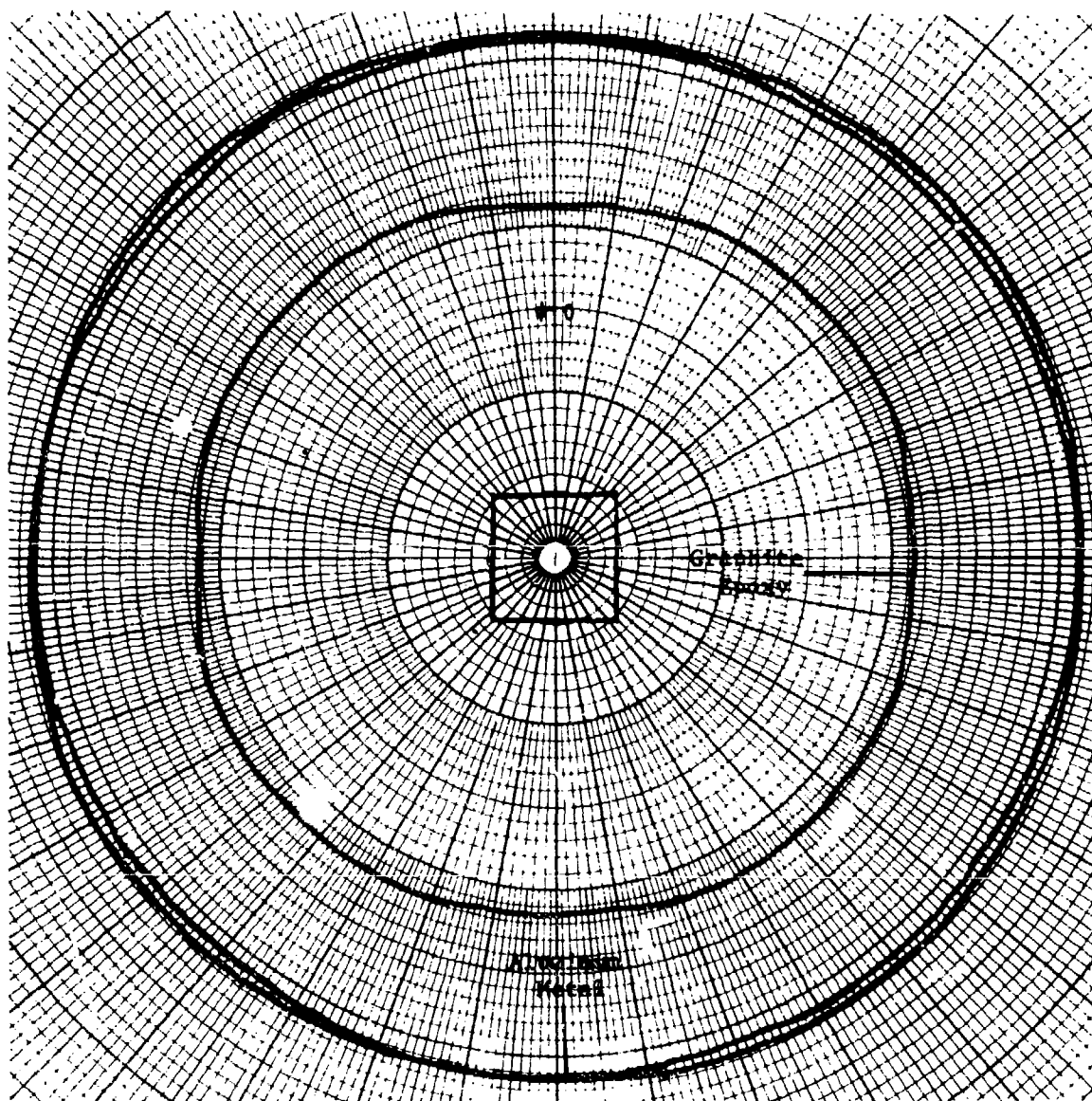


Figure 6-5 Monopole Antenna at 370 MHz
Conical antenna pattern at $\theta=70^\circ$

NOTE POWER LEVEL DIFFERENT GOT THESE TWO PATTERNS

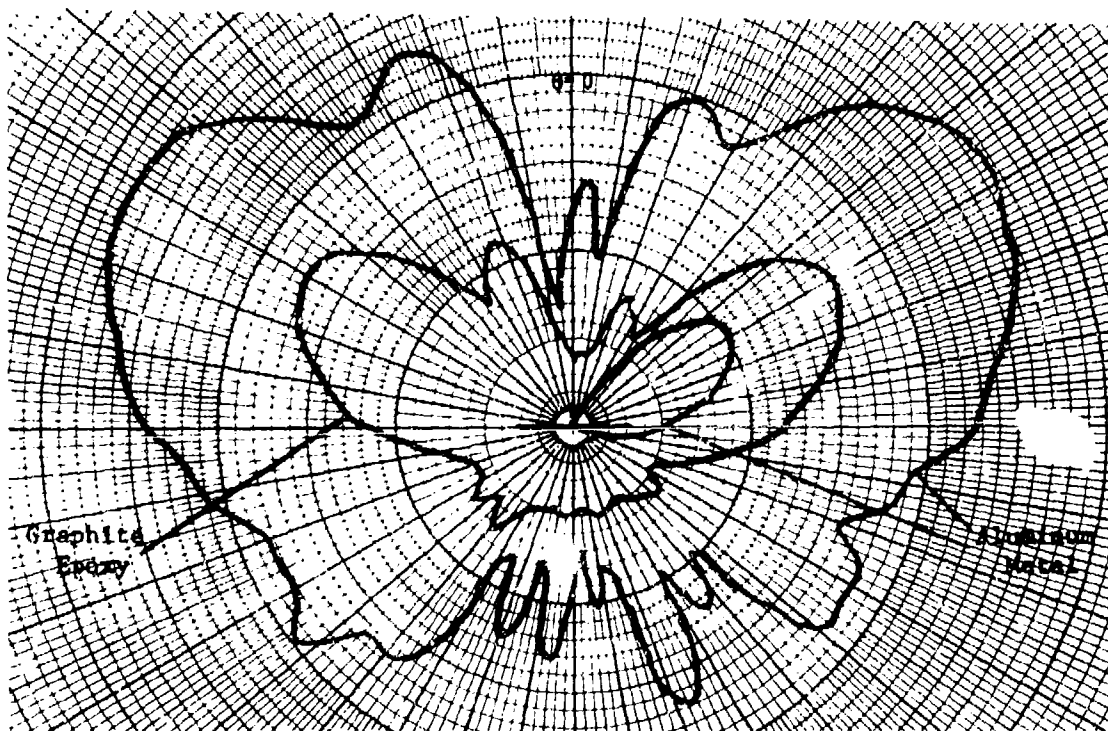


Figure 6-6 Monopole antenna at 837 MHz.
Antenna pattern in the $\phi=0$ plane.

NOTE POWER LEVEL DIFFERENT FOR THESE TWO PATTERNS

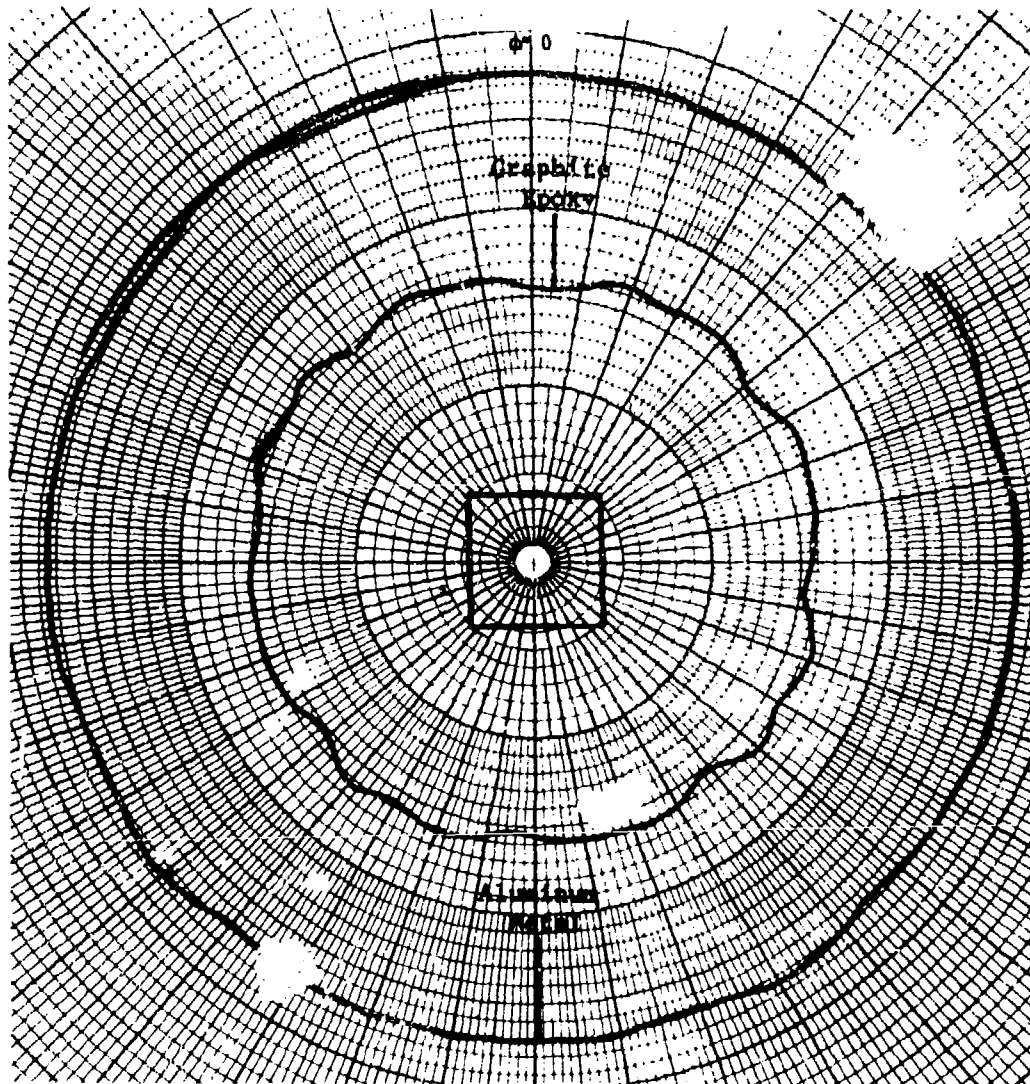


Figure 6-7 Monopole antenna at 837 MHz.
Conical antenna pattern at $\theta=70^\circ$.

6.3.2 Dipole Antennas

At 370 MHz the dipole was 36.6 cm long and was mounted 22.5 cm above the ground plane. The patterns obtained are given in Figures 6-8 through 6-10.

At 837 MHz the dipole was 15.7 cm long and was mounted 13.8 cm above the ground plane. The patterns obtained are given in Figures 6-11 through 6-13. The coordinate system is shown in Figure 6-3b.

6.3.3 Blade Antenna

One pattern was measured using a UHF blade antenna of the type used on the F-4 aircraft. The antenna is 15.2 cm high and 9.2 cm wide. The pattern is shown in Figure 6-15 for 370 MHz. The coordinate system is shown in Figure 6-14.

NOTE POWER LEVEL DIFFERENT FOR THESE TWO PATTERNS

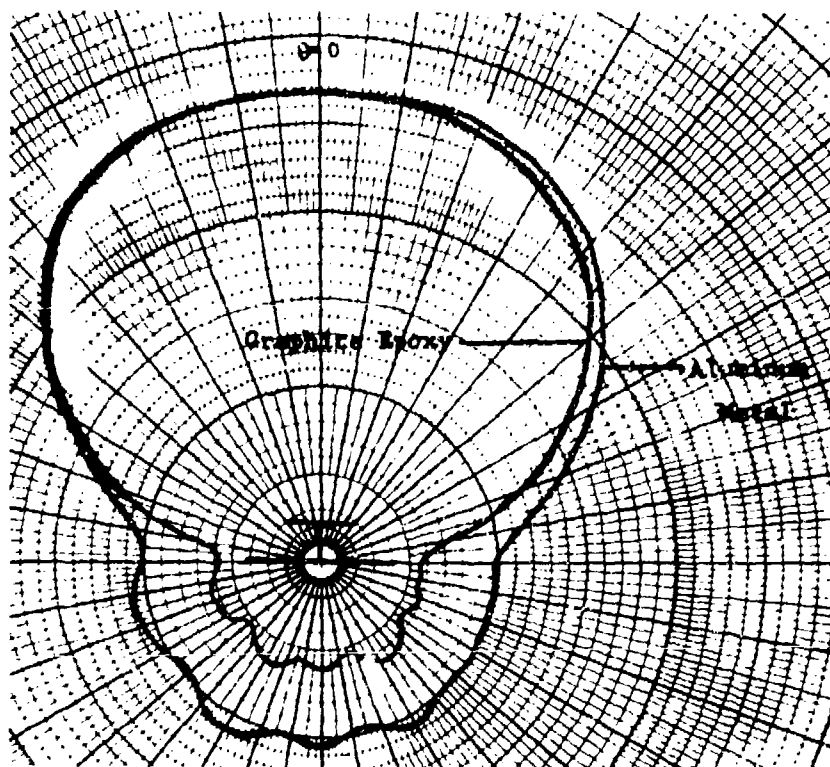


Figure 6-8 Dipole antenna at 370 MHz.
Antenna pattern in the $\phi=90^\circ$ plane.

NOTE POWER LEVEL DIFFERENT FOR THESE TWO PATTERNS

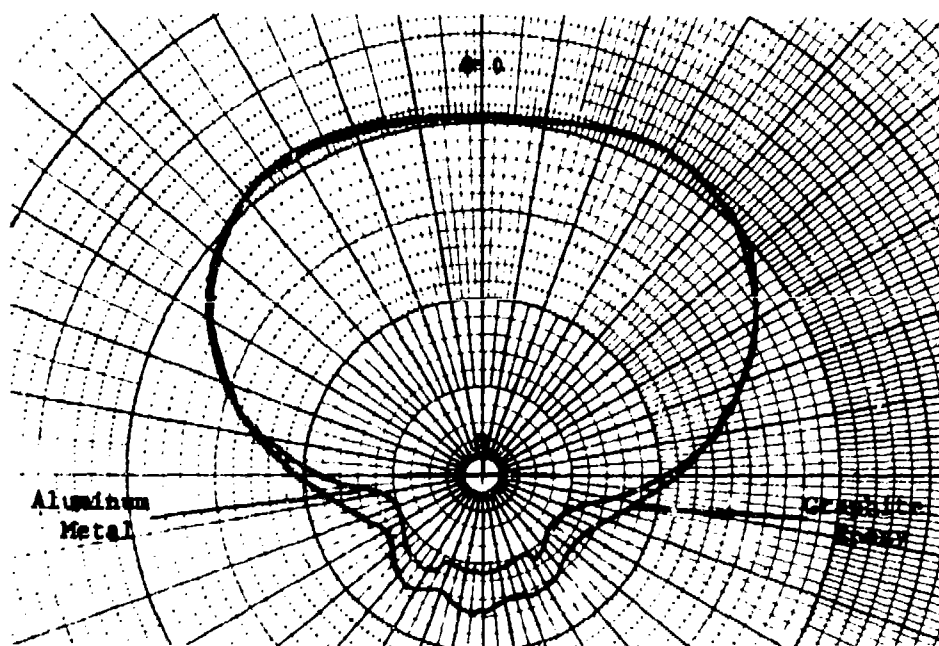


Figure 6-9 Dipole antenna at 370 MHz.
Antenna pattern in the $\phi=0^\circ$ plane.

NOTE POWER LEVEL DIFFERENT FOR THESE TWO PATTERNS

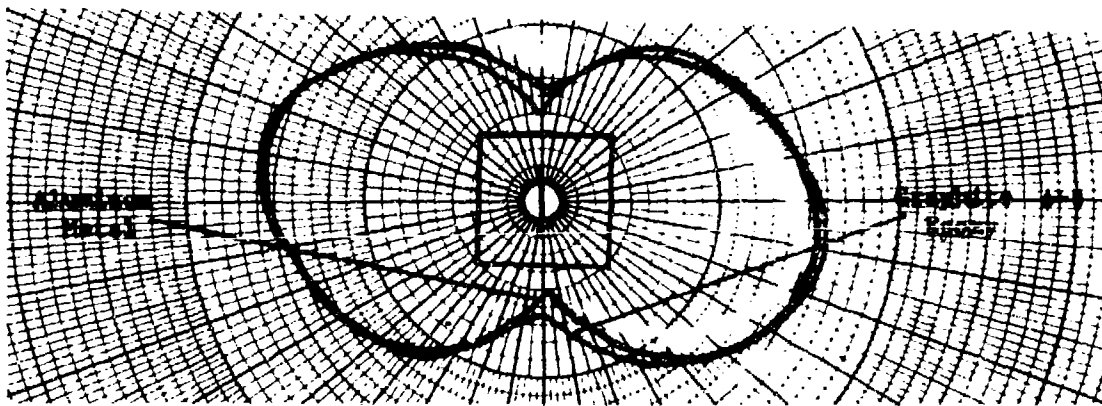


Figure 6-10 Dipole antenna at 370 MHz.
Conical antenna pattern for $\theta=70^\circ$.

NOTE POWER LEVEL DIFFERENT FOR THESE TWO PATTERNS

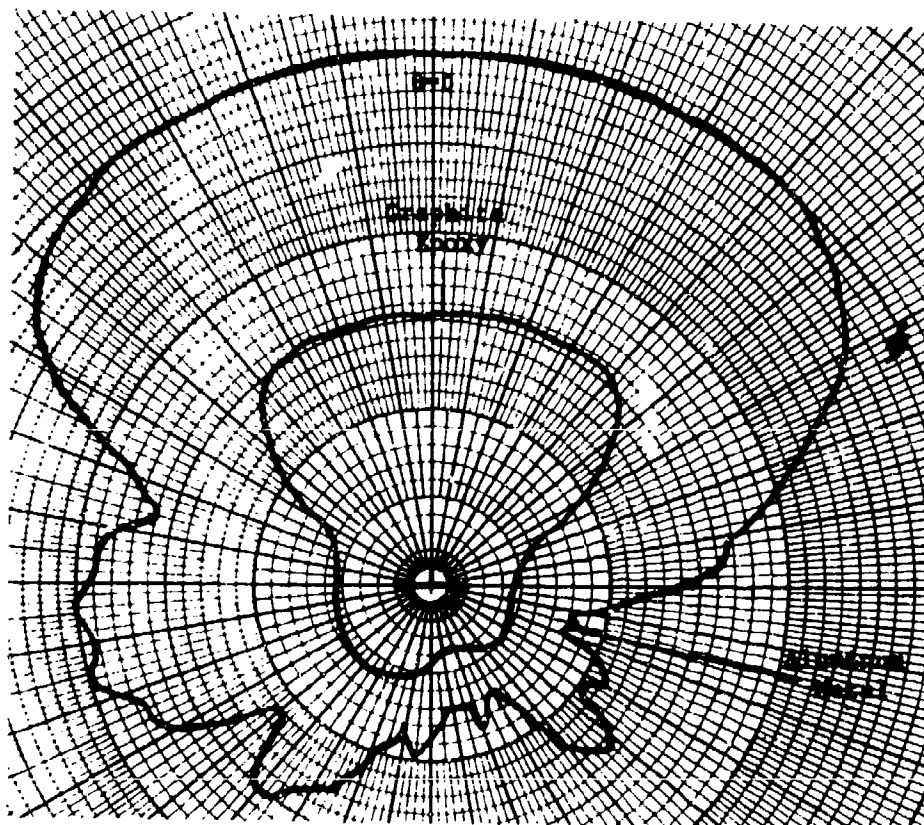


Figure 6-11 Dipole antenna at 837 MHz.
Antenna pattern in the $\phi=90^\circ$ plane.

NOTE POWER LEVEL DIFFERENT FOR THESE TWO PATTERNS

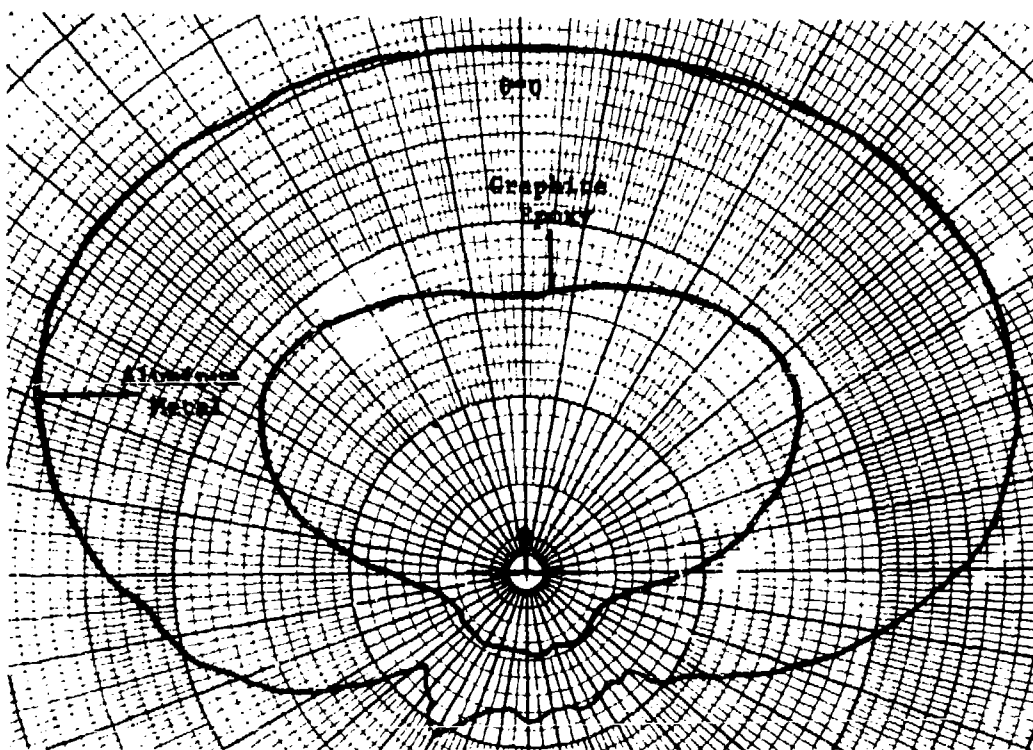


Figure 6-12 Dipole antenna at 837 MHz.
Antenna pattern in the $\phi=0^\circ$ plane.

NOTE POWER LEVEL DIFFERENT FOR THESE TWO PATTERNS

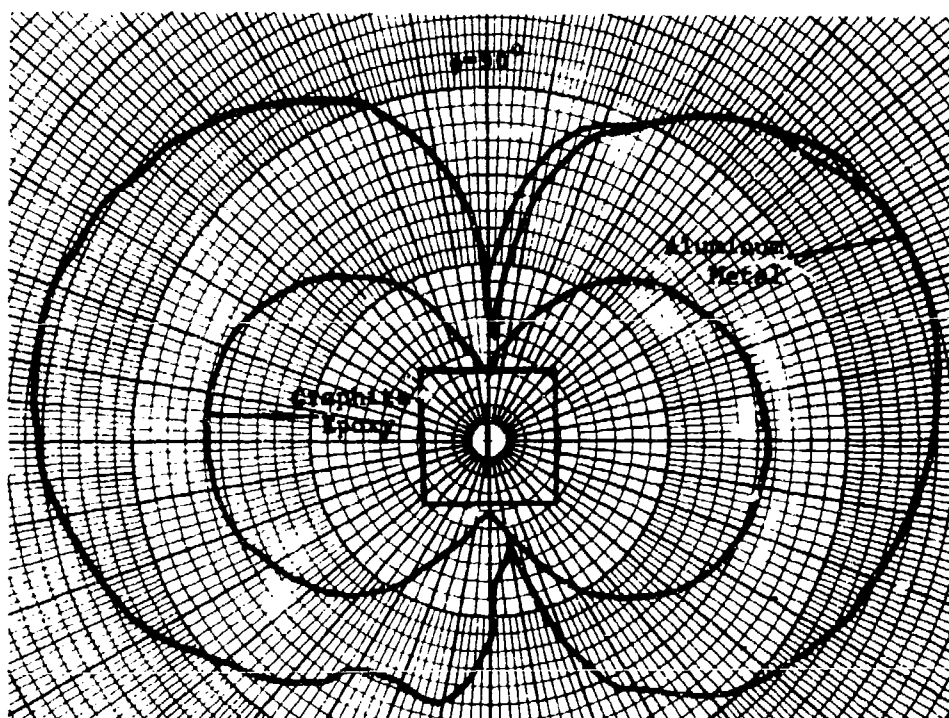


Figure 6-13 Dipole antenna at 837 MHz.
Conical antenna pattern at $\theta=70^\circ$.

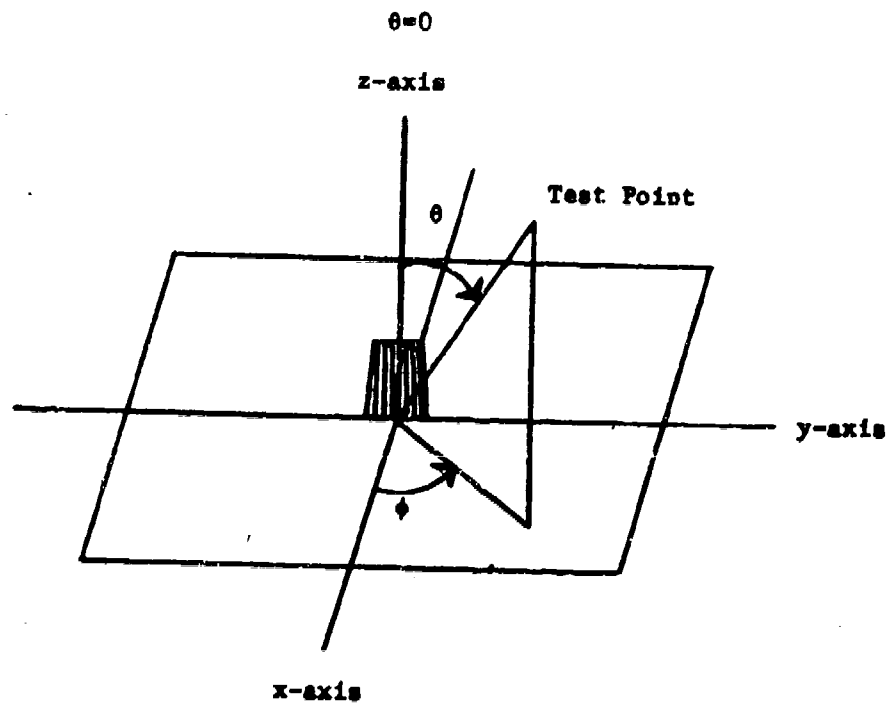


Figure 6-14 The coordinates used on the blade antenna

NOTE POWER LEVEL DIFFERENT FOR THESE PATTERNS

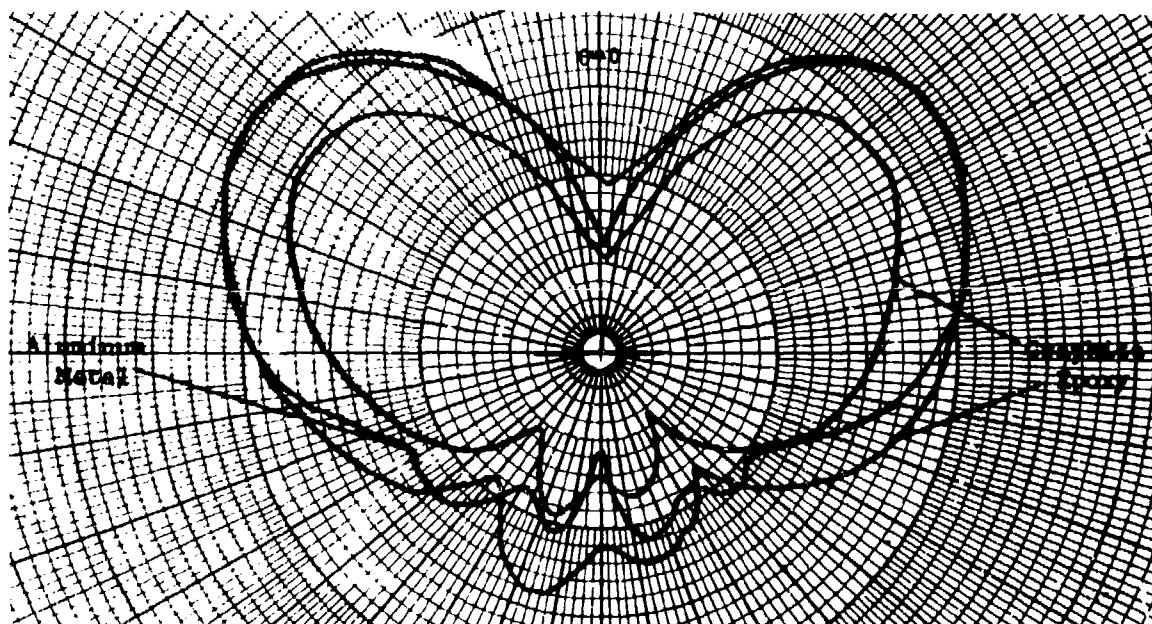


Figure 6-15 Blade antenna at 370 MHz.
Antenna pattern in the $\phi=0$ plane.

REFERENCES

- 6-1 Capt John E. Erickson, Lt. Col. Oscar D. Graham, Maj Jerry D. McCannon,
Capt Michael J. O'Brien, Performance of Graphite/Epoxy as an Antenne
Ground Plane, To be published by the U.S. Air Force Academy, CO.

MISSION of Rome Air Development Center

RADC plans and conducts research, exploratory and advanced development programs in command, control, and communications (C³) activities, and in the C³ areas of information sciences and intelligence. The principal technical mission areas are communications, electromagnetic guidance and control, surveillance of ground and aerospace objects, intelligence data collection and handling, information system technology, ionospheric propagation, solid state sciences, microwave physics and electronic reliability, maintainability and compatibility.



Best Available Copy